ULTRASOUND TRIGGERED RELEASE OF TRASTUZUMAB-CONJUGATED

IMMUNOLIPOSOMES TARGETING BREAST CANCER

by

Amal Elsadig Elamir Ahmed

A Thesis presented to the Faculty of the
American University of Sharjah
College of Engineering
In Partial Fulfillment
of the Requirements
for the Degree of

Master of Science in
Chemical Engineering

Sharjah, United Arab Emirates

December 2018

Approval Signatures

We, the undersigned, approve the Master's Thesis of Amal Elsadig Elamir Ahmed

Thesis Title: Ultrasound triggered release of Trastuzumab-conjugated immunoliposomes targeting breast cancer.

Signature   **Date of Signature**
                                                       (dd/mm/yyyy)

_____   _____
Dr. Ghaleb Husseini
Professor, Department of Chemical Engineering
Thesis Advisor

_____   _____
Dr. Rana Sabouni
Assistant Professor, Department of Chemical Engineering

Thesis Co-Advisor

_____   _____
Dr. Nabil Abdel Jabbar
Professor, Department of Chemical Engineering
Thesis Committee Member

_____   _____
Dr. Lutfi Albasha
Professor, Department of Electrical Engineering
Thesis Committee Member

_____   _____
Dr. Naif Darwish
Head, Department of Chemical Engineering

_____   _____
Dr. Ghaleb Husseini
Associate Dean for Graduate Affairs and Research
College of Engineering

_____   _____
Dr. Richard Schoephoerster
Dean, College of Engineering

_____   _____
Dr. Mohamed El-Tarhuni
Vice Provost for Graduate Studies

Acknowledgement

Dedication

To my loving family…

Abstract

Cancer is one of the deadliest diseases in this era. Since conventional treatment has many side effects, its use is limited, which augments the need for new smart drug delivery systems, such as nanocarriers, capable of shielding the healthy cells from the adverse side effects of chemotherapy. To this endeavor, liposomes are the most widely used and researched nanovehicles in the fight against cancer. They can be engineered to specifically target cancer cells by modifying their surface with targeting moieties. In this thesis, Trastuzumab was used as the targeting moiety for HER2-positive breast cancer. Once these drug-loaded liposomes reach the tumor, their release can be triggered using ultrasound, an external modality capable of accelerating the cytotoxic effects of the drug. The purpose of this study is to test the ultrasound-triggered release of calcein (a model drug) from immunoliposomes and compare it with the control (non-targeted) liposomes, under the utility of low-frequency ultrasound. The overall goal is to obtain an engineered immunoliposomes that specifically targets malignant tissue using acoustic power. The liposomes were categorized to be unilamellar vesicles (ULVs) with average radii of 89 nm and 101 nm for non-targeted liposomes and immunoliposomes, respectively. Next, the attachment of Trastuzumab was confirmed resulting in 9 Trastuzumab molecules per liposome. Low-frequency ultrasound (at 20 kHz) results showed the sono-sensitivity of both carrier types, with immunoliposomes being more acoustically sensitive, releasing 92% of the model drug, compared to 86% released from NH_2 liposomes. Results also showed an increase in the release rate as the power density increased from 7.46 to 17.31 (mW/cm^2). Finally, both types of liposomes were tested for their release kinetics, and results showed adherence to the Korsmeyer-Peppas model with an n > 0.45 which indicates a non-Fickian diffusion of the drug through the liposomal membrane. Statistical analysis showed that the release rate constants were significantly different at different power densities. Release rates (k_{kp}) at 7.46 (mW/cm^2) for immunoliposomes and NH_2 liposomes were 2.098 x 10^2 and 2.094 x 10^2, respectively. Using ultrasound and targeted liposomes, we envision a drug delivery system capable of reducing the side effects of conventional chemotherapy.

Keywords: *liposomes; active targeting; breast cancer; cancer therapy; drug delivery; Trastuzumab; ultrasound; triggered release; human epidermal receptor.*

Table of Contents

List of Figures

List of Tables

List of Abbreviations

ACE	Angiotensin Converting Enzyme
ADCs	Antibody Drug Conjugates
BCA	BicinChoninic Acid
C.C.	Cyanuric Chloride
CDRs	Complementarity-Determining Regions
CFR	Cumulative Fraction Release
CMC	Critical Micelle Concentration
CTLA4	Cytotoxic T-Lymphocyte-Associated protein 4
DDS	Drug Delivery Systems
DLS	Dynamic Light Scattering
DOPE	1,2-DiOleoyl-sn-glycero-3-PhosphoEthanolamine
Dox	Doxorubicin
DPPC	DiPalmitoylPhosphatidyl Choline
DSPE	1,2-DiStearoyl-sn-glycero-3-PhosphoEthanolamine
EGFR	Epidermal Growth Factor Receptor
EPR	Enhanced Permeability and Retention
ER-positive	Estrogen-positive
Fab	antigen-binding Fragment
FDA	Food and Drug Administration
HER2	Human Epidermal Receptor 2
HPMA	N-(2-HydroxyPropyl)MethacrylAmide
LFUS	Low Frequency Ultrasound
LUVs	Large Unilamellar Vesicles

mAb	monoclonal Antibody
MDR	Multi Drug Resistance
MI	Mechanical Index
MLVs	Multi-Lamellar Vesicles
MOFs	Metal Organic Frameworks
MPS	Mononuclear Phagocyte System
PBS	Phosphate-Buffered Saline
PD	Poly Dispersion
PEG	PolyEthylene Glycol
PR-positive	Progesterone-positive
PSMA	Prostate-Specific Membrane Antigen
RES	Reticulo Endothelial System
RGD	Arginine-Glycine-Aspartic acid
RTKs	Receptor Tyrosine Kinases
scFV	Single-Chain Variable Fragment
SUVs	Small Unilamellar Vesicles
TAA	Tumor Associated Antigen
TSL	Temperature Sensitive Liposomes
ULVs	Uni-Lamellar Vesicles
VEGFR	Vascular Endothelial Growth Factor Receptor

Chapter 1. Introduction

1.1. Overview

Cancer is one of the most epidemic diseases in this era. Considering the amount of effort put into treatments, cancer treatments still lack specificity and efficiency, especially in late stages when chemotherapy is applied. Chemotherapy suffers from severe side effects because it harms healthy cells along with cancerous cells. Some cancers develope resistance towards drugs. All these shortcomings can be overcome using smart drug delivery systems, mainly nanocarriers such as liposomes. Nanocarriers shield healthy tissue from the drug and enhance efficacy. They also control the rate at which the drug is released. Controlling the amounts and levels of the drug is important in order to sustain therapeutic levels, and to reduce administration frequency to be more convenient for the patients.

Liposomes are biodegradable, and biocompatible nanocarriers. They do not need to be surgically implanted nor removed. They can encapsulate both hydrophilic and hydrophobic drugs in their inner aqueous compartment, and hydrophobic bilayer, respectively. Liposomes enhance the drug distribution and pharmacokinetics, preventing interaction with fluidic molecules, while only releasing the drug at the tumor site. Liposomes physically accumulate at tumor sites due to the enhanced permeability and retention effect that characterizes malignant tissue. This happens when the tumor tissue is too leaky that liposomes of certain sizes enter the tumor and are retained onsite. This ensures the accumulation of liposomes at the tumor tissue, hence only affecting cancer cells, while protecting healthy cells from damage caused by the chemotherapeutic tissue.

Liposomes selectivity to tumors is further enhanced by conjugating targeting moieties to their surface. To target tumors, it is important to know that cancer cells overexpress certain receptors on their surface. Each receptor specifically binds to a ligand. A ligand can be a molecule, hormone, protein, or an antibody. This conjugation results in more specific targeting towards cancer, which is needed to enhance the treatment.

Once the liposome-encapsulated drug reaches the tumor site, its contents can be released using various triggers such as light, change in pH, increase in temperature,

and ultrasound. Ultrasound is a reliable mechanism used to trigger and control the release of drugs from liposomes. It is safe to use and cheap. Ultrasound has a synergetic effect when used with chemotherapy, which increases its cytotoxicity effects. The waves of ultrasound induce cavitation events which are considered the main reasons for triggering drugs release from liposomes. Cavitation events are believed to increase with increased intensity of ultrasound. Ultrasound needs to be optimized for its parameters including frequency, intensity, and mode of operation.

Breast cancer is the first leading cancer death in women. Human epidermal receptor 2 (HER2) positive breast cancer is the most aggressive type. It coincides with decreased survival rates. HER2 receptor is uniformly overexpressed on cancer cells and continuously exist in the entire malignant process. HER2 receptor can be targeted using the monoclonal antibody Trastuzumab as a ligand. Trastuzumab is approved by the FDA to be used in immunotherapy to hinder the homo-dimerization of the HER2 and to prevent its signal implicated in causing the growth of cancer cells. Trastuzumab is solely attracted/has the affinity towards the HER2 receptor, which assures specific binding.

In this study, HER2-positive breast cancer is targeted using the monoclonal antibody Trastuzumab as a ligand conjugated on the liposomal surface. The ligand assures the liposomes selectivity toward cancer cells. Ultrasound is used to trigger the model drug calcein encapsulated in the liposomes, which are synthesized, then characterized. The attachment of the antibody is confirmed, and then the ultrasound release is studied at low frequency. Release profiles are compared for both Trastuzumab-conjugated liposomes, and control plain liposomes. Finally, the release kinetics of each type is modelled using the best fitting model among nine suggested ones.

1.2. Problem Statement

Conventional treatments of cancer such as chemotherapy suffer from the severe side effects; due to the damage to healthy cells. This thesis is intended to overcome the side effects of chemotherapy by encapsulating the drug in nanocarriers, namely liposomes, preventing its interaction with healthy cells. It also aims to increase the cytotoxicity effect of the chemotherapy by acoustically triggering the release of the encapsulated drug within liposomes, using ultrasound. Ultrasound is

17

known to have a synergistic effect with chemotherapy, hence significantly controlling and retarding cancer development. The targeted receptor on the surface of cancer studied in this thesis is HER2. The targeting ligand attached to liposomes surface, for this receptor, is the monoclonal antibody, Trastuzumab.

1.3. Thesis Objectives

The main objective of this thesis is to test immunoliposomes response to low-frequency ultrasound and confirm their sono-sensitivity. Additionally, immunoliposomes are compared to control liposomes in order to test the effect of the conjugated antibody, Trastuzumab, on ultrasound response of liposomes. The detailed description objectives of the thesis are:

- The synthesis of anti-HER2 stealth immunoliposomes encapsulating calcein as a model drug.
- The synthesis of control non-targeted liposomes encapsulating calcein as a model drug.
- The characterization of both types of liposomes using Dynamic light scattering.
- Measuring the lipid concentrations of liposomes using the Stewart assay.
- The verification of the antibody conjugation using the BCA assay.
- The evaluation of calcein release from both types of liposomes using LFUS.
- Testing release kinetics against nine different kinetic models and showing the best fitting model that represents the liposomes triggered release.

1.4. Research Contribution

This thesis is the first to suggest ultrasound triggering from immunoliposomes, to target HER2-positive breast cancer. Previous publications show that ultrasound can be used as a trigger to release encapsulated drugs from liposomes, but this triggering modality has never been used in conjunction with Trastuzumab-conjugated immunoliposomes targeting HER2 positive breast cancer.

1.5. Thesis Organization

In chapter two, a brief biological background of cancer is first presented, mainly to understand how to tackle the challenges faced with treatments. Then, a detailed description of breast cancer is presented, showing all types of breast cancer

and the commonly expressed receptors of each type, emphasizing HER2 receptor. After that, the different types of treatments are presented with all their advantages and limitations. Afterwards, smart drug delivery systems are introduced, emphasizing the most important ones. Liposomes, the drug delivery vehicle of choice in this thesis, are thoroughly detailed, including their composition, modifications, evolvement, applications, classification, advantages and disadvantages. Then, I move on to explain how nanocarriers exhibit the EPR effect, which is followed by explaining active targeting in detail. In the active targeting section, details about receptors and ligands for each receptor are discussed, including antibodies as ligands. In this section, Trastuzumab is mentioned for the first time. Afterwards, a closer look into monoclonal antibodies is taken, where Trastuzumab is detailed. Lastly, ultrasound is introduced and detailed. Finally, studies done with active targeting, and ultrasound triggered release are presented. Chapter three provides the materials and methods used in this thesis, detailing each methods and choice of material. Methods including attachment/conjugation, validation, and testing of the proposed treatment system are included. Chapter four discusses the results of the thesis, including attachment, ultrasound triggering, and kinetics modelling. Chapter five interprets the results and provides recommendations about the use of the results. It also suggests what work should follow this research.

Chapter 2. Background and Literature Review

In this chapter, the concepts of cancer/cancer development are outlined with specific emphasis on breast cancer. Then, an overview of conventional cancer treatments, including targeted therapy and its related receptor-ligand biology, are presented. Afterwards, the advantages of smart nano-drug delivery systems in chemotherapy treatment are introduced with an emphasis on liposomes. Additionally, the characteristics and mechanisms of delivery using liposomes are outlined, which include passive and active targeting. Finally, a brief overview of ultrasound and its role in triggering drug release from nanocarriers is presented, along with relevant *in vitro* and *in vivo* studies.

2.1. Overview of Cancer

Cancer is a widespread disease in the USA with 1.6 million new cases diagnosed in 2015. The most common types, responsible for more than half of the cases, are breast, prostate, lung, and colon cancer. By far the most common cancer in women and the second leading cause of cancer death among American women is breast cancer [1, 2]. It is also a global concern that endangers women lives worldwide. Breast cancer is the most frequent cancer in women and the second overall (23% of all cancers). With 4.4 million cases diagnosed within the past five years, only 1.4 million survived breast cancer [3].

2.1.1. The etiology and epidemiology of cancer. Most normal cells replicate, but tumor cells are damaged cells that cannot stop growing. They can escape programmed cell death (apoptosis) due to abnormalities in cell proliferation, differentiation, and survival [4]. These cells are either benign or malignant. Malignant cells (cancer) usually proliferate faster and spread throughout the body invading other organs in a process called metastasis [5].

Solid tumors that stem from cells of mesenchymal origin (connective tissue) are known as sarcomas, and they spread via the bloodstream. Cancer cells that arise from epithelial cells are called carcinomas. They are the most common tumor type that constitutes 90% of human cancers, and they spread through the lymphatic channels. Leukemias and lymphomas, which constitute 8% of cancer cases, arise from the cells of the blood and the immune system, respectively [4, 5].

The tumor starts from a single cell that mutates. Mutations include the activation of oncogenes that promote cell proliferation and damage in tumor suppressor genes that causes cell failure (to differentiate normally). It proliferates fast requiring extensive blood vessels and nutrients during proliferation. After that, these cells form a cluster, refered to as an *in situ* carcinoma. Then, they penetrate the basement membrane (extracellular matrix of tissue) to invade the underlying connective tissue, as can be seen in Figure 2.1. Once this happens, cancer cells can circulate throughout the body and spread the tumor to other organs, in a process called metastasis, and cause metastatic cancers. Metastasis is the main reason why localized therapy eventually does not work in cancer treatment [4, 6]. Furthermore, dissolution of the basement membrane tissue makes it permeable and easy to penetrate, which is considered a characteristic of the malignant tissue.
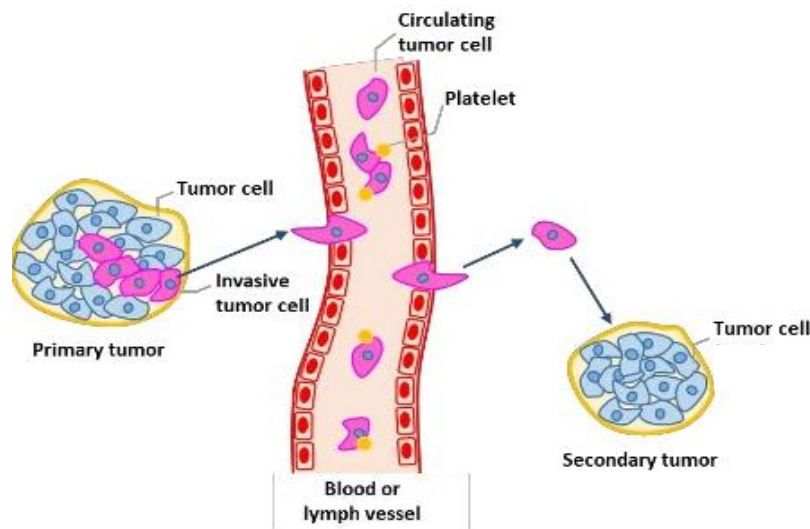
Figure 2.1: The metastasis process of cancer cells [7].

Apoptosis resistance contributes to the development of the tumor and also creates resistance to chemotherapeutic drugs that are based on damaging the DNA [4].

2.1.2. Cancer cells characteristics. The Hallmarks of cancer cells can be summarized as follows [4, 6]:

1. Normal cells proliferate in the presence of growth factors, while cancer cells have a reduced requirement for growth factors. This can be due to the

unregulated activity of growth factor receptors and intracellular signaling systems in cancer cell.

2. Some cancer cells produce their own growth factors, auto-stimulating cell division (autocrine signaling).

3. Cancer cells are less responsive to cell-cell interactions. This results in their disordered multilayered growth patterns in which they push neighboring cells to grow, and eventually put pressure on the organ.

4. They secrete chemicals that digest the extracellular matrix components allowing for more invasions.

5. They also produce growth factors that stimulate angiogenesis which results in the formation of new capillaries around the tumor. It can also help in metastasis since these capillaries are easy to penetrate by cancer cells.

6. Divided cells lose the capacity to differentiate.

7. Cancer cells fail to respond to signals promoting apoptosis, contributing to the survival of damaged mutated cells.

8. Some cancer cells produce immunosuppressive factors in an attempt to avoid detection by the immune system.

9. Lower pH around the tumor is caused by lactic acid formation due to the lack of oxygen which is a result of a higher oxygen consumption rate in proliferation (higher than what angiogenesis can provide). This also contributes to immune system evasion where high lactic levels disturb T cells function [8].

Cancer progresses through a series of abnormalities that accumulate over time, so there can be several factors that induce cancer. These factors are called carcinogens. Carcinogens include environmental factors; chemicals, radiations, and viruses. Factors that contribute to the proliferation of the mutated cells are called tumor promoters, which include increased accumulation of hormones and/or collagen [4, 9].

2.1.3. Breast cancer and its cells receptors. As mentioned above, breast cancer is the most frequent cancer among women and the second overall [3]. Ductal carcinoma (cancer origins from cells lining the milk ducts) constitutes 80% of breast cancer and lobular carcinoma, and other special histologic types form the rest 20% [1]. Breast cancer most commonly spreads to the regional lymph nodes, and in

advanced stages, it could also spread to the bones, lungs, and liver. Some of the factors that increase the risk of breast cancer are early menarche, late menopause, as well as obesity and increased uptake of alcohol. Breast cancer develops as a result of a series of changes in oncogenes and cell mutations that include mutations in BRAC1 and BRAC2 genes. These two genes are tumor suppressor genes that help repair DNA damage. Mutations of these genes are present in basal breast cancers (triple negative breast cancer, i.e. those that are HER2 negative, ER-negative and PR-negative), and they account for 20-25% of heredity breast cancers and 5-10% of all breast cancers. Local estrogen production helps in the growth of both cancer cells and breast stromal cells [3, 10]. Cancer cells differentially express estrogen and progesterone receptors compared to normal breast tissue, and this is why it is referred to as ―hormone receptor positive" breast cancer. It occurs most commonly in older patients and progresses slowly. This type of cancer is expressed in up to 60% of breast tumors and can be treated with tamoxifen (an estrogen antagonist). Vascular endothelial growth factor receptors (VEGFR) can also be overexpressed in breast cancer. They are essential for angiogenesis which is in turn required for cancer growth, invasion, and metastasis. Insulin-like growth factor receptors are also expressed in high levels in breast cancer compared with normal breast tissue. Lastly, the most important family of receptors that regulate cell proliferation and apoptosis are the human epidermal growth factors family that includes HER1 (EGFR), HER2 (ErbB2), HER3 (ErbB3), and HER4 (ErbB4) that belong to a family of transmembrane receptor tyrosine kinases (RTKs) [11-13].

HER2 encodes 1225 amino acids, and is normally expressed at low levels in the epithelial cells of various organs such as the lung, bladder, pancreas, breast, and prostate [3, 14]. HER2 overexpression occurs in 20% to 30% of patients with breast cancer, and it is more prevalent among younger woman. HER-2 positive cancer progresses rapidly; hence coincides with decreased survival rates, with 20% less survival rate for HER-2 positive women than a HER-2 negative woman in the five-year period following surgery [11-13]. It is noteworthy that HER2 overexpression in breast cancer cells corresponds to overexpression of VEGF, and thus induces angiogenesis [15]. HER2 is continuously overexpressed throughout the malignant process, and homogeneously distributed within the tumor. These characteristics make it an appealing choice as a target in cancer targeted therapy. HER2 does not have a

known ligand (orphan receptor) but it heterodimers with other receptors in the family to enhance signaling. Overexpression or gene amplification of HER2 induces ligand-independent homodimerization; hence the activation of the HER2 signaling pathways that include PI3K/AKT and RAS/RAF/MAPK pathways which leads to uncontrolled cell proliferation, growth and survival as well as invasion and angiogenesis, thus leading to cancer development. The HER family of receptors bind to a variety of different ligands as shown Table 2.1. It was found that prolidase (peptidase D) may act as a ligand for HER2 and inhibit downstream signaling using immune-precipitation [11]. Additionally, mutations in the PI3KCA gene have been detected in 25% of breast cancers [13]. Table 2.1 shows that HER-2 positive tumors tend to include P53 tumor suppressor gene mutation [11, 12].

Table 2.1: Ligands of the human epidermal growth factors (HER) family [11].

Ligand	HER1 (EGFR)	HER2	HER3	HER4
Transforming Growth Factor alpha (TGFα)	yes	-	-	-
Amphiregulin (AR, AREG)	yes	-	-	-
Epidermal Growth Factor (EGF)	yes	-	-	-
Betacellulin (BTC)	yes	-	-	yes
Heparin-binding EGF like Growth Factor (HBEGF)	yes	-	-	yes
Epigen (EPG)	yes	-	-	-
Epiregulin (EPR)	yes	-	-	yes
Heregulin	-	-	1,2	1,2,3, 4

2.1.4. Treatments. In recent years, there has been several ways to treat cancer depending on the type of malignancy, stage, and pathologic features (including receptor status and tumor grade). A plan for each patient depends on the purpose of treatment, either to shrink the tumor, stop the tumor growth, or just enhance the patient's quality of life in late stages. Treatments include surgery, radiation,

chemotherapy, biological therapy (includes immunotherapy), and targeted therapy. It can also be a combination of the above treatments. In the early stages before the metastasis of cancer, surgery combined with radiation (localized treatments) can be applied. But once the tumor has spread, chemotherapy and sometimes chemotherapy combined with immunotherapy are used. Adjuvant treatment is then followed to make sure that new tumors are eliminated. Sometimes chemotherapy is used before surgery in order to shrink the tumor size [16].

2.1.4.1 Chemotherapy and its challenges in cancer treatments. In chemotherapy, drugs inhibit cell division and eventually kill these cells. Nitrogen mustard was the first chemotherapeutic agent to be used against cancer. It targets fast proliferating cells which unfortunately include some other normal cells as well (i.e. stems cells). Folic acid antagonists are the second group developed and are used to inhibit the cancer cell ability to produce folic acid which is necessary for growth. Nucleic acid antagonists are the third group used. They inhibit nucleic acid which is needed for cell growth and proliferation. Tyrosine kinase inhibitors work by deactivating this protein which is responsible for facilitating signaling pathways related to cell proliferation activities. And antitumor antibiotics such as doxorubicin are also used in cancer treatment [16].

The challenge of using chemotherapy resides within the non-selective action resulting in the severe side effects of these chemical agents to normal cells which limit the dosage given in therapy. These side effects include nausea, vomiting, diarrhea, anemia, and hair loss. They also cause damage to the heart, the kidneys, and the bone marrow and may result in the death of the patient in some cases.

Another challenge is the ability of the tumor to develop resistance to the anti-neoplastic drug, rendering them ineffective in the fight against malignant tissues. In drug resistance (also known as multi-drug resistance-MDR), the cancer cells develop a mechanism that reduces the ability of cancer cells to take up the chemical agents or reduce expression of some proteins that guide the agent to the diseased cell. An additional MDR mechanism is developed when the tumor is grown, where some cells slow their proliferation and hence become non-detectable as malignant cells. Also, heterogeneous tumors that consist of cells with different characteristics and different sensitivity to chemotherapy are considered drug resistant. As most chemotherapy

25

drugs kill cancer cells using apoptosis, defective apoptosis allows the survival of these cells, and make them resistant in the process [16].

MDR can be treated by the administration of a combination of drugs that follow different cytotoxic mechanisms, increasing the drug dosage, using chemotherapy with a combination of other therapies (immunotherapy), hyperthermia therapy, or delivering the drug more efficiently using advanced drug delivery systems.

Hyperthermia therapy is one solution to drug resistance. It works by heating the tumor region above 40 ºC, a temperature at which cancer cells and tissue are rendered more porous, hence increases the uptake of the drug. It also facilitates the delivery of the drug as a result of dilated blood vessels to the tumor. Hyperthermia can also be used in combination with radiation therapy.

2.1.4.2 Biological therap. Biological therapy includes: inducing the host defence (immunotherapy), inhibiting tumor growth, and prompting cell differentiation (remission). To explain remission, we need to know that cell differentiation is coupled with cell division in such a way that whenever a cell is matured and fully differentiated, it stops replicating, hence cancer development is controlled.

Inhibiting tumor growth works by inhibiting angiogenesis that provides nutrients needed for proliferation. This is mainly accomplished by blocking growth factors receptors signals to prevent tumor development [4, 6].

Immunotherapy includes the enhancement of the human's own immune system to attack cancer cells. One way is to alter cells of a specific tumor to be more antigenic (provoking to the immune system) to help the tumor be identified and consequently produce antibodies for that tumor. Another way is to grow antibodies that are sensitive to the tumor and inject them into the patient, where these antibodies mark the cells for destruction [17, 18]. Lastly, antibodies can be used to block proliferation cells signaling and thus control cancer development [2, 18]. One example is the use of Trastuzumab (Herceptin) in blocking human epidermal receptor two (HER2). Another example is the use of Bevacizumab in targeting vascular endothelial growth factor VEGF receptor (that is necessary for angiogenesis), and Cetuximab that binds the epidermal growth factor receptor (EGFR or HER-1) [16]. Also, some antibodies are used in blocking immune checkpoints created by cancer cells in an attempt to avoid detection by the immune system [19].

2.2. Drug Delivery Systems

Scientific and medical professionals are trying to overcome the challenges in cancer treatment (discussed in the previous sections) including severe side effects, a limited dosage, and drug resistance by developing new strategies of drug delivery including smart drug delivery systems. For the reasons mentioned above, we need to be able to use higher doses and to target cancer cells effectively without harming the healthy surrounding tissue. This endeavor can be accomplished using smart drug delivery systems [16].

Drug Delivery vehicles control the rate at which a drug is released and the location in the body where it is released, which subsequently controls the therapeutic agent infusion rate and the required tissue drug levels. Some systems can control both. They not only improve safety and efficacy but also permit new therapies that once were considered too risky or toxic to be delivered via conventional ways. Release patterns can significantly affect the therapeutic response. Additionally, it is more economical to enhance drug delivery systems than it would be to treat the side effects associated with the conventional chemotherapy. These systems include mechanical pumps (implants), polymer matrices (micro-particulates), externally applied transdermal patches, and drug delivery vehicles. Each method has advantages and disadvantages, and not all methods can be used for every medication. Implants require surgical administration and removal while microparticles suffer from being too large for drug targeting and intravenous administration [20, 21].

Nanoparticles such as liposomes and macromolecular drug carriers such as polymers are classified as nanomedicines; a field encompassing nanoscale drug delivery devices, aiming at optimizing selectivity, prolonging the agent's activity, and controlling drug release and cellular uptake. The most significant advantages of this technology are the ability to cross physiologic barriers, overcome drug resistance, and significantly reduce side effects [13]. Their small size helps them leave the vascular system and extravasate at the tumor sites. It has also raised the possibility for intracellular targeting and gene delivery [22].

The recent advancement in nanotechnology has provided a variety of nanocarriers, with a size range of 10-800 nm. Nanocarriers include nanocrystals (quantum dots), nanosuspensions, nanotubes, nanowires, micelles, liposomes, metal-

organic frameworks (MOFs), ceramic nanoparticles, dendrimers, solid lipid nanoparticles, and hydrogel nanoparticles. Micelles and liposomes are the most widely applicable nanocarriers [23]. Micelles are smaller, so they have limited capacity. They also have stability issues in the serum. Additionally, they can only encapsulate hydrophobic drugs [24].

2.2.1. Liposomes. Liposomes are one of the most widely used nanocarriers in drug delivery. They were first introduced by the British scientist Alec Bangham in the 1960s. Hence their former name was bengasomes [23-25].

Liposomes and nanocarriers have the ability to passively target tumor cells by utilizing the enhanced permeability and retention (EPR) effect. Additionally, they can be actively targeted to have increased selectivity for tumors in general. After reaching the tumor site, liposomes can be triggered to release their contents faster. Triggering nanocarriers internally can be achieved via several stimulators such as change in pH, temperature, pressure, or enzymes concentration. Otherwise, nanocarriers can be triggered externally by light, magnetic or electric fields, and ultrasound [24, 26].

2.2.1.1 Composition and function. Liposomes are spherically shaped phospholipid bilayers (lamellae) with a diameter range between 20 and 1000 nm. Each of these monolayers consists of amphipathic molecules; that is a hydrophilic (polar) head and hydrophobic (nonpolar) tail, as can be seen in Figure 2.2. It can also contain other molecules such as cholesterol, carbohydrates and proteins [24, 26, 27]. Liposomal membranes are considered similar to some cells membranes structures, rendering them safe to use in clinical trials (biocompatible and biodegradable). The aqueous compartment inside the core has the ability to entrap hydrophilic drugs, whereas the hydrophobic region within the bilayer can entrap hydrophobic drugs, as can be seen in Figure 2.4 [23]. Some of the chemotherapeutic drugs that can be loaded into liposomes include doxorubicin, annamycin, daunorubicin, vincristine, cisplatin derivatives, paclitaxel5- fluorouracil derivatives, camptothecin derivatives, and retinoids [28]. Liposomes can also be used to entrap various types of other molecules including: vaccines, plasmid DNA, peptides, hormones, antisense oligonucleotides or ribozymes, nutraceuticals and cosmetics [26]. The properties of liposomes can be tailored to perform various functions by controlling their lipid composition, particle size, surface charge, lipid membrane fluidity, and steric stabilization [26].
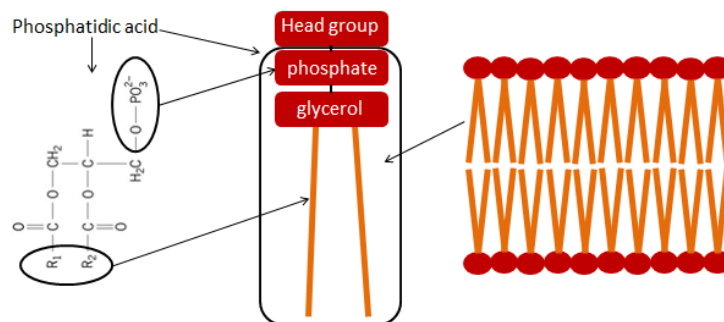
Figure 2.2: The amphipathic molecule composed of a phosphoglyceride (a class of phospholipids).

2.2.1.2 Classification. Liposomes are classified, depending on their number of bilayers, into multilamellar vesicles (MLVs) and unilamellar vesicles. In multilamellar vesicles (MLVs) more than one fluid compartments are present and separated by lipid bilayers. As can be seen in Figure 2.3, they range in size between 500 and 5000 nm, while Unilamellar vesicles (ULVs) contain only one internal aqueous compartment. The later can be further classified into small unilamellar vesicles (SUVs) that range in size between 50 and 100 nm and large unilamellar vesicles (LUVs) with a size in the range of 100 to 250 nm, respectively. Most liposomes used in drug delivery belong to the SUVs type due to their optimal size and high drug capacity [26, 29]. Even though MLVs can exhibit slower drug release and higher loading capacities for hydrophobic compounds, they still have limited industrial applications due to their heterogeneity in size, large diameter, multiple internal compartments, and inconsistent methods of preparation [30].
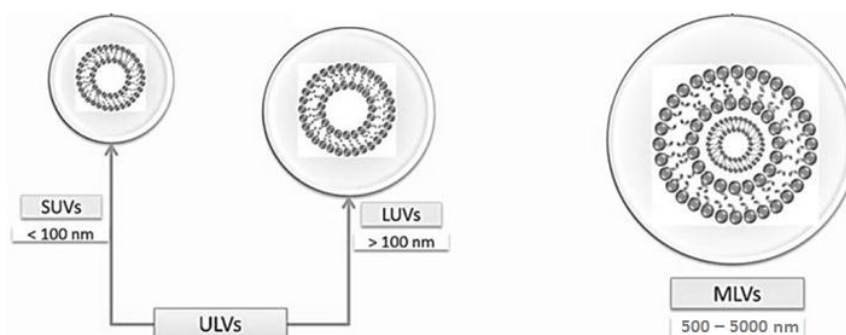
Figure 2.3: Classification of liposomes based on size into MLVs and ULVs [26].

2.2.1.3 Liposomes modifications. Nanocarriers face many unexpected hurdles upon interaction with body fluids. Liposomes are rapidly cleared from the human

body because they are considered foreign bodies. This can be avoided by covalently attaching moieties to their surface in order to render them more stable and less immunogenic, which increases their blood circulation time, and protects them from degradation in the plasma [29]. Liposomes blood circulation time depends on their size, their surface charge, and degree of unsaturation of the lipid chains [31]. Liposomes can also be engineered to better target cancer cells, by attaching ligands on their surface. These ligands have a binding affinity toward receptors on cancer cells. Commonly used targeting moieties attached to the liposomal surface include antibodies, hormones, and proteins, as is extensively detailed in section 2.2.3 [32].

Sterically-stabilized liposomes (also referred to as stealth liposomes) have the hydrophilic poly ethylene glycol (PEG) attached to their surface as can be seen in figure 2.4 (C). This protective polymer helps in avoiding hydrophobic interactions with plasmatic proteins (specifically opsonin proteins (f) in Figure 2.4 (C)) and their subsequent adsorption by the liposome membrane. This reduces the trapping of liposomes by macrophages of the mononuclear phagocyte system (MPS also known as the reticulo endothelial system (RES)), in a process called opsonisation, thus resulting in prolonged blood circulation time. Basically, increasing the hydrophilicity of the liposomes creates a steric barrier to prevent detection by the MPS, which subsequently prevents liposomes clearance. This is needed as long as the liposomes target does not include one of the RES organs such as spleen, liver, or bone marrow. Stealth liposomes also have the ability to cross biological barriers and are used in the treatment of solid tumors [26]. Coating liposomes with PEG was found to increase their half-lives up to 12 to 30 hours in animal models and 21 to 54 in humans. But unfortunately, the PEG polymer can also prevent cells interactions, so a trade-off for the amount of PEG coating layer should be done if a targeting moiety was to be used [23]. It was reported that some stability issues arose with PEG stealth liposomes. Due to their hydrophobic nature, they can act against the hydrophilic property of the head group and cause destabilization. To counteract this effect, a sufficient amount of cholesterol (a rigidifying agent) is added into stealth liposomes [33]. Other coating polymers have been suggested but because of PEG's ease of preparation, relatively low cost, controllability of molecular weight and linkability to lipids by a variety of methods, it was generally preferred [31, 34]. It was also reported that the size and the fluidity of the liposomes could affect its uptake by the RES; the smaller their size and

the more rigid they are, the better chance they have to avoid clearance [28]. Another approach to deal with liposomes clearance is to render them less foreign and more recognized as self-proteins by the macrophages of the MPS using coats of natural glycolipids, gangliosides. However, this approach was not pursued due to some difficulties [28].

Targeting ligands can be attached on liposomes surface to enhance treatment, as can be noticed in Figure 2.4 (B). To have both properties of long circulation time and targeting ability, antibodies are attached to distal ends of PEG molecules, as can be seen in Figure 2.4 (D) [20, 23].

Liposomes can also be modified with cell-penetrating peptides like viral proteins. It has been proven that using TAT protein (found in HIV-1) as a ligand on liposomes surface facilitates its delivery into cells [29].
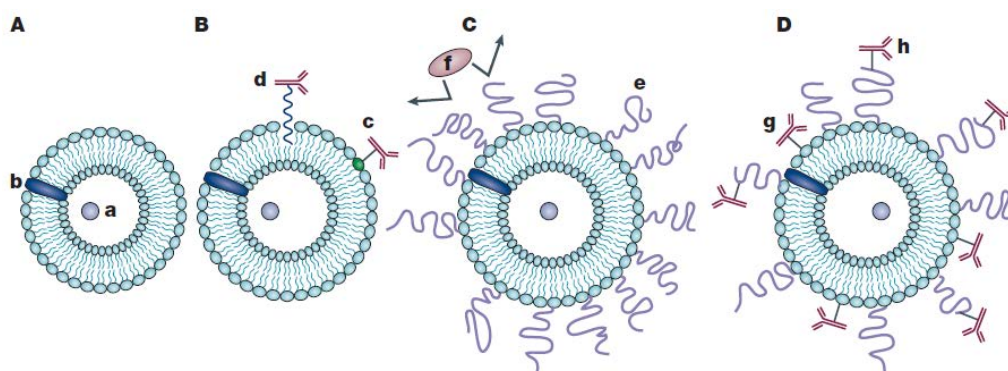
(A) describes the hydrophobic region where the hydrophobic drug (b) is trapped and the aqueous compartment where the hydrophilic drug (a) can be loaded, (B) describes liposomes after the attachment of antibodies covalently to the surface groups (c) or hydrophobically anchored into the membrane (d), in (C) stealth liposomes are described where the protective polymer (e) hinders the opsonin proteins (f), finally in (D) the incorporation of both the antibodies and the protective polymer is presented, where attachment directly to the surface is seen in (g) and to the distal ends of the protective polymer is seen in (g).

Figure 2.4: Liposomes structure and evolution [29].

2.2.1.4 Advantages of liposomes. Advantages of liposomes include:

- They enhance drug pharmacokinetics, distribution, and solubility by preventing drug interaction with bodily fluids, and hence prevent early degradation.

31

- They prolong the duration of tumor drug exposure and control the drug release rate.

- They naturally accumulate around the tumor area which increases the drug's concentration at the diseased site compared to healthy tissue.

- They can be actively targeted to bind to cancer cells more preferentially, enhancing tumor uptake and also intracellular drug delivery.

- Liposomes can be modified to make them more appealing to be used in many domains other than drug delivery, including diagnosis, regenerative medicine, and gene therapy.

- They allow the use of new drugs since they have the ability to control their release and help increase drugs solubility.

- They are considered biocompatible and bio-degradable and weekly immunogenic.

- Using liposomes can overcome multi-drug resistance.

- Liposomes have the ability to deliver various types of drugs, and also have increased loading capacity compared to other nanocarriers.

- Liposomes can be remotely triggered to release their contents.

2.2.1.5 Limitations of liposomes. limitations include:

- Sterically-stabilized immunoliposomes show enhanced accumulation at the tumor site, but less blood circulation time than conventional liposomes (more clearance).

- Sometimes liposomes still end up in the liver due to insufficient time to interact with the cancer cells.

- Some studies reported certain side interactions with liposomes.

2.2.2. Passive targeting. The first generation of nanocarriers used in nanomedicine is based on the enhanced permeability and retention (EPR) effect, also called passive targeting. Then in the second generation, targeting moieties were introduced to the surface of the nanocarriers for enhanced selectivity. The third line of treatment could further include the intracellular uptake, which is needed for some drugs to be fully effective.

EPR effect is naturally occurring due to the physical properties of solid tumors tissue. The enhanced vasculature and system permeability to molecules and nanoparticles in and around the tumor area is due to the defectiveness of the tumor vascular structure; this structure helps in entrapping those particles for prolonged periods of time before their subsequent clearance by the lymphatic system. Due to the impaired lymphatic system at the tumor site, particles clearance is slowed [23].

Enhanced tumor permeability is a physical phenomenon that depends on blood vessels morphological differences between normal and healthy tissue; this difference exists due to rapid angiogenesis. Normal blood vessels are linear and stacked regularly. However, blood vessels in tumors have openings in the endothelium and are weak due to the lack of an external muscle layer, leading to high blood pressure in the tumor site. Tumor blood vessels also show polymeric leakage at the capillary level. These structural deviations and vascular permeability render cancer vessels leaky, and as a consequence, macromolecules and lipid particles are allowed to extravasate from the blood vessels into the tumor interstitial space and accumulate as time passes by [35]. This can be seen in Figure 2.5 Permeability is also enhanced by the cancer cells increased production of permeability mediators such as bradykinin, nitric oxide, prostaglandins, and VEGF (or vascular permeability factor), in or near the most solid tumors [36].

EPR is normally applied to biocompatible lipidic particles and macromolecules with large molecular weights, whereas low molecular substances are observed to return to the circulatory system by diffusion [36]. Usually, long circulation times (around 6 hours) are needed for the accumulation of any drug to take place due to EPR effects [23].

In a study, it was reported that blue albumin (67 kDa) exhibited EPR effects because its tumor concentration was 10-fold more than that of blood after 145 hours. But this was not observed for low molecular weight proteins [38]. Another study showed rapid uptake of HPMA copolymers in tumors, except for those that are 40 kDa or smaller, which were diffused back to the bloodstream and cleared by renal excretion. This demonstrates the molecular weight significance for the EPR effect [39].

It was reported that endothelium openings range from 300-4700 nm, which are not found in normal tissue. These molecules exhibit the EPR effect, but as the size increases, the intracellular uptake rate decreases [40]. Generally, liposomes that range from 90-200 nm are known to exhibit increased accumulation due to EPR effects [41].
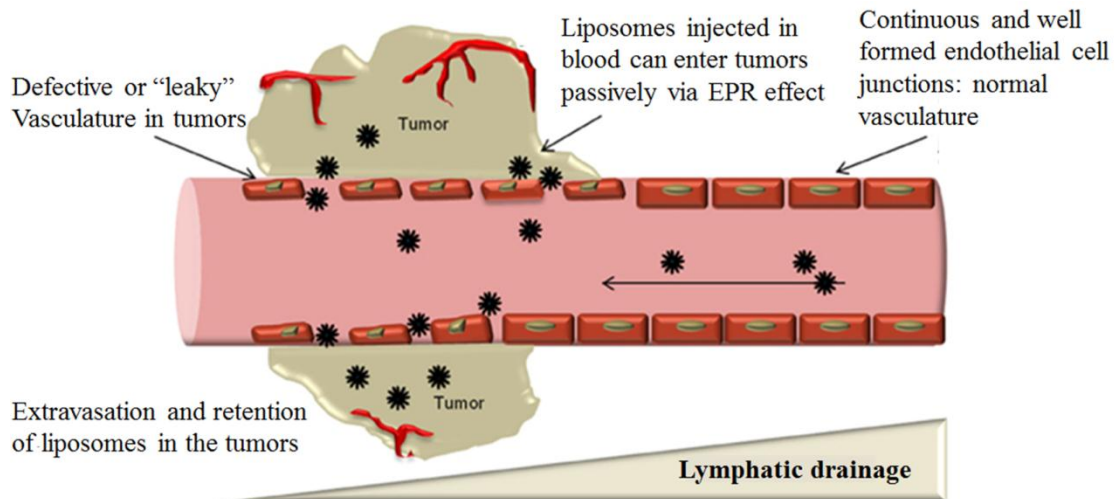
Figure 2.5: Enhanced permeability and retention effect of nanocarriers [37].

Even though EPR is an important breakthrough discovery, the heterogeneous nature of tumors reduces EPR effects. Additionally, some tumors have less vascular density leading to less EPR effect (pancreas and prostate). Measures suggested to enhance the EPR effect include raising the systemic blood pressure, increasing nitrogen oxide (NO) concentration utilizing NO-releasing agents, and increasing kinin (bradykinin) concentration using ACE inhibitors [35].

In order for the penetrated materials to accumulate, they need to escape clearance. This happens as a result of functional defectiveness of the lymphatic system that usually removes foreign particles from the interstitial space [23].

2.2.3. Active targeting. As passive targeting provided a novel approach to cancer treatment, it does not exclusively target tumors, as inflammation also exhibits EPR effects. Additionally, it does not guarantee intracellular uptake of the drug. Moreover, the issue of molecules diffusing back to the bloodstream is considered another drawback. So, it has become clear that relying on EPR effects alone for targeting is not adequate.

One way to achieve more selective cancer treatment is through the development of liposomes to target specific receptors expressed on the surface of cancer cells. Receptors are proteins on cells surfaces that help regulate cells processes. They are vastly more over-expressed on cancer cells than healthy ones. Normal targets include receptors that play a role in cell growth and survival. Each receptor binds to its specific ligand. Ligands are signaling molecules that transmit information between cells. They include ions, hormones, neurotransmitters, peptides, growth factors, proteins, and antibodies [4]. Attaching these ligands on liposomes surface enhances targeting toward cancer cells and can also increase cellular uptake of the liposome, if the receptor can internalize its ligand by receptor-mediated endocytosis.

After EPR effects lead liposomes close enough to the affinity of the tumor tissue, the conjugated ligand on the surface of the liposome is recognized by its receptor on the cancer cell surface, leading to more efficient targeting, as can be seen in Figure 2.6. This, of course, is based on the prolonged circulation time and controlled slow release that liposomes already exhibit [23].
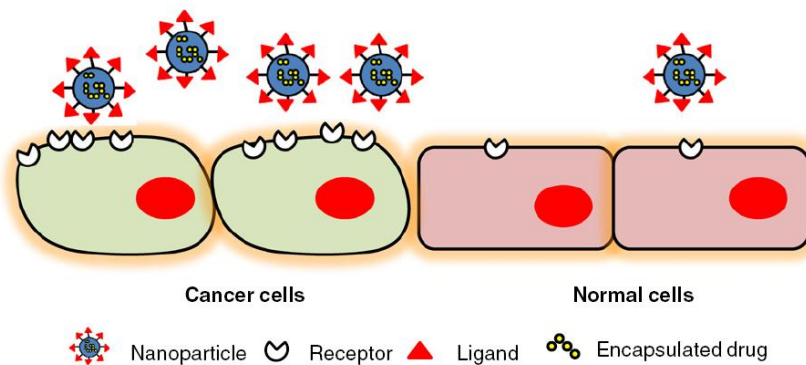
Figure 2.6: Active targeting of liposomes to cancer cells surface [42].

Generally, most cancers over-express VEGF receptors, integrins, and vascular cell adhesion molecules which are all related to cancer angiogenesis. Folate receptors were also known to be extensively over-expressed in many tumors such as lung, brain, breast, kidney, and ovary cancers, in order to improve their growth [32]. Other cell division receptors are human epidermal receptors (HER) family including EGF receptors (HER1) that are commonly found in multiple cancer types such as head and neck, bladder ovarian, cervical, and oesophageal cancer [43]. Also, the transferrin

receptors are of importance in cell division. Hence they are generally over-expressed in multiple tumors including brain capillary endothelial cells [23].

Some cancers overexpress receptors that are specific to the type of the tumor, and these depend on the malignancy, location, and stage of the tumor. They have been extensively reviewed for breast cancer earlier in this thesis in section 2.1.2. Ligands used in ligand-targeted drug delivery include glycoconjugate, oligopeptide, nucleic acids, aptamers, carbohydrates, vitamins, whole proteins, peptides, and antibodies and antibody fragments against tumor markers [32, 44].

2.2.3.1 *Ligands for targeting.* Ligands for targeting include:

2.2.3.1.1   Folate receptor targeting ligands. It was reported that the attachment of folic acid to micelles (in the PEG copolymer side) entrapping doxorubicin significantly increased cellular uptake of the drug than those which are folate unconjugated micelles against KB cells over-expressing folate receptors [45]. It was also reported in another study that FA-PEG-liposomes exhibited much greater cellular uptake [44]. In another study, folate-PEG-cholesterol liposomes showed 38 times more toxicity compared to non-targeted liposomes towards KB cells [46].

2.2.3.1.2   Transferrin receptor targeting ligands. It was shown that coupling PEG end of Doxorubicin-loaded liposomes to transferrin significantly increased the cellular uptake of the glioma cell line in vitro [47]. It was also observed that OX26 monoclonal antibody (mAb) could be used to better target liposomes towards the transferrin receptor when attached to the distal end of the PEG molecules conjugated to the surface and coating the liposomes [48].

2.2.3.1.3   EGFR targeting ligands. EGFR has various ligands; they include EGF, antibodies, antibodies fragments, aptamers, and EGFR-specific low-molecular-weight peptides. FDA approved antibodies with affinity to EGFR, such as Trastuzumab, and the chimeric monoclonal antibody, cetuximab. Peptides used for EGFR targeting include D4 and GE1. Anti-EGFR aptamers, a class of functional oligonucleotides similar to the antibodies in their binding affinity, have been successfully used to specifically deliver gold nanoparticles to EGFR [49].

2.2.3.1.4   Antibodies as targeting ligands. Liposomes that have monoclonal antibodies or antibody fragments conjugated to their surface are called

immunoliposomes. Antibodies can identify antigens overexpressed on the targeted cells surface. Each Antibody binds to a specific antigen, making it possible to selectively target that cell, hence avoiding undesired interactions with healthy cells [20]. Some tumors are highly immunogenic, and some are not. The presence and the type of antigen vary from one type of malignancy to another, which eventually affects the efficacy of the immunoliposomal therapy [29]. Potential highly investigated targets for antibodies include VEGFR, EGFR, HER2, transferrin receptors, and prostate-specific membrane antigen (PSMA) [50].

HER2 receptors have the ability to internalize their ligands resulting in the endocytosis of the antibody-mediated nanoparticles. A known humanized monoclonal antibody targeting HER2 is the Trastuzumab, which is already approved by the FDA to be used in immunotherapy. Nanoparticles coupled with Trastuzumab have been intensively investigated for HER2 positive breast cancer. Another known chimeric monoclonal antibody is the Cetuximab which has a high affinity towards the EGF receptor. Cetuximab-targeted gold nanoparticles were investigated for delivery of chemotherapeutics to many cancers including pancreatic and colorectal carcinoma, and results showed significant tumor growth inhibition. Cetuximab immunomicelles were suggested as delivering vehicles for doxorubicin agent, as well as immunoliposomes conjugated with cetuximab to deliver boron in glioma cells overexpressing EGF receptors. Anti-transferrin receptor antibodies include OX26 and R17217 monoclonal antibodies. Also, antibodies for Prostate‑specific membrane antigen (PSMA) include J591 monoclonal antibodies. Recently in 2005, Bevacizimab (Avastin) was successfully implemented in combination with chemotherapy in the treatment of metastatic breast cancer, in which it was targeted against VEGFR overexpressed as a result of angiogenesis [15]. Lastly, rituximab, an anti-CD20 monoclonal antibody is used as a conjugate in nanoparticles to target lymphoma tumors overexpressing CD20 receptors. CD20 receptors do not internalize their Anti-CD20 monoclonal Antibodies contrast to CD19 receptors [50, 51].

2.2.3.1.5 Antibody fragments. Due to the large size of monoclonal antibodies which could pose an obstacle for intracellular drug delivery, antibody fragments were suggested because of their small size and similar affinity to their corresponding antigens as whole antibodies do. Antibody fragments used in nanomedicine include single-chain variable fragments (scFV) and antigen-binding

fragments (Fab). Nanocarriers decorated with antibody fragments exhibit reduced clearance by the RES. Also, their small size allows for better penetration. scFV that bind specifically to an isoform of fibronectin was found to enhance the targeting ability of liposomes. Also, scFV-CM6 was found to bind specifically to a protein extensively overexpressed on surfaces of tumor cells (TEM1) and was used successfully in making immunoliposomes. It was also reported that efficient internalization was shown when liposomes were conjugated with single-chain anti-EGFR antibody. Additionally, some antigen-binding fragments (Fabs) of monoclonal antibodies were successfully used as conjugates to liposomes. These include Fabs targeting β_1 integrins that are overexpressed in lung cancer and Fab of the mAb anti-GD(2) that targets disialoganglioside which is overexpressed on the surface of neuroblastoma cells. Also, human B-cell lymphoma was targeted using immunoliposomes conjugated with mAb anti-CD19 or its Fab fragments. Finally, Fab fragments of Trastuzumab were used to target HER2 overexpressing breast cancer cell lines. Results in vitro showed increased cytotoxicity, and in vivo showed enhanced tumor growth inhibition [50].

2.2.4. Monoclonal antibodies and immunogenicity of tumors. An antigen is any molecule that can interact with an antibody, and its binding site is called epitope. An antigen can be a cell receptor, a peptide, a lipid, a carbohydrate, a nucleic acid, or any other molecule. Any substance that can induce an immune system response is defined as immunogenic. All immunogens are antigens, but not all antigens are immunogens (they also include allergens and tolerogens). Depending on the immunogen size, chemical composition, conformation, and its ―foreignness", it has the ability to provoke an immune response [52].

Some antigens that are marked ―self" do not stimulate an immune response; these are normally expressed on normal, healthy cells. But mutations in cancer cells result in either altering these proteins making them more foreign or overexpressing them. Both cases should lead to an immune response [18].

Antibodies are naturally produced by B-cells as a response to the antigen representation by helper T-cells. Antibodies belong to proteins of the blood called immunoglubins. They are classified into five different classes; IgM, IgD, IgG, IgA, and IgE. Each class has a similar component in its structure, and a small variable

fragment (Fv) part, the N-terminal (amino-terminal) domains, which is found in the antigen binding fragment (Fab). That variable fragment is unique for each antigen-antibody binding [53, 54]. Antibodies consist of dual heavy and light chains joined by disulfide bonds with an average molecular weight of 150 kDa [55].

Monoclonal antibodies are antibodies produced in a laboratory by culturing antibody-producing cells. Their production depends on immunizing a mouse with a pathogen or any other immunogenic substance. Normally, these complex antigens have many antigenic sites which result in the production of various antibodies in the bloodstream for that one complex antigen. Each antibody is produced by a specific antibody-producing cell in the spleen. Köhler and C. Milstein have taken antibody-producing spleen cells and fused them with immortal myeloma cells to have hybrid cells that contain both immortal properties and antibody secreting ability of parent cells. These can then produce polyclonal antibodies. Each hydridoma is then cultured individually to produce separated clones that secrete one specific type of antibodies, called monoclonal antibodies. By using monoclonal antibodies, we can ensure the precise binding to only one antigenic site of the tumor, and not worry about whether or not it will affect other targets [56].

Monoclonal antibodies can be used as homing devices to guide nanocarriers to tumor targets (receptors) and hook with them, or in immunotherapy to interfere with cell signals and specific molecules functions that are necessary for tumor growth and angiogenesis as previously discussed in targeted therapy section 2.1.3.2 [57].

Limitations to monoclonal antibodies include expensive production, immunogenicity, and limited conjugation density on nanocarriers due to their large size [49]. Also, mouse-derived antibodies were shown to induce some allergic-like reactions when used in humans, which raised the need for creating chimeric, or humanized murine-derived antibodies, or fully human monoclonal antibodies [56]. Chimeric monoclonal antibodies are considered less compatible with humans than humanized ones; they have the variable fragment from a murine source and the constant region from a human. While humanized monoclonal antibodies have only the complementary determining regions of the variable regions (CDRs) from a murine source, fully human monoclonal antibodies are developed using phage-display

technologies. Usually, fragments of antibodies display less immunogenicity and are considered a good approach when it comes to nano-medicine [55, 58].

Modifications to mAbs are needed for conjugation purposes. Sites for chemical binding in antibodies, and proteins, in general, include thiol groups (sulfhydryl groups) that are found in cysteine residue of the protein, amine groups that are located in the lysine residue, and carbohydrates. Usually, sulfhydryl bonds in proteins are found in their reduced version as disulfide bonds (in cystine), which first need to be activated into a free thiol group in order for the conjugation to be successful. These modifications are known to affect the antigen-antibody binding sites except for the carbohydrate modification. For disulfide modification at low pH, damage control can be achieved [55, 59].

Trastuzumab is used in this work. Trastuzumab, also called Herceptin, is a humanized IgG(1) kappa monoclonal antibody (145.5 kDa) with high and specific affinity towards the HER2 receptor overexpressed in breast tumor cells [41, 60]. Trastuzumab can prevent HER2 hetero-dimerization and stop cells signaling related to tumor development, so it is considered HER2 receptor antagonist. This is why it has been approved by the FDA to be used in immunotherapy, as previously mentioned. Trastuzumab showed to reduce the risk of recurrence when used as adjuvant therapy and was also shown to augment the effects of chemotherapy. It is commonly used in combination with Paclitaxel, Docetaxel, Navelbine, Gemcitabine, and Capecitabine in Antibody drug conjugates (ADCs). Pertuzumab is another monoclonal antibody specific to HER2 but binds to a different epitope than Trastuzumab [13, 60].

2.3. Ultrasound as a Trigger for Liposomes Drug Release

Triggering mechanisms allow controlling the release at tumor sites, resulting in dismissing side effects on healthy cells, while avoiding inducing drug resistance that is due to long accumulation time. They also facilitate penetration into the tumor, and endosomal release [41]. Releasing the drug too early or too fast results in damaging healthy cells, while releasing the drug too slow or too late won't allow for the concentration to reach the cytotoxic dose, thus a controlled release is needed. Once the drug-loaded nanocarriers reach the tumor site, spatial and temporal controlled release can be obtained by applying ultrasound. Ultrasound is widely used as a mechanism for triggered release due to its low cost, safety, and focused feature.

Ultrasound also has a synergetic effect when used with chemotherapy, and hence it will be used as a triggering mechanism in this work [24].

Ultrasound is a cyclic sinusoidal acoustic wave that has high-pressure phases (compression) at the upper peaks and low-pressure phases (refraction) at the lower peaks. It propagates through the medium, by transferring energy through the oscillation of particles, thus it propagates faster in solids than in fluids. Ultrasound waves are just like any other waves with frequency, wavelength, amplitude, speed, and attenuation. The ultrasound frequency ranges are above the human hearing range (20 kHz) [24]. Attenuation is the loss of intensity as the wave travels through some medium, where energy is lost either by absorption or transformed to other forms [61].

Parameters of ultrasound that are of importance in US-triggered drug release include its frequency, intensity (power density), and mode of operation.

Low-frequency ultrasound (LFUS) which is generally less than 1 MHz is applied to trigger drugs release. High-frequency ultrasound (> 5 MHz) is used in diagnostic imaging in medicine. Generally, it is known that as the frequency of the applied ultrasound increases, less penetration into tissue occurs. It is noteworthy to mention that several studies reported drug release at low frequencies but not at high ones. This was explained by the fact that at low frequencies cavitation increases [24].

Ultrasound intensity is the energy carried per cross-sectional area of the applied beam. Several studies report a proportional relationship between drug release and ultrasound power intensity. Low-intensity ultrasound usually does not induce hyperthermia in contrast to high-intensity ultrasound (HIUS) that is frequently used as a treatment of cancer in hyperthermia treatment. As previously described, elevated temperatures have the ability to damage cells.

The mode of continuously applying ultrasound has been used in triggered therapy as well as the discontinuous mode (pulsed mode), where ultrasound has on and off periods for specific periods.

To understand ultrasound mechanism in triggering drug release from nanocarriers, first, we need to understand its effects and interactions with surrounding substances. Ultrasound has thermal effects and non-thermal effects (mechanical

effects). Thermal effects (hyperthermia) previously described are the result of energy dissipation of HIUS into thermal heat rising tissue temperature.

Mechanical effects result from the acoustic wave propagation and pressure variations. One such effect is acoustic cavitation, which is the formation of gas bubbles in a liquid, due to changes in pressure. Cavitation depends on the intensity of the US, and it only occurs at a certain threshold. At low-pressure amplitude, the gas bubbles exhibit stable oscillation, in which they contract and expand slightly. This is referred to as stable cavitation. On the other hand, inertial cavitation results from high-pressure amplitude that leads to gas bubble collapse. The bubbles increase rapidly in size until they reach their resonant size, at which they collapse resulting in high pressure and temperature, a sonic jet of fluid (near solid surfaces) that damages nearby cells, shock waves that shear open the cells, and the formation of new small bubbles that reinitiate the cycle. Stable and inertial cavitation can occur in the same situation following each other; they are not separate phenomena. Another mechanical effect is acoustic streaming which is a direct result of the ultrasound wave propagation through some medium. In acoustic streaming, particles move in the direction of the flow, resulting in micro-streaming, bulk-streaming or both. The latter is considered a powerful mechanism that facilitates the delivery and distribution of drugs [23].

An important acoustic parameter is the mechanical index (MI), which is the probability of collapse cavitation to happen.

In triggered drug delivery, the aim is to find the optimum ultrasound parameters that permit enhanced drug delivery without harming healthy cells. This could be better achieved if we understood the mechanism by which enhanced triggered delivery works. Several mechanisms that could be the cause of successful triggered drug delivery were suggested. They are as follows: disruption of the drug nanocarriers, enhancement of drug distribution in tumor tissue, enhanced intracellular drug uptake by endocytosis, and increased cellular uptake of the nanocarriers by enhancing the cell permeability.

The first suggested mechanism states that shear stress resulting from both wave pressures and cavitation can lead to disruption of the nanocarriers membrane. Ruptures resulting from cavitation are particularly important for site triggered drug

delivery to avoid drug release near healthy cells. In the second mechanism, micro-streaming is thought to enhance the distribution of the encapsulated drug by diffusion through the tumor tissue. Moreover, cavitation has an enhancement effect on the motion of the fluid near the tumor cells, in which drug dispersion occurs. Gas bubbles of the cavitation phenomenon can pull denser materials (nanocarriers for example) towards them, resulting in their rupture. In the third mechanism, the uptake of micelles into tumor cells was reported in several studies, suggesting nonspecific endocytosis. Lastly, cell membrane permeability is a direct result of events resulting from cavitation. Shock waves, sonic jets, and micro-streaming induce pore formation on cells membranes and thus facilitate the drug uptake into cells [23].

Liposomes can be modified to be more sensitive to ultrasound. Echogenic liposomes are rendered sensitive to ultrasound by entrapping gas into their core, thus releasing their contents as soon as ultrasound is applied. eLiposomes contain nanoemulsions that change phase from liquid to gas in response to ultrasound, thus leading to subsequent drug release [23].

2.4.   Controlled Release and Modeling Kinetics

Controlled release became a vital part of the modern therapeutic treatment. Its concept is that an initial large dose of the drug is needed, to be followed by a slower release to maintain the drug therapeutic level as long as possible. Control release is needed since some drugs leak too fast from liposomes, before getting to the tumor, and others too slow that the therapeutic effect ca not take place [62].

Controlled release aims to reduce the frequency of the treatment and increase the patients comfort level [63]. It has also brought engineers and scientists in the medical field together to optimize dosing and drug delivery mechanisms. For this purpose, modeling is needed in the optimizing stage, where the patterns of the release can be predicted without the need for unnecessary studies. It may also provide some insight into the mechanisms by which the drug is released and some other physical aspects as well [64]. Several release mechanisms are common; they include but are not limited to: release by drug diffusion through the polymer membrane, or by the degradation of the polymer, or by chemical disassociation of the drug [65, 66].

The kinetics of drug release of liposomes in Phosphate-buffered saline can give an idea about the release behavior in vivo, thus reducing studies done in vivo.

Models describing drug dissolution differ based on their assumptions, but they can be categorized as follows: slow zero order, first order, and ones that start rapidly and then reduce to either of the previously mentioned types [67]. Kinetics are influenced by the type of drug, particle size, solubility, and the amount used. Nine models are used in this thesis to discuss the release kinetics of the model drug calcein under low-frequency ultrasound [68].

2.5. Literature Review

2.5.1. Relevant studies on breast cancer using immunoliposomes targeted towards HER2.
A study of doxorubicin-loaded immunoliposomes (ILs) was conducted in vitro and in vivo. Sterically stabilized liposomes (70-100 nm in diameter) were conjugated to anti-HER2 mAb fragments. Delivery of these immunoliposomes into HER2 overexpressing cells resulted in intracellular uptake of 600 times higher than non-targeted stealth liposomes, but they exhibited similar uptake in non-HER2 overexpressing cells, which demonstrates the effectiveness of targeting moiety. Also, ILs exhibited 700 times more accumulation in targeted tissue than in negative cells. In vivo studies conducted on xenograft that overexpresses HER2, reported that ILs loaded with doxorubicin yielded improved anti-tumor activity in contrast to all other treatment options used which included: free Dox, free mAb (Trastuzumab), liposomal Dox, free Dox conjugated to the mAb, and liposomal Dox linked to Trastuzumab. However, tumor tissue levels of ILs and liposomes were the same, but ILs exhibited intracellular uptake opposite to non-targeted liposomes that accumulated in the tumor stroma, which resulted in 10-30 times higher cytotoxicity. It was also repeated that the administration of ILs did not increase clearance, hence showing that anti-HER2 mAb fragments did not affect the stabilization or the non-immunogenicity of sterically stabilized liposomes [69].

Another study investigated the effect of using immunoliposomes (140 nm in diameter) conjugated with Trastuzumab mAb to deliver both Paclitaxel (PTX) and Rapamycin (RAP) therapeutic drugs into 4T1 cells that are triple negative breast cancer cells and SKBR3 cells which are HER2 positive breast cancer cells. The encapsulation efficiency was about 56% and 70% for PTX and RAP respectively, and the conjugation of Trastuzumab was above 70% using a thioether bond. Results in cell studies showed increased cytotoxicity of SKBR3 cells for the ILs compared to the

control liposomes (non-targeted liposomes). This was believed to be a result of the enhanced uptake mediated by the mAb bound to the HER2 on the cells. The in vivo study investigated the immunoliposomes co-loaded with both drugs, control liposomes, and solution of PTX/RAP against human xenograft HER2 overexpressing tumors. Immunoliposomes showed better anti-tumor growth activity. It is noteworthy that that RAP can increase PTX induced apoptosis, hence produce synergetic effects in the presence of Trastuzumab [70].

It is worth mentioning that the stability of actively targeted liposomes is not affected much in circulating conditions. A study demonstrated that liposomes in circulating conditions leaked 20% of their contents after 5 hours and 42% after 8 hours. Liposomes in cell culture conditions leaked 5% after 5 hours and 9% after 8 hours. This is still a long circulation time, and liposomes are considered stable in circulating conditions in times up to 8 hours [71].

2.5.2. Antibody conjugation methods related studies. Attachment methods of targeting ligands to liposomes include covalent and non-covalent bonds. The attachment done to the distal ends of the PEG-PE anchor was found more efficient than linking directly to the surface of the liposome. The approach of conjugating the ligand to liposomes after their synthesis was considered better than linking them to lipids prior to liposomes synthesis [72].

Types of linkages used in the conjugation methods include thioether bonds, disulfide bond, amide bonds, Hydrazide bonds, and crosslinking primary amines. All these methods have been extensively reviewed and compared in literature [59, 70, 72-80]

A study demonstrated that ILs-PEG-mAb linkage displayed increased binding, but reduced internalization compared to ILs-mAb linkage (but still contains PEG on their surface parallel to the mAbs). Attaching the mAbs to distal ends (ILs-PEG-mAb) showed that binding was independent of the PEG density. Additionally, they showed that increasing mAb density on immunoliposomes enhanced binding and internalization. A conjugation efficiency of 70-90% resulted using a thioether covalent bond in conjugation [69].

Also, in agreement with the previous study, stealth immunoliposomes were prepared with Trastuzumab Fab conjugated to the surface for one approach and

conjugated to the distal ends of PEG chain for another approach; both in which they used thioether bonds. Increasing PEG density decreased the binding with the first approach but did not affect the second approach. Also, it is noteworthy that binding and internalization was much higher in HER2 positive cells than in negative ones for both approaches [80].

Some studies, concerned with the binding strategies of the antibodies to liposomes, mentioned that using a thioether bond in which the liposomes were thiolated instead of the antibodies had more advantages in controlling side reactions and drug loading methods [78, 81]. But in literature, this method applied directly to liposomes surface was reported to have less efficiency and was not used much like the one where antibodies were thiolated and liposomes were maleimided [72]. When the attachment was done directly to the stealth liposomes surface, the PEG polymer affected its efficiency by hindering the antibodies away from the surface. So, in this study, they coupled the distal ends of the polymer, and they got high conjugation efficiencies.

Thioether bonds require pre-derivatization of both liposomes and antibodies, which is considerably complicated and not feasible when the antibody is especially expensive.

A new simple and more efficient approach was introduced by Bendas and co-workers, where they use Cyanuric chloride as a linkage between the PEG distal end and the antibody to prepare immunoliposomes [34]. This method required no prior derivatization to the antibody and no extra chemicals as well [82]. Binding efficiency for the immunoliposomes was also established which means no harm was done to the binding site. Immunoliposomes stability was also confirmed [34]. R.R. Hood used Cyanuric linkage to form immunoliposomes in a continues process [83]. Cyanuric chloride was also used to bind DNA to beads [84]. This is why this method is used in this thesis to bind Trastuzumab to liposomes.

2.5.3. Studies including ultrasound triggered drug delivery. Ultrasound release is studied under the effect of frequency and power density when the liposomes nature is not changing. The liposomes parameters affecting ultrasound are lipid ratio, surface charge, and PEG polymer density.

In one study, calcein (a model drug) release from liposomes was reported to be higher at LFUS than at HFUS. The amount released increased with increasing exposure time and the mechanical index. It was suggested that enhanced release was due to mechanical effects rather than thermal effects [85].

The dependency of the release on the liposome membrane structure was studied in dox-loaded liposomes under LFUS effects. Results showed 30% higher release using DOPE based liposomes than DSPE based liposomes. This showed that DOPE-based liposomes are sonosensitive lipids [86].

It was reported that PEGylated liposomes showed 10-fold more permealization upon exposure to LFUS than the control non-PEGylated liposomes. This is because of the absorption of energy by the PEG groups which are considered sonosensitive [87].

In targeted therapy, the effect of targeting moiety was studied. It was reported that estrone-targeted calcein-loaded immunoliposomes upon exposure to LFUS exhibited higher initial release rates than the non-targeted ones, but the same final release rate for both liposomes types [25].

Chapter 3. Materials and Methods

In this work, sterically stabilized liposomes with functional groups at their ends are synthesized, using a mixture of lipids. The functional group is related to the type of linkage used, and it is placed at the end of the PEG chain on the liposomal surface, hence the ligand will be attached to the distal end of this chain, after the formation of liposomes. Briefly, lipids are first dissolved in an organic solvent, then dried until a lipid film forms. After that, it is hydrated with a suitable material (distilled water or the encapsulating material), which leads to the formation of MLVs liposomes. In order to convert it to ULVs, several techniques for applying mechanical stresses could be used including sonication or extrusion. Finally, the liposomes should be purified to get rid of unreacted substances and formed micelles, by gel chromatography, based on size (micelles and other molecules are very small compared to liposomes). This yields the control liposomes [30, 88]. For the actively-targeted liposomes, one more step is needed to attach the antibody to the functional groups at the distal ends by a suitable reaction depending on the type of bond. This work is done following Bendas Work [34, 83].

For simple, fast, and clean ligand binding, Cyanuric chloride-PEG-liposomes are used, with Cyanuric chloride being the functional group. This reaction does not damage the antigen binding site on the antibody, thus does not prevent their specific activity. The process includes non-toxic materials, and it doesn't require the pre-modification of the monoclonal antibody [34].

Attaching the antibodies to the liposomes directly can prevent their activity and also increase their clearance by the reticulo endothelial system (RES), but conjugating them to the distal ends of PEG chains yields long-circulating, fully functioning immunoliposomes. Sometimes, it can also enhance the binding efficiency of the ligand to the liposome [76].

The choice of saturated phospholipids in this work (DPPC and DSPE) was made to avoid chemical degradation, and more precisely, to avoid oxidation which could lead to an increase in the permeability of the bilayers. Oxidation can also be minimized using high-quality lipids and avoiding high temperatures [30].

The choice of the buffer used, the pH, the temperature, and the charge of the liposome can affect the hydrolysis of the phospholipids [30].

The choice of the lipid:cholesterol molar ratio was based on the stability of the liposomes. Basically, the addition of cholesterol to saturated lipids (used in this work) increases their fluidity (in contrast to unsaturated lipids), and thus all the gaps that are formed in the lipid bilayers due to the trigger will reclose immediately, which is unwanted. But the addition of cholesterol aims to reduce the phase transition temperature of the lipid mixture [89].

The choice of PEGyhlated lipid to non-PEGylated one was made to control aggregation, which should be below 6% [59, 76].

The choice of PEG chain length was based on the fact that too long chains can prevent the target binding of immunoliposomes [76].

The protein density should approximately be 7.5-30 molecules per liposome vesicle to yield a strong affinity towards its target [41, 90].

The gel-liquid crystalline phase transition temperature (T_m) of DPPC bilayer is 41 ºC, while it is 74 ºC for DSPE, so the operating temperature for the preparation of liposomes was chosen to be around 60 ºC [91]. This is reasonable because the resulting lipid transition temperature ranges from 41 Cº for pure DPPC to 43 Cº for 15% DSPE–PEG(2000) lipid mixture, and the cholesterol helps to lower the transition temperature as well [92].

Finally, for calcein release experiments, a fluorescence marker was used as a model drug instead of doxorubicin because the latter is highly toxic and significantly more expensive. Also, calcein is generally used to model hydrophilic drugs, and it is easily dissolved in the lipid solution after adjusting the buffer pH [93, 94].

Some of the materials used in this work and their properties are listed in Table 3.1.

3.1. Materials

The Dipalmitoylphosphatidyl choline (DPPC) and 1,2-distearoyl-sn-glycero-3-phosphoethanolamine-N-[amino(polyethylene glycol)-2000] (DSPE-PEG(2000)-NH2) were obtained from Avanti Polar Lipids Inc. (Alabaster, AL, USA). Calcein disodium salt, and the bicinchoninic acid (BCA) kit were obtained from Sigma-

Aldrich Chemie GmbH (Munich, Germany). Cholesterol was obtained from AlfaAesar (Ward Hill, MA, USA). Chloroform was obtained from Panreac Quimica S.A. (Spain). Sephadex G-100 and Sephacryl S200 HR were obtained from Sigma-Aldrich (Sweden). Trastuzumab was obtained from a local pharmacy. Cyanuric chloride (C.C.) was a generous donation from the chemistry department at the American University of Sharjah.

Table β.1: Properties of the materials used in the synthetic process.

Material/properties	Molecular weight (g/mole)	Transition temperature (ºC)
DPPC	734.039 [95]	41 [91]
DSPE	748.08 [96]	74 [97]
DSPE-PEG (2000)-NH2	2790.486 [98]	-
cholesterol	386.65	-
Trastuzumab	145531.5 [41]	-

3.2. Methodology

3.2.1. Preparation of DSPE-PEG-NH$_2$ control liposomes. Liposomes were prepared using cholesterol, DPPC, and DSPE-PEG (2000)-NH$_2$ at molar ratios of 30:65:5, respectively. The materials were dissolved in 4 ml chloroform to a final concentration of around 10 mg lipid/ml solvent (normal values range from 5-20 mg/ml) in a round-bottom flask at 60 ºC. Then chloroform was dried in a rotary evaporator under vacuum for 15 minutes, until a thin film was observed on the walls. After that, the lipid film was hydrated using 2 ml of 30 mM calcein solution and the pH adjusted to 7.4. Then the solution was sonicated at 40-kHz using 100% power for 15 minutes in a sonicator bath (Elma D-78224, Melrose Park, IL, USA). The liposomal solution was then extruded three times using 200-nm polycarbonate filters (Avanti Polar Lipids, Inc., Alabaster, AL, USA). Lastly, for the removal of free calcein and spontaneously formed micelles, purification using size exclusion chromatography on a Sephadex G-100 column was performed, after equilibrating it

with borate buffer pH 8.5. All of the previous steps were performed at 60 ºC; above the transition temperature of the lipid. Finally, dense liposome fractions were collected and both were used to prepare immunoliposomes or stored at 4 ºC after changing their buffer to PBS pH 7.4.

3.2.2. Preparation of sterically stabilized immunoliposomes with antibody-PEG linkage. This is done in two steps; first modifying the liposomes with Cyanuric Chloride (C.C.), and then adding the antibody at a pH 8.5 to be linked to the Cyanuric Chloride. This can be summarized in Figure 3.1.
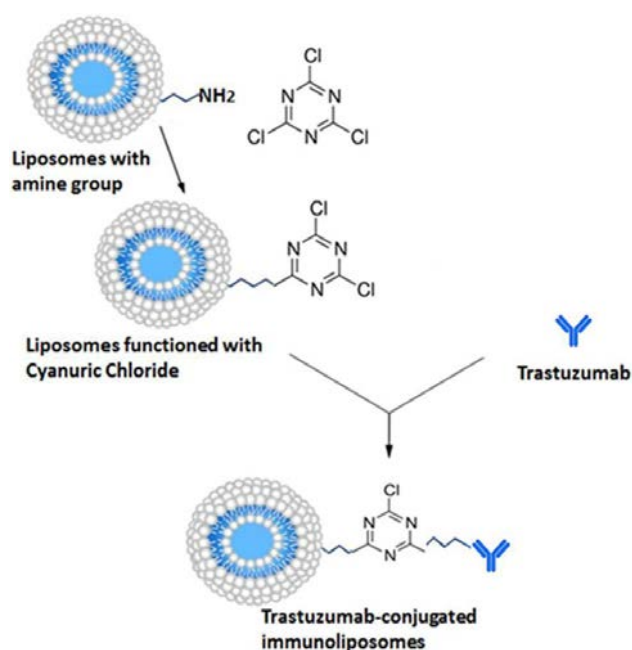

Figure β.1: Preparation of immunoliposomes using cyanuric chloride.

Liposomes previously made were used here. All the steps were done in an ice bath. First, Cyanuric chloride was dissolved in acetone to make a 10 (mg/ml) solution. Then, 9.23 (µl) of that solution was diluted in 0.5 (ml) di-ionized water, because alcohol hurt liposomes. This amount was added to 1 (ml) liposomes solution, to achieve 1:1 molar ratio of Cyanuric Chloride to DSPE-PEG-NH2 respectively. The reaction at pH 8.5 and 0 Cº was stirred for 3 hours to allow for the nucleophilic substitution of chloride particle on the Cyanuric Chloride with the proton on the NH2 group on liposomes. Then after that, Trastuzumab was added in excess amounts (1 mg) after being dissolved in 0.5 ml borate buffer (pH 8.5). This reaction was kept

stirring overnight to allow to reach completion, where the N-terminus on amino acids of the Trastuzumab were linked to Cyanuric Chloride. Finally, the excess Trastuzumab and any free calcein were purified in a Sephacryl S-200 HR column equilibrated with PBS (7.4 pH) and eluted with PBS (pH 7.4) [34, 83]. The liposomes are collected and stored at 4 ºC until use.

3.3. Characterization of Liposomes

3.3.1. Liposomes size using dynamic light scattering. Size distribution is a fundamentally important property when dealing with drug carriers, commonly determined either by dynamic light scattering (DLS), electron microscopy, or right-angle light scattering and turbidity.

In this work, the liposome size distribution will be determined at room temperature by DLS using DynaPro® NanoStar™ model from Wyatt Technology Corp. (Santa Barbara, CA, USA). Viscosity and concentration of liposomes are important parameters and will be measured considering a medium viscosity of 1.020 and medium refractive index of 1.333. First, the samples are diluted with PBS pH 7.4 and filtered using 450-nm PVDF disk filters, then placed inside the machine for analysis, where a laser is directed toward the sample. The way it works by detecting fluctuations in the intensity of the light scattered, due to movement of particles. This intensity differs for large particles compared to smaller ones, and based on a previous calibration process, measurements of size distribution can be obtained. Acceptable readings correspond to <20% poly dispersity (PD) and the relatively low sum of squares (SOS), which are all shown on the software used.

Data obtained from the software will be analyzed using two fits: cumulant and regularization. Cumulant fit analysis assumes the presence of one model, i.e. a uniform size distribution, however, we anticipate that this will not be the case. We need to confirm that only liposomes exist and not micelles or other impurities. Therefore, the regularization fit will be used, and the particles will be assumed to behave as multimodal particles distribution.

3.3.2. Liposomes concentration quantification. A rapid method to detect phospholipids was presented by Stewart in 1980 [99]. It is based on complex formation between ammonium ferrothiocyanate and phospholipids, which can be

detectable in spectra at 485 nm. The solution is insoluble in chloroform, whereas the phospholipids are. Mixing the two and separating the phases will result in a lower layer of chloroform in which the complex formed is dissolved in, and an upper layer of the remaining solution is formed. Detecting the spectra absorption of the lower layer, after separation, will indicate the phospholipids concentration in the sample. The assay is sensitive to small amounts down to 0.01 mg lipids in 2 ml chloroform (0.005-0.05 mg/ml) [99]. Diluted samples can be used if needed and then the results can be adjusted with the dilution factor.

A calibration curve for the DPPC was prepared with increasing concentrations from 0.0025 (mg/ml) to 0.025 (mg/ml). The liposomes samples were dried in vacuum and then dissolved in chloroform, with a dilution factor of 20. Then the solution was sonicated to properly dissolve and break the liposomes to its constituent lipids. Six replicates were made by adding specific amounts to 2 ml ammonium ferrothiocyanate. Then the mixtures were vortexed for 20 seconds for proper mixing. After that, they were centrifuged to separate the chloroform layer. Finally, the light absorption at 485 nm was read using a spectrofluorometer and results were used to calculate the DPPC concentration in each sample. An average of the six measurements was taken.

Liposomes are formed mainly by DPPC, so the amount of the NH2-PEG-DSPE lipids was safely neglected.

3.3.3. Antibody conjugation confirmation using BCA assay. Protein conjugation efficiency is normally determined by the BCA assay (Smith assay), Lowry protein assay, Bradford protein assay (spectroscopic analytical procedure) or biuret test. Compared to Lawry assay, the BCA was found more straightforward and allowed for more flexibilities. And it was found more objective than the Bradford assay since, at higher temperature, peptide bonds begin to take part in the reactions [100].

The science behind it follows a two-step reaction. The first is the reduction of copper Cu^{2+} to Cu^{1+} upon interacting with amino acids and peptide bonds. The second is a change in color from green to purple upon interacting with BCA reagent. This purple colored complex highly absorbs light at 562 nm. Reduced copper is proportional to the amount of protein in the sample [101].

Using the micro BCA assay in this work, to determine the total protein concentration in a solution, working reagents A, B, and C were added together at molar ratios of 25:25:1, respectively. One milliliter of the resulting solution was added to one milliliter of the buffer (PBS) and 100 µL of the sample (liposomes solution). Then, they were mixed for 30 seconds using the vortex machine, and finally, they were incubated at 60 ºC for 1 hour. A calibration curve to compare the absorption spectra with protein solutions of known concentrations can give direct concentration measurements [102].

Conjugation efficiency can be determined as the ratio of the amount of protein in immunoliposomes after purification to the ones before purification. Sometimes purification is not 100% efficient, so some free antibodies that were not attached can be detected in the assay. To overcome that, control liposomes were prepared by simply mixing them with the antibody without performing the reaction, and then they were purified. The difference in the protein amount between the two samples indicates the number of attached antibodies, not the free ones.

Six replicates per liposome batch were used to confirm the amount attached. The procedure was repeated for three batches of liposomes to confirm the attachment and the consistency of the results.

3.3.3.1 The number of Trastuzumab molecules attached to each liposome vesicle. The number of antibody molecules attached to each liposome was determined assuming an average radius of liposomes of about 100 nm, which indicates that each liposome vesicle have around 80,000 phospholipid molecules [80]. With the knowledge of the molecular weight of Trastuzumab and DPPC, the number of Trastuzumab per vesicle can be calculated after quantifying the protein and lipids amounts using BCA assay and Stewart assay.

3.4. Release Experiments

Generally, calcein release rate is dependent on liposomes composition, fluidity, permeability, and bending elasticity [103] and upon ultrasound triggered drug release, the release is affected by the mode of operation, the power intensity, the duration of the pulse, and liposomes composition, gas encapsulated, and concentration in the sample [93]. Thus, various power densities will be tested to achieve optimal drug release. In literature, the release at LFUS obtained better results than HFUS [85].

One particular study showed release at 20 kHz was superior to 1 MHz and 3 MHz [104]. So only LFUS will be applied to test release kinetics.

3.4.1. Online (continues) release experiments applying LFUS using phosphorescence/fluorescence spectrofluorometer. To trigger the release of the calcein, a model for hydrophilic drugs, from liposomes, 20-kHz LFUS will be used. The amount released will be quantified by fluorescence changes using QuantaMaster QM 30 Phosphorescence Spectrofluorometer (Photon Technology International, Edison NJ, USA). Calcein is a fluorescence molecule and has an excitation and emission wavelengths of about 495 and 515 nm, respectively. It is used as an indicator for the liposomal leakage and drug release as follows: when it is encapsulated in fluorescent quenching concentrations ($\geq$30 mM), no fluorescent can be detected, but upon releasing to the surrounding aqueous solution due to acoustically trigger release, it is diluted and the release can be measured by monitoring the increase in fluorescent. Calcein fluorescence is dependent on pH at acidic conditions (pH<4.5), but independent at pH values ranging between 6.5 and 10 [103]. Release experiments will be conducted at a pH of 7.4.

First, the synthesized liposomes will be diluted using a solution of PBS at a pH of 7.4 in a fluorescence cuvette and placed inside the spectrofluorometer. For ultrasound exposure, 20-kHz ultrasonic probe (model VC130PB, Sonics & Materials Inc., Newtown, CT), will be inserted 2 mm in the cuvette, so it does not cross the path of the emitted light through a special opening in the spectrofluorometer. Then, for data normalization, the initial fluorescence concentration (F_o) will be measured for 60 seconds before sonication. Then, ultrasound will be applied in a pulse mode, with 20 seconds ‒on" and 10 seconds ‒off" periods, until fluorescence concentration plateaus. To normalize release, 2% (w/v) Triton X-100 will be added to achieve a final concentration of 0.48 mM. The surfactant will be used to lyse the liposomes and monitored fluorescence concentration (F_1) to achieve 100% release. This will be repeated for three different power settings (20%, 25% and 30%), corresponding to three different power densities 7.46, 9.85, and 17.31 (mW/cm^2) [105]. Now, to calculate the dimensionless fluorescence concentration at a given time, the following equation will be used:

$$\text{Cumulative fraction of drug released (CFR)} = \frac{F_t - F_0}{F_1 - F_0} \tag{1}$$

The data for three batches of liposomes, with three replicates collected for each run.

3.5. Statistical Analysis

Means and standard deviations of release will be calculated for both control liposomes and the targeted ones. Pairwise comparisons will be performed using ANOVA tests. Based on the assumption that both populations having similar variances, two values will be considered significantly different if $p<0.05$ and if $F<F_{critical}$ (unless otherwise stated).

Chapter 4. Results and Discussion

In this chapter, the conformational results of the synthesis of NH2 liposomes, and immunoliposomes, are presented, providing the BCA assay and Stewart assay results for attachment confirmation, with the DLS results to confirm the successful synthesis of both types of liposomes. In addition, the calcein release data upon the application of ultrasound on both types of liposomes, NH2 liposomes and immunoliposomes, will be shown and compared. Finally, the release kinetics will be modeled using nine different nine models, in which the best one will be further discussed.

4.1. Dynamic Light Scattering (DLS) Results

The dynamic light scattering measurements are performed to ensure the formation of liposomes and to measure the size and ensure that they are almost uniform. A poly-dispersity (Pd) upper limit of 20% is generally acceptable for these measurements, as previously mentioned. Table 4.1 summarizes the averages of the three batches with their standard deviation for both types of liposomes. It can be seen that both liposomes radii fall within the range of SLVs, and they are within the optimal range for the EPR effects to take place, as previously discussed.

A slight increase in radius after attachment is noticed with the radius going from 89.54 nm to 101.10 nm for NH2 liposomes and immunoliposomes, respectively. This is expected since the Trastuzumab molecule is large and attached to the distal end of the liposomes.

Table 4.1: Summary of dynamic light scattering results.

liposomes	Radius (nm)	Pd %
NH2 liposomes	89.54 ± 0.50	11.28 ± 1.11
immunoliposomes	101.10 ± 1.13	17.22 ± 2.34

A single ANOVA analysis has been conducted between the radii of the NH2 liposomes and the immunoliposomes. Results in Table 4.2 show an extremely high value of F compared to F critical and a value for p-value lower than the standard alpha

value (0.05). This indicates that the two types have statistically different radii as expected.

Table 4.2: Single-factor ANOVA analysis of radius measurements.

Source of Variation	SS	df	MS	F	P-value	F crit
Between Groups	725.08	1	725.08	66.73	8.43E-08	4.35
Within Groups	217.31	20	10.87			
Total	942.39	21				

4.2. Trastuzumab Attachment Confirmation

To confirm the attachment of the mAb Trastuzumab to liposomes, the BCA assay and Stewart assay were used. As discussed, BCA was used to determine the concentration of protein in the sample (µg/ml), while the Stewart assay was used to determine the DPPC concentration in the sample (mg/ml). By combining the two methods, we can obtain a w/w ratio of protein to lipids in (µg/mg). This is done to exclude the effect of different concentrations. The results for three batches of liposomes were averaged to confirm attachment consistency and calculate a standard deviation. Finally, the number of liposomes attached per each liposomes vesicle was calculated, using some assumptions that will be discussed later.

The control liposomes used here are NH2 liposomes that are mixed with the antibody but without performing the attachment reaction. They were purified using the same purification column of that of immunoliposomes. This is done to confirm that any increase in the protein level is only due to the attached Trastuzumab, and not free.

The summary of the results of the Stewart assay, BCA assay and final protein concentration for each batch of liposomes are shown in Tables 4.3, 4.4, and 4.5, and could be visualized in Figure 4.1. In Figure 4.1, the apparent increase in the protein for immunoliposomes clearly confirms the antibody attachment. The consistency of results can also be observed from batch to batch, with w/w protein to lipids ratio is about 1:48.

58

It can also be noticed that both liposomes types have approximately the same lipids concentration, which is expected because they were both made following the same procedure except when adding cyanuric chloride with acetone, where acetone alone was added. This finding can help in excluding unnecessary Stewart assay measurement in future work.

Additionally, the protein increase was found to be a critical function of the cyanuric chloride added, which can be shown for the last batch where a slight increase of about 2 µl resulted in slightly higher protein amount. The reason why cyanuric chloride addition was controlled is the homopolymerization of mAb-mAb or the possibility of the liposome-liposome attachment.
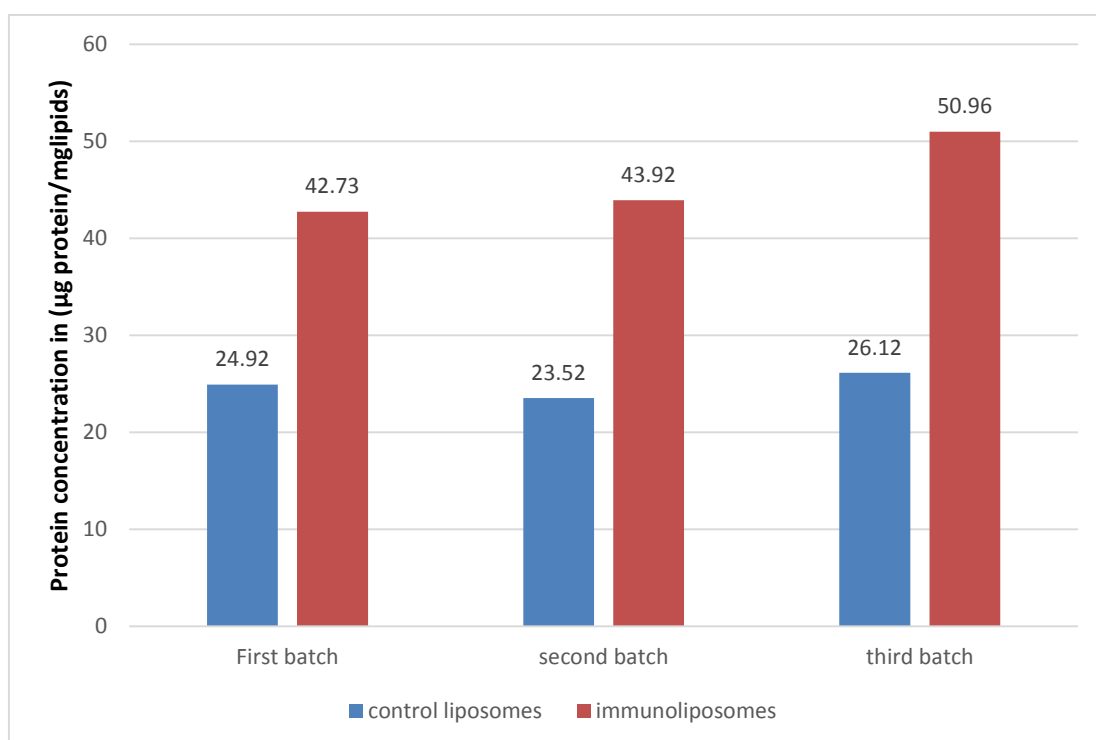
Figure 4.1: Protein concentrations per mg lipids for control and immunoliposomes confirming attachment of Trastuzumab.

Table 4.3: Trastuzumab attachment results summary for batch 1.

	µg protein/ml	mg lipids/ml	µg protein/mg lipids
control liposomes	69.62	2.79	24.92
immunoliposomes	121.48	2.84	42.73
Trastuzumab			17.80

Table 4.4: Trastuzumab attachment results summary for batch 2.

	μg protein/ml	mg lipids/ml	μg protein/mg lipids
control liposomes	76.81	3.27	23.52
immunoliposomes	147.44	3.36	43.92
Trastuzumab			20.40

Table 4.5: Trastuzumab attachment results summary for batch 3.

	μg protein/ml	mg lipids/ml	μg protein/mg lipids
control liposomes	78.50	3.01	26.12
immunoliposomes	172.71	3.39	50.96
Trastuzumab			24.85

4.2.1. Stewart assay for measurements of lipids concentrations. Normally, lipids solutions absorb light at 485 nm. A calibration curve of known concentrations of DPPC in mg/ml versus absorbed spectra was constructed. Samples were compared against that curve, and each spectra value was converted to a concentration. Six replicates per batch were used for both types of liposomes. This calibration curve was linear which allowed for more accuracy and flexibility in calculations.

4.2.2. BCA assay for measurements of Protein concentrations. Similar procedure was adopted when running the BCA assay, where a calibration curve was first constructed for known Trastuzumab solution concentrations. Then each sample spectra was compared against that curve to yield the protein concentration in μg/ml. The protein sources in the samples were the amino acids in the antibody and the peptide ponds in the liposomes themselves. To account for the difference, protein concentrations for the control liposomes were measured as well. Therefore, the difference in protein amounts could be attributed only to the amino acids in the attached Trastuzumab. This is feasible because of the linearity of the calibration curve, where the protein concentration can be additive and subtractive. Additionally, the nature of the control liposomes accounted for the calculation of attached mAb only. Some of the subtracted protein was due to the presence of free Trastuzumab in that sample, leaving only the effect of protein coming from attached Trastuzumab.

4.2.3. The number of Trastuzumab molecules attached to each liposome vesicle. Assuming a liposomes size of 100 nm in radius and an average area for a single phospholipid molecule of about 75 A°, the average number of lipid molecules constructing a single liposomes vesicle was 80,000 [80]. Knowing the concentrations of the lipids and Trastuzumab and their molecular weights, it was found that almost 9 Trastuzumab molecules were conjugated per liposome This is considered to fall within the optimal range necessary to induce sufficient cells cytotoxicity [90].

4.3. Safe Limits for Ultrasound Used

Mechanical index (MI) is a measurement of the likelyhoood of cavitation and damage to cells and tissues. At different mechanical indices, different effects start to happen. For collapse cavitation to start, the mechanical index has to reach 0.3, while for biological effects, it has to reach 0.6. Tissue damage begins at a mechanical index of 1, where the limits set by the Food and Drug Administration (FDA) is MI = 1.9. The following relation is used to calculate the MI [106].

$$MI = \frac{P^-[Mpa]}{\sqrt{f[MHz]}} \tag{2}$$

where $P^- \equiv$ the negative pressure in [Mpa]

$f \equiv$ frequency in [MHz]

The negative pressure can be calculated using the specific acoustic impedance of water which is 1.48 (MPa.s/m) and the intensity [107]. This is shown in equation (2a) below.

$$P = \sqrt{2Iz} \text{ [Pa]} \tag{2a}$$

where $I \equiv$ power density in W/m^2

$z \equiv$ specific acoustic impedance of water in [Pa.s/m]

It is noticed that the power densities and frequencies calculated correspond to mechanical indices of 0.11, 0.12, and 0.16 for power densities of 7.46, 9.85, and 17.31 (mW/cm^2) respectively. These values are well below the safe limits of any biological effects. It can be concluded that higher power densities can be safely implemented in future work (up to 60 (mW/cm^2) which corresponds to a mechanical index of 0.3, when using a frequency of 20 (kHz) ultrasound.

4.4.   Low-Frequency Ultrasound (LFUS) Online Release Studies

As mentioned previously, the ultrasound release studies were conducted at 20 kHz; because it was previously reported that liposomes exhibit higher release rates at this frequency [104]. LFUS was implemented and at three power densities, 7.46, 9.85, and 17.31 mW/cm^2; these are believed to best induce release at safe conditions [105]. Pulsed ultrasound at 20 seconds on and 10 seconds off was used for a total duration of 6.3 minutes, corresponding to an actual duration of 4.2 minutes. As calcein is released, an increase in the fluorescence level should be observed. The baseline at before sonication was measured for 60 seconds before pulsed sonication was initiated. Then sonication was applied until a plateau was reached. After that, a sharp increase in the fluorescence level was noticed when liposomes were lysed to spill all their contents. Finally, the data were normalized using equation (1). For both types of liposomes, three batches were used, with three replicate measurements for each batch.

The control liposomes used in the LFUS studies are the NH$_2$ liposomes, but the buffer was lowered from 8.5 to 7.4 in pH. Buffer changing was done using the purification column. Immunoliposomes went through the conjugation process before changing the pH buffer to 7.4.

4.4.1. Low-Frequency Ultrasound Release Studies for NH2 liposomes. Calcein release for NH$_2$ liposomes at LFUS and relatively low intensities was established as shown in Figure 4.2, and no agglomeration occcured among the liposomes. These results are important because LFUS can be used to penetrate further into the human body. Also, high-intensity ultrasound can cause unwanted effects such as hyperthermia.

The ultrasound parameters considered here are satisfactory to achieve a controllable release that is appropriate for medical purposes. They are optimum because they are safe to use, and they induce cavitation events in a moderate rate which are not too drastic to cause complete release of the drug in one pulse. The lowest MI to cause cavitation is 0.3, but in this thesis, MI of 0.11 was shown to be sufficient for drug release. Also, the range of intensities does not endanger human cells. These parameters are a starting point to achieve drug release *in vivo*, and consequently in animal tests and clinical trials.

The release trend can be seen in Figure 4.2, in which the average cumulative fraction release data (CFR) for the three batches, for each power density, were plotted. It can be seen that as the power density increases the release rate becomes steeper; this is expected due to the increase in cavitation events as the power density increases [61]. It can also be seen that NH_2 liposomes released most of their contents (86.35%) within 3 minutes, which demonstrate their strong sonosensitivity. Additionally, the release trend at 17.31 mW/cm^2 can be seen to decrease slightly after the plateau; which can be explained by the thermal effects liposomes start to exhibit. As they approach their transition temperature, the drug can diffuse back into liposomes. In conclusion, the release rate is a function of both the power density and exposure time. This was also supported by literature [108].

From the same graph, it is clear that as sonication stops, the release also ceases, which means that there was no delay, and any events occurring upon sonication disappeared immediately. This suggests the occurrence of stable cavitation (mechanical effects), rather than thermal effects at LFUS. The absence of thermal effects makes sense since low-intensity ultrasound was used and no increase in temperatures was measured during that period.

The suggested mechanism was that LFUS causes pore-like defects in the liposomes membrane upon exposure, which heals immediately in off periods.

It is also seen that the release is accumulative, so the drug can be released continuously, or pulsed, resulting in the same CFR (after the same exposure time). These findings are very important in controlling the release rate over any desired periods of time. This is also important for the control of the hyperthermia effects upon the continuous exposure to ultrasound.

As summarized in Table 4.6, NH_2 liposomes released almost 86.35% of their content after 140 seconds (7 pulses) of actual sonication at 7.46 (mW/cm^2), 100 seconds (5 pulses) at 9.85 (mW/cm^2), and 60 seconds (3 pulses) at 17.31 (mW/cm^2). It was previously reported in literature that liposomes with no sonication released about 3% in 3 minutes [108]. Higher release rates were attributed to more cavitation events. It also shows the range of ultrasound parameters that can be selected to achieve the desired release rate which corresponds to an optimum treatment.
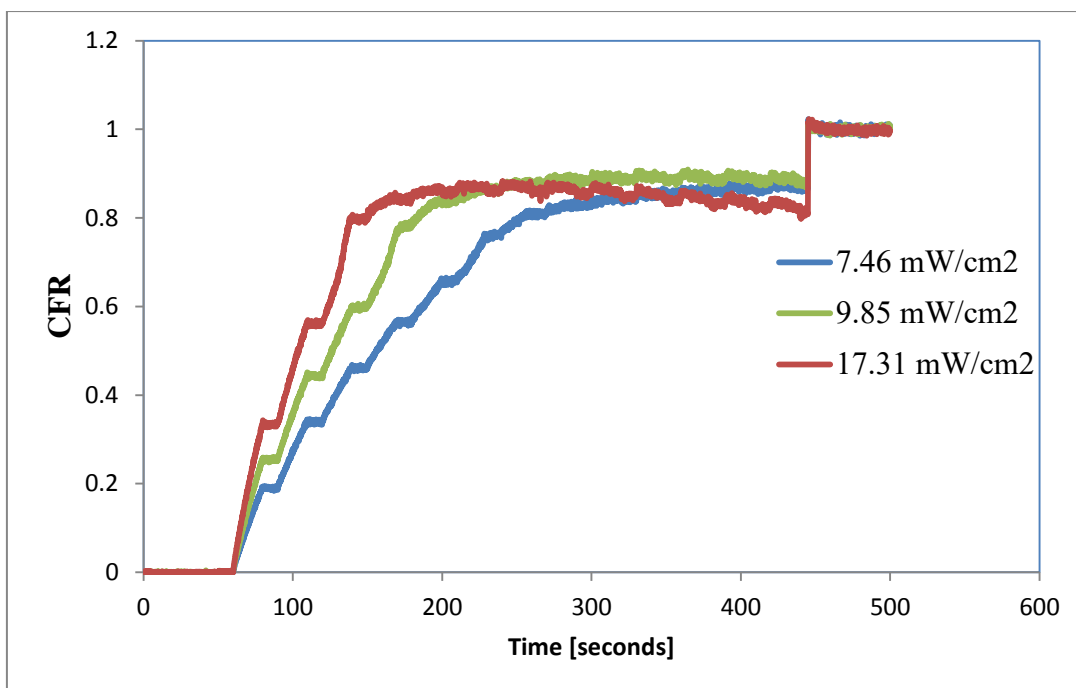
Figure 4.2: Online release profile for 3-batch averaged NH2 liposomes.

Table 4.6: Release data summary of NH2 liposomes showing total release CFR at the plateau.

Power density (mW/cm^2)	CFR at Plateau	Pulses to reach plateau	Time to reach plateau (seconds)
7.46	0.8530	7	140
9.85	0.8820	5	100
17.31	0.8554	3	60
average	0.8635		

A closer look into the release data can be seen in Figure 4.3, where the CFR values clearly increase as power density increases. Also, the amount released after the third pulse for the lowest power density (7.46 mW/cm^2) was almost 46% of the total drug encapsulated within liposomes, which occurred after 1 minute of actual sonication only. These results support the above-concluded results and show the sono-sensitivity of NH$_2$ liposomes.
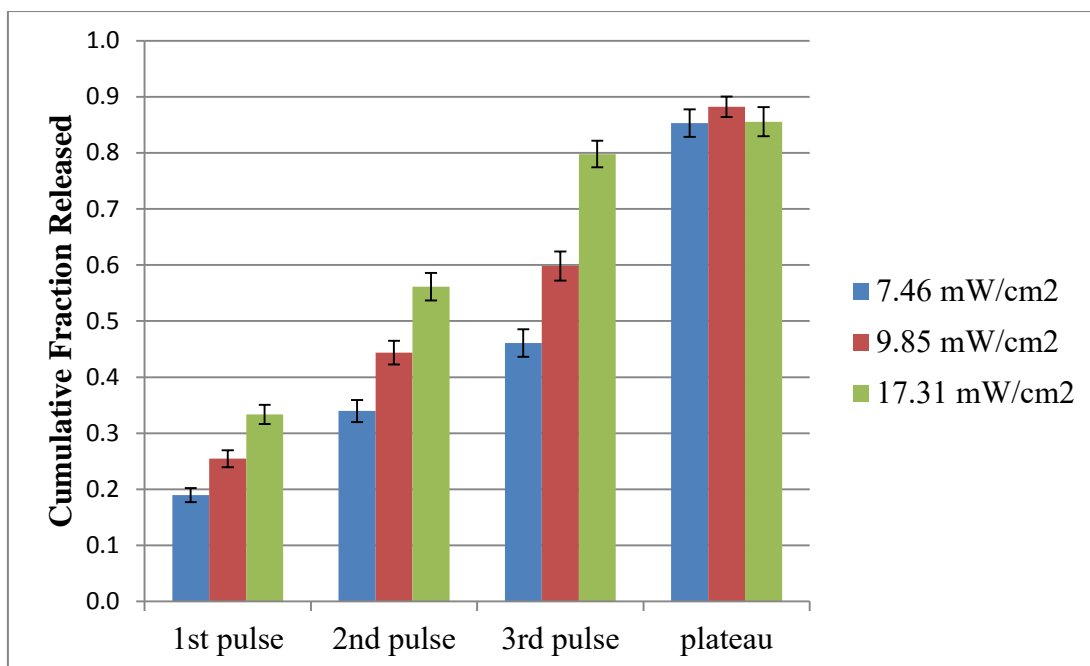
Figure 4.3: Cumulative fraction released measured at different pulses, and the final plateau for NH2 liposomes.

The last Figure in this section, Figure 4.4, shows the fraction released for each pulse separately (not cumulatively) and it can be seen that the highest fractional release of the drug was in the first pulse. Similar results are also noticed for other power densities (see appendix A). This is important in which high initial levels of the drug are needed for biological effectiveness, and consequently less amounts to follow to retain that level are needed. The plateau is shown to happen after the 7th pulse after which the release decreased significantly.

4.4.2. Low-Frequency Ultrasound Release Studies for immunoliposomes.

Figure 4.5 illustrates the online release rate of calcein from immunoliposomes at the three power densities, averaged for the three batches of liposomes tested. Release upon exposure to ultrasound is established, and no agglomeration occcured among the liposomes. The same experimental procedure used for NH_2 liposomes was also followed for these immunoliposomes Similar discussed was made for NH_2 liposomes in detail in section 4.4.1.

As observed with NH_2 liposomes, the release rate in immunoliposomes also increases as power densities increase. Also, release happened only upon exposure to

ultrasound, and it was cumulative. These characteristics are very important in drug delivery as previously discussed for NH_2 liposomes in section 4.4.1.
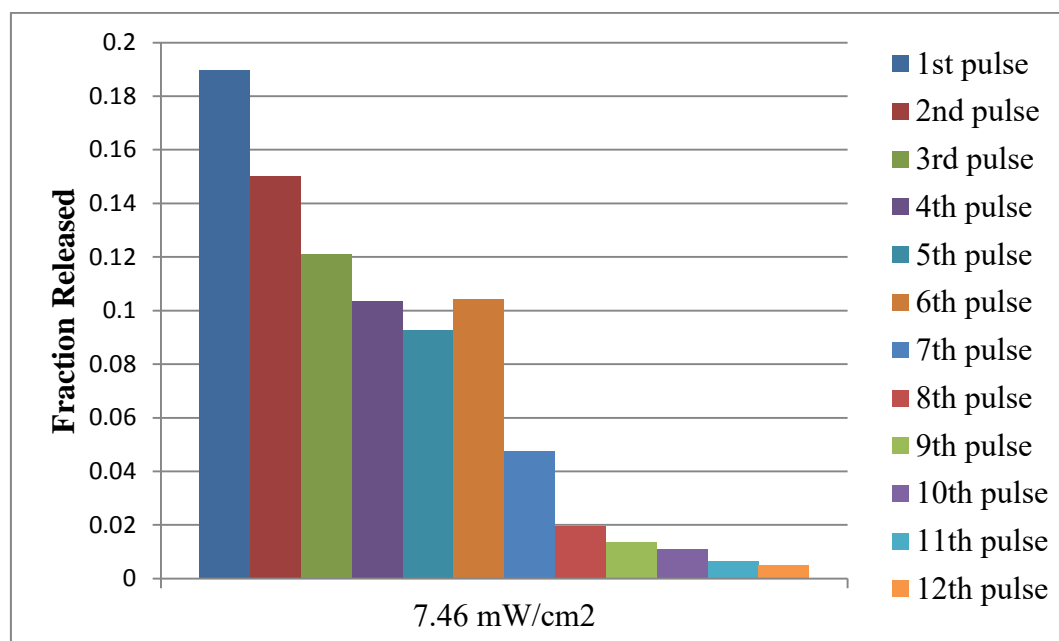
Figure 4.4: Fraction released at the 1st, 2nd, and 3rd pulses for NH2 liposomes at 7.46 (mW/cm^2).

Release continued for a few seconds in the off period at the highest power density, probably due to the fact that thermal effects started to occur [61].

Additional observation can be seen at a power density of 17.31 (mW/cm^2) where the drug starts to get internalized into the liposomes again after the plateau. The reason could be thermal effects allowing the drug to diffuse back, where liposomes membrane become fragile. Normally, ultrasound exposure will stop before reaching that stage.

The almost complete release of the liposomes content (92%) happened after 6 pulses (120 s), 4 pulses (80 s), and 3 pulses (60 s), for 7.46, 9.85, and 17.31 mW/cm^2 respectively. The data are summarized in Table 4.7 and is attributed to the increased occurrence of cavitation events that accompany higher intensities. It also shows the range of ultrasound parameters that can be selected to achieve a specific release rate.

Figure 4.6 shows that values clearly increase with increasing intensities. After 1 minute only, the amount released from immunoliposomes was 47 % at a power

density of 7.46 (mW/cm^2), whereas the complete release was achieved at that same duration for the 17.31 mW/cm^2 power density.
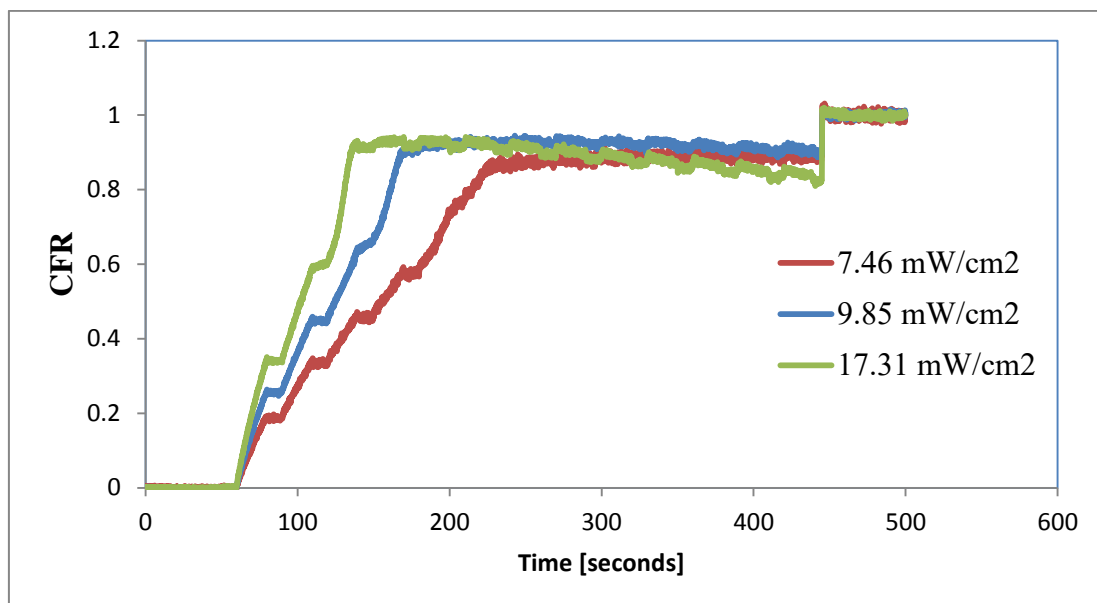
Figure 4.5: Online release profile for 3-batch averaged immunoliposomes.

Table 4.7: Release data summary of immunoliposomes showing total release CFR at the plateau.

Power density (mW/cm^2)	CFR at Plateau	Pulses to reach plateau	Time to reach plateau (seconds)
7.46	0.9109	6	120
9.85	0.9257	4	80
17.31	0.9246	3	60
average	0.9204		

Figure 4.7 shows the non-cumulative fraction of drug released at each pulse at 7.46 (mW/cm^2) for immunoliposomes. Similar observations with NH$_2$ liposomes can be seen as the highest fraction released of the drug was observed after the first pulse. As previously mentioned, it is important to initiate a high therapeutic dosage at the beginning and to maintain that level for prolonged periods. The plateau is shown to happen clearly after the 6th pulse, and incremental release is very low after that.
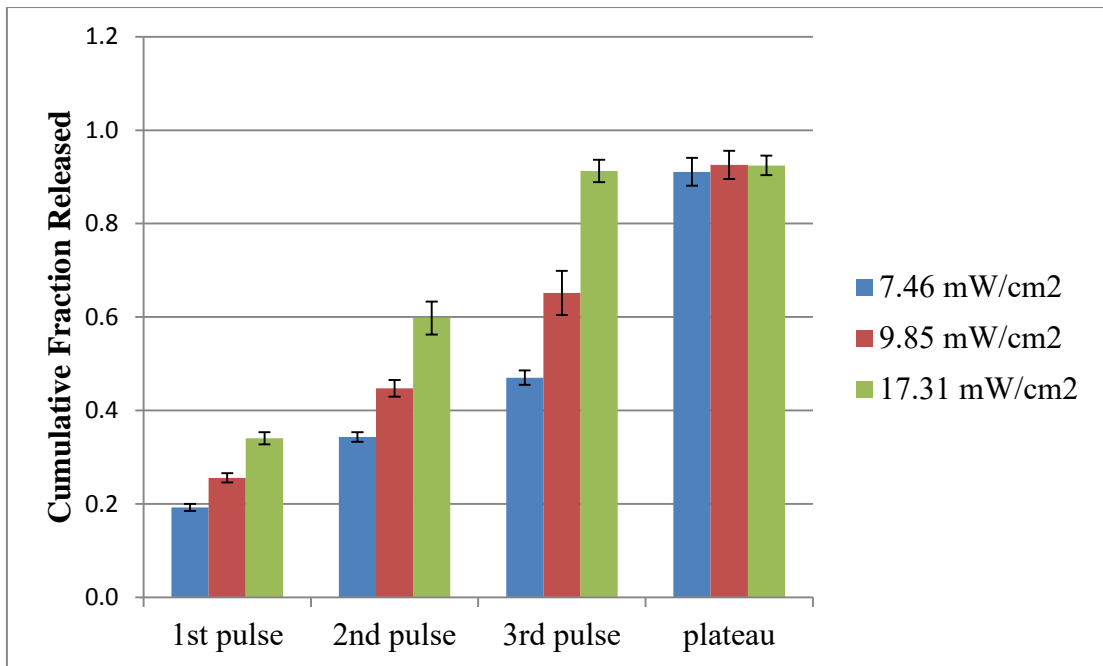
Figure 4.6: Cumulative fraction released measured at different pulses, and the final plateau for immunoliposomes.
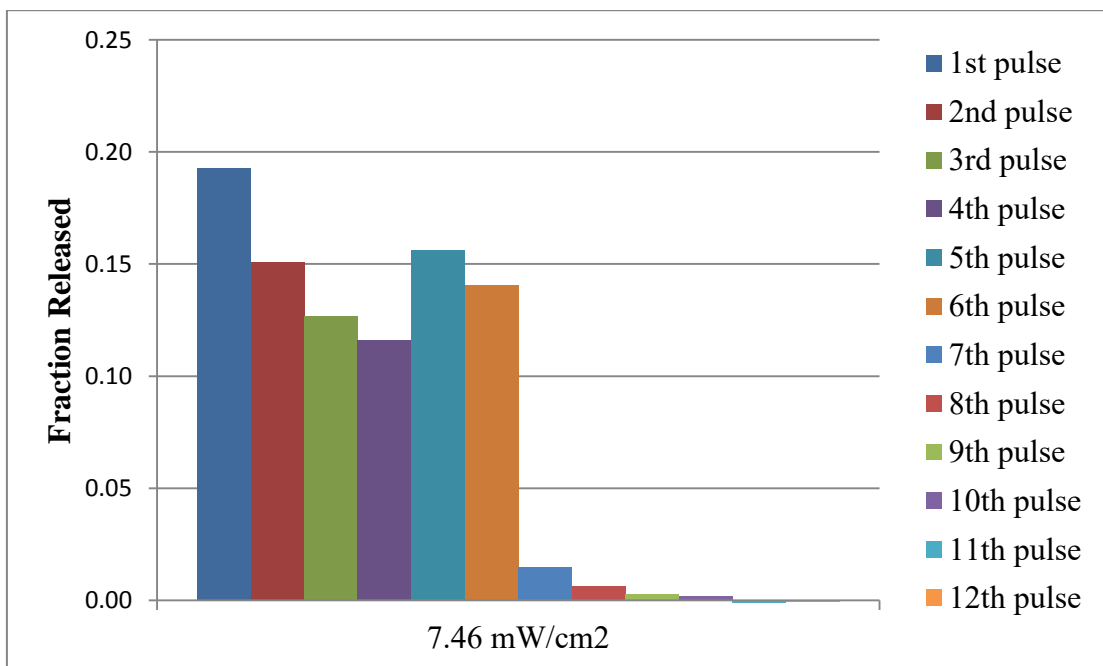
Figure 4.7: Fraction released at the 1st, 2nd, and 3rd pulses for immunoliposomes at 7.46 (mW/cm^2).

4.4.3. Comparison between the NH$_2$ liposomes and immunoliposomes release rates. Both liposomes types demonstrated ideal release profiles for drug-

controlled release, as can be seen in Figure 4.8. The steeper release for immunoliposomes indicates its higher sono-sensitivity. This is due to the fact that the targeting moiety (Trastuzumab) makes liposomes absorb more acoustic energy. Increased sono-sensitivity of immunoliposomes is considered a plus in ultrasound triggered release; because it could be used to reach therapeutic levels in shorter exposure times.
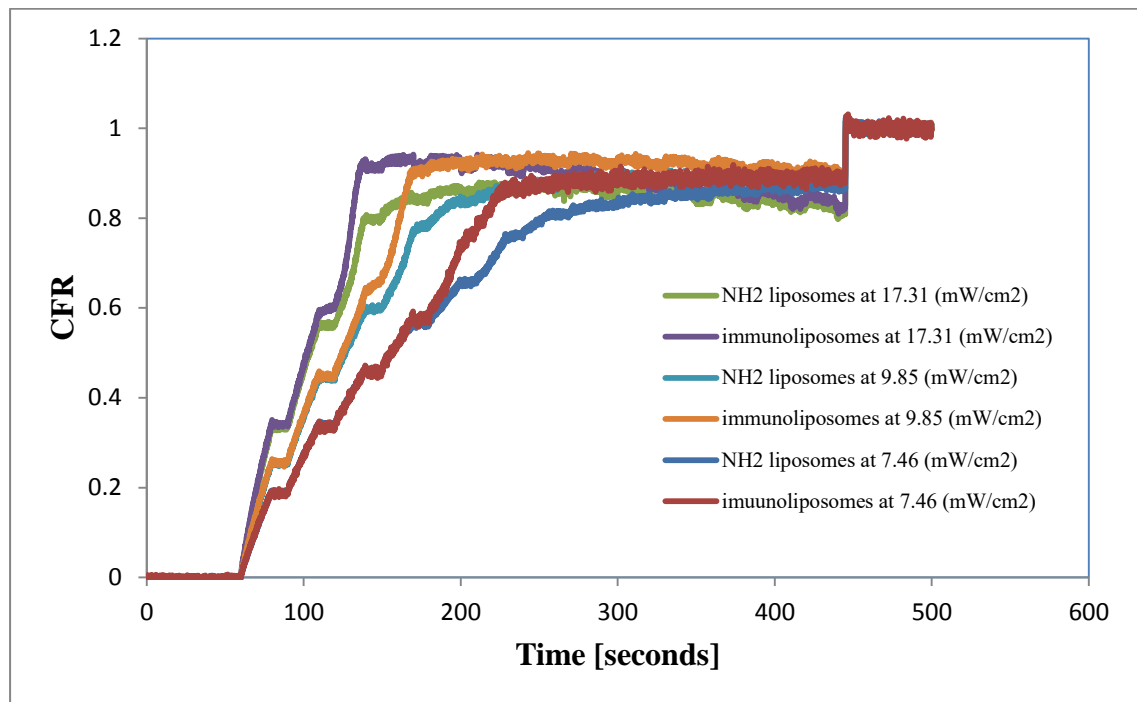
Figure 4.8: Release profiles for NH2 liposomes and immunoliposomes at different power densities.

Figures 4.9, 4.10, and 4.11 illustrate clearly the higher drug release amounts for immunoliposomes after the first pulses, and the final amount of calcein that liposomes were able to release. Keeping less than 8% encapsulated within immunoliposomes compared to 13% for NH_2 liposomes at the end of the sonication period.

4.4.4. Comparison with other targeted liposomes under LFUS. In comparison with other targeted liposomes triggered by LFUS, a similar release profile was observed for RGD-targeted liposomes using the same ultrasound parameters in this study. Similarly, RGD-liposomes were found more sono-sensitive than control liposomes. RGD-liposomes and control ones demonstrated an average release of 80% at the end of the sonication time (6 minutes with pulse mode) compared to our

liposomes that released almost 90% in less than 4 minutes in pulsed acoustic mode. This lower value can be attributed to the difference in liposomal solution concentration between the two studies. Generally, the higher the concentration, the more time is needed to fully release the drug. No thermal effects were observed in this study, hence the release is attributed solely to cavitation/mechanical effects [105].
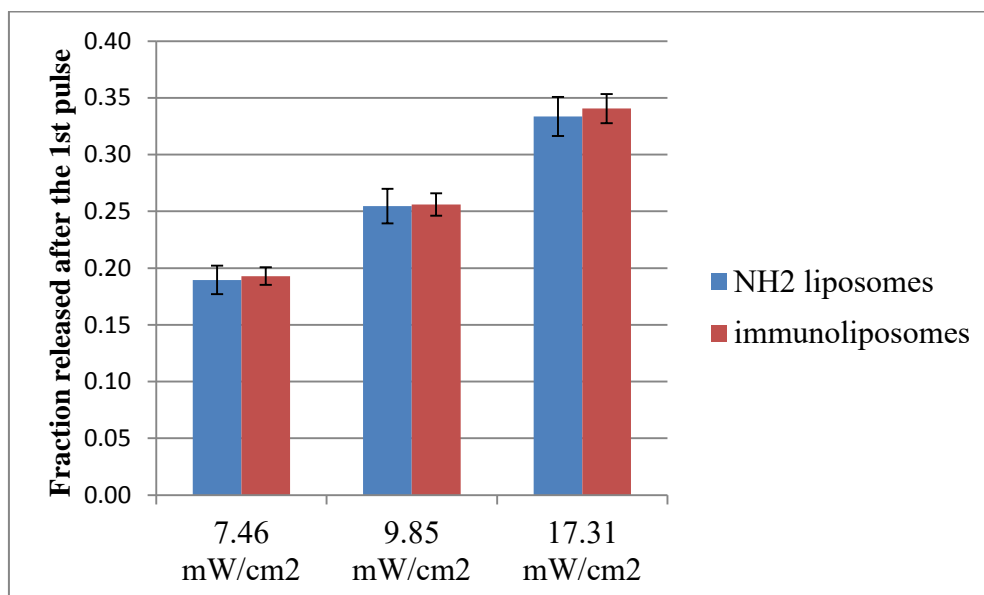
Figure 4.9: Fraction released after the first pulse for both types of liposomes at each power density.
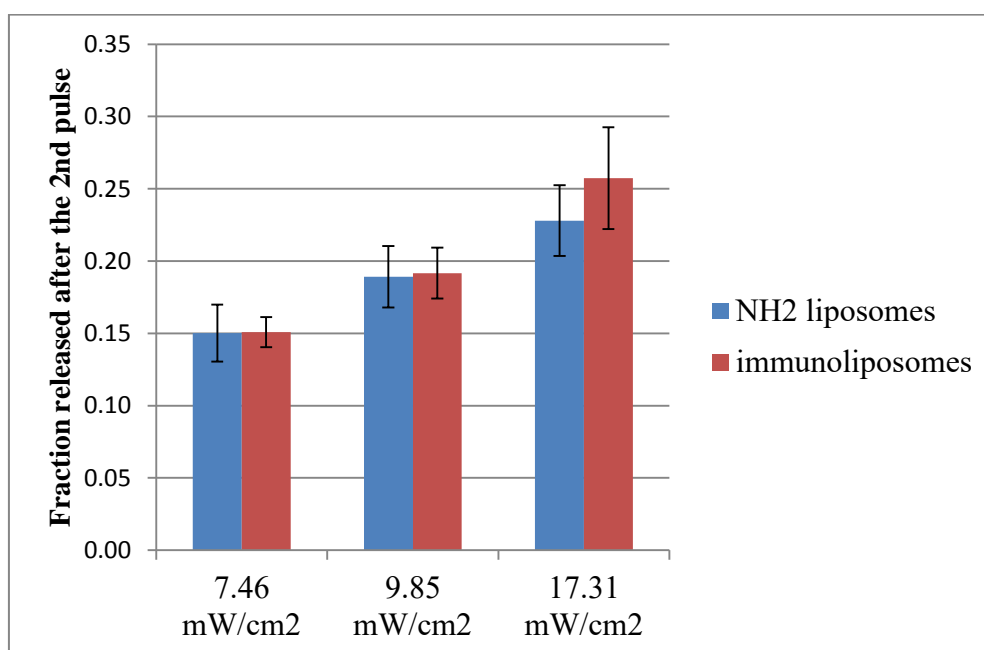
Figure 4.10: Fraction released after the second pulse for both types of liposomes at each power density.
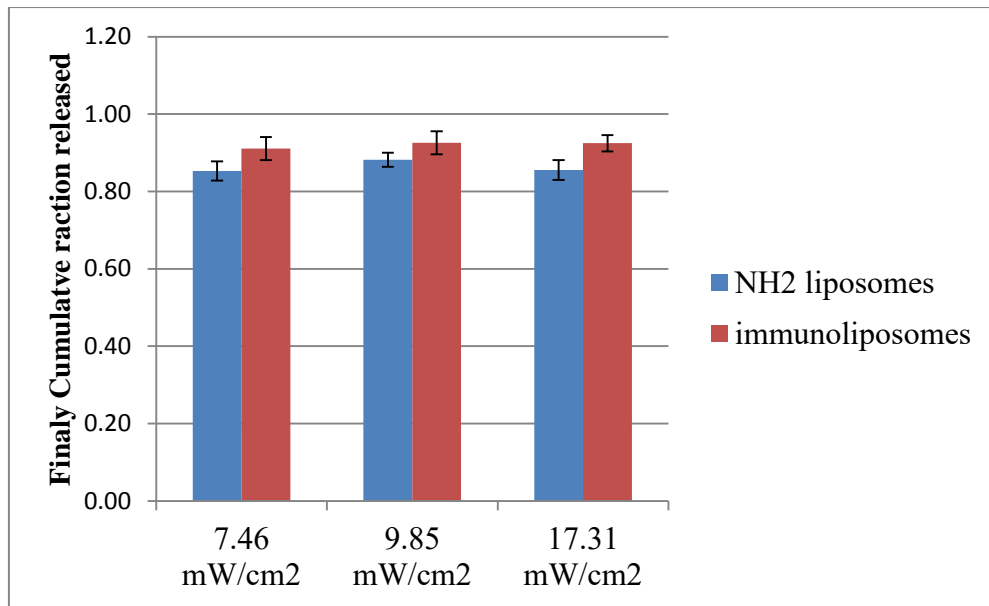
Figure 4.11: Final cumulative release fraction from both types of liposomes at each power density.

A previous study conducted made by Mohammad shows that Estrone-liposomes also exhibited a similar release profile as our immunoliposomes at power densities ranging from 6.08 to 11.83 mW/cm^2. Also, results showed that Estrone-liposomes were more sono-sensitive than control liposomes; exhibiting a steeper release rate [25].

Turki showed that adding albumin as a targeting moiety slightly decreased liposomes sensitivity toward ultrasound. Albumin captures calcein and can hence decrease its apparent release. Another possible reason is that albumin increased liposomes stability. Eventually similar release profiles were observed for albumin-liposomes compared to our immunoliposomes [93].

In conclusion, targeted liposomes seem to exhibit sono-sensitivity toward LFUS at 20 kHz and intensities ranging between 6 and 17 mW/cm^2. They also have similar release profiles and show steeper release rates than their controls. Additionally, no heat effects are seen within those conditions. Lastly, it can be concluded that the release rate is governed by liposomes concentration, when their composition and ultrasound parameters are kept the same.

4.5. Release Kinetics Studies

Modeling the release kinetics may help in predicting release at different conditions including lipid and the agents' composition, power density and frequency. In addition, it helps to design equipment to optimize release. The data presented above can be used to find the best fitting model that can successfully represent calcein release from targeted and non-targeted liposomes. Nine models were inspected to find the best fit for the release data

4.5.1. Zero-order model. The zero-order model is derived from a basic understanding of the physical process of the nanocapsules where the drug is released very slowly at a constant rate. Assuming that the area is constant and no equilibrium conditions are obtained, equation (3) represents the model [109]:

$$Q_t - Q_0 = K_0 t \tag{3}$$

where $Q_t \equiv$ the amount of drug dissolved in time t

$Q_0 \equiv$ the initial amount of drug in the solution

$K_0 \equiv$ zero-order release constant

Rearranging the equation to fit our normalized data, is presented in equation (4):

$$CFR = k_0 t \tag{4}$$

where $CFR \equiv$ cumulative fraction released

$t \equiv$ time in seconds

$k_0 \equiv$ zero-order release constant in percentage per second.

A plot of CFR vs. time will deliver the release constant as the slope.

4.5.2. First-order model. This model assumes that dissolution includes a surface action [110]. It can be used accurately to model the release of water-soluble drugs in porous matrices [67]. It is mathematically represented by equation (5):

$$\frac{dc}{dt} = -k_1 C \tag{5}$$

where $C \equiv$ drug concentration at time t

$k_1 \equiv$ first-order rate constant in seconds^{-1}

After integrating and rearranging to make it compatible with the data taken, it yields equation (6):

$$\log CFR = k_1 t + constant \tag{6}$$

A plot of log(CFR) versus time will yield the slope k_1.

4.5.3. Higuchi model. This model was the first to describe drug release from matrix systems. It was first introduced by Higuchi in 1961 [111]. It describes release as a diffusion-based process. Applications of the model include transdermal systems and matrix tablets carrying water-soluble drugs. The model assumes the following:

1) Diffusion is in one dimension only.
2) The concentration of the drug inside the matrix is higher than its solubility.
3) The drug molecules are much smaller than the matrix thickness.
4) Constant drug diffusivity.
5) The matrix change in dimensions is negligible.
6) Perfect sink conditions in the release environment.

The simplified equation for the Higuchi model can be seen in equation (7) [67]:

$$Q = k_H \sqrt{t} \tag{7}$$

where $k_H \equiv$ Higuchi release constant

$Q \equiv$ the amount of drug released in time t

Rearranging to convert Q to CFR yields equation (8) which can be used to obtain Higuchi release constant upon plotting CFR versus square root of time.

$$CFR = k_H \sqrt{t} \tag{8}$$

4.5.4. Korsmeyer-Peppas model. Korsmeyer derived a simple model describing the release from porous hydrophilic polymers. Korsmeyer-Peppas or the power -law as it is sometimes called is a more general model than Higuchi. It takes into account the effects of swelling and dissolution, and it does not assume a diffusion-based release [112]. At small t, the model can be simply shown as in equation (9) [113]:

$$\frac{M_t}{M_\infty} = k_{kp} t^n \tag{9}$$

where $\frac{M_t}{M_\infty} \equiv$ is the fraction of drug released at time t

$k_{kp} \equiv$ the Korsmeyer-Peppas release rate constant

$n \equiv$ the release exponent

The rate constant changes with different shapes and structures. The exponent value indicates the mechanism of the release. For the case of cylindrical shapes, if n ≤ 0.45, then the release follows Fick's law (diffusion –dependent), if 0.45 < n < 0.89 then the release is non-Fickian, if n = 0.89 the release follows relaxation transport, and if n > 0.89 then the release is considered super case transport. This is why this model is used to study the release when the mechanisms are not known [67, 109].

After adjusting the model to our type of data and linearizing, equation (10) is realized, and a plot of the log(CFR) versus log(t) can yield log(k$_{KP}$) as the intersect and the n value as a slope.

$$\log(CFR) = \log(k_{kp}) + n \log(t) \tag{10}$$

4.5.5. Hixson-Crowell model. Hixson in 1931 built his equation based on the proportionality of the sphere regular area to the square root of its volume. The relation can be seen in equation (11) [109].

$$W_0{}^{1/3} - W_t{}^{1/3} = k_{HC}t \tag{11}$$

where $W_0 \equiv$ the amount of drug initially inside the liposome

$W_t \equiv$ the remaining amount of drug in the liposomes

$k_{HC} \equiv$ the proportionality constant

Rearranging the resultant equation to get CFR on one side, yields equation (12).

$$(1 - CFR)^{\frac{1}{3}} = 1 - k_{HC}t \tag{12}$$

This model assumes that release is controlled by the dissolution of the drug particles and not by their diffusion through the pores of the matrix. It also takes into account the reduction in the particle size as it dissolved in the solution [109]. Plotting 1-(1-CFR)$^{1/3}$ versus time should yield a straight line with -k$_{HC}$ as the slope after setting the intercept at 1.

4.5.6. Baker-Lonsdale model. Baker described the release from spherical matrices by developing the Hugichi model. The expression is shown in equation (13) [67, 114]. The resultant equation when converting the release in terms of CFR is described in equation (14).

$$\frac{3}{2}\left[1-\left(1-\frac{M_t}{M_\infty}\right)^{2/3}\right]-\frac{M_t}{M_\infty}=k_{BL}t \tag{13}$$

where $M_t \equiv$ the drug release amount at time t

$M_\infty \equiv$ the total amount released at infinite time (initial amount inside the liposomes)

$k_{BL} \equiv$ the release constant

$$\frac{3}{2}\left[1-(1-CFR)^{2/3}\right]-CFR=k_{BL}t \tag{14}$$

Plotting the left hand-side of equation (14) versus time will result in a straight line with k_{BL} as the slope.

4.5.7. Weibull model. The Weibull model is a general empirical relation that describes different dissolution rates of matrix type systems [67, 109]. The relation is shown in equation (15) and the altered form to incorporate our data is shown in equation (16), whereas the linearized form can be seen in equation (17). Since this is an empirical relation and does not represent any physical phenomena, it had limited use in literature [109].

$$m = 1 - e^{\left[\frac{-(t-T)^b}{a}\right]} \tag{15}$$

where $m \equiv$ accumulated fraction of the drug

$a \equiv$ a scale parameter that describes time dependence

$b \equiv$ a parameter that depends on the shape of the dissolution curve

$T \equiv$ accounts for the time lag in dissolution process (taken = 0)

$$1 - CFR = e^{\left[\frac{-(t)^b}{a}\right]} \tag{16}$$

$$\log(-\ln(1-CFR)) = b\log(t) + \log k_w \tag{17}$$

where $k_w \equiv \frac{1}{a} \equiv$ Weibull rate constant

Plotting the left-hand side expression of equation (17) versus log(t) will yield b as the slope and log(k_w) as the intersection.

4.5.8. Hopfenberg model. In 1976 Hopfenberg developed a relation modeling the release from the erodible surface polymers, for different shapes including slaps, cylinders, and spheres. Hopfenberg assumes that the surface remains constant while eroding. He also assumes that a zero-order mechanism will take place throughout the eroding process, whether the drug was loaded chemically (attached), or physically (dissolved, dispersed). The model considers the diffusion process to be so rapid that it cannot be rate determining [115]. The cumulative fraction released at time t is described by the model in equation (18) [67].

$$\frac{M_t}{M_\infty} = 1 - \left[1 - \frac{k_0 t}{C_L a}\right]^n \tag{18}$$

where $\frac{M_t}{M_\infty} \equiv$ cumulative fractional released

$k_0 \equiv$ the zero-order rate constant describing the eroding

$C_L \equiv$ the initial drug loading

$a \equiv$ the system's half thickness (radius for a sphere)

$a \equiv$ 1, 2, or 3, for a slap, cylinder, and a sphere respectively

Rearranging yields equation (19) in terms of CFR, which is similar to the Hixson-Crowell equation after rearranging. This is not surprising since some relations can reduce to others in special cases. Plotting the left-hand side against time will result in a straight line of a slope k_{HF}.

$$1 - (1 - CFR)^{\frac{1}{3}} = k_{Hf} t \tag{19}$$

where $k_{Hf} = \frac{k_0}{C_L a}$

4.5.9. Gompertz model. Gompertz model is for drugs with good solubility and intermediate release. The relation is exponential and is shown in equation (20). The model has a sharp increase, which then converges gradually to a plateau [67, 113].

$$\frac{X_t}{X_{max}} = e^{-\alpha e^{\beta \log t}} \qquad (20)$$

where $X_t \equiv$ fraction dissolved at time t

$X_{max} \equiv$ maximum dissolution

$\alpha \equiv$ a scalar parameter describing non-dissolved portion at time t=1

$\beta \equiv$ dissolution rate per unit time

Rearranging assuming X_{max}=1 is shown in equation (20).

$$\ln(-\ln CFR) = k_G \log t + \ln \alpha \qquad (21)$$

where $k_G = \beta$

According to equation (21), plotting the left-hand side versus log(t) will result in a straight line with k_G as the slop and ln(α) as the intersection.

4.5.10. Models accuracy for NH$_2$ liposomes. Previously stated cumulative fraction release of each batch of NH$_2$ liposomes were used in equations (4), (6), (8), (10), (12), (14), (17), (19), and (21) to construct the following graphs. To test the models representation of the drug release kinetics, a straight line should appear in the graph, if the model was accurate. The suitability of each model was determined upon creating a straight trendline of the plot. Then to test how close the data points are to this straight line, R^2 was calculated. Generally, R^2 is an indication of the model capability to accurately represent the release data.

Additionally, Parity plots were also used to demonstrate the best fitting model.

Figures 4.12 to 4.20 were constructed using the data from the three batches of NH$_2$ liposomes at a power density of 7.46 (mW/cm^2), where each R^2 is shown on the graph. The rest of the data for the remaining batches and the other power densities for NH$_2$ liposomes and immunoliposomes can be found in Appendices A and B respectively.

The R^2 values of the models for all the NH$_2$ liposomes batches at each power density are summarized in Tables 4.8 and 4.9, in which averages of each model fitting parameter (R^2) is shown at the bottom of the table. It can be seen that Korsmeyer-Peppas shows the highest R^2 averaged values for NH$_2$ liposomes (0.9952), meaning that it is the best model to fit the release data. This can also be visualized in the parity

plots in Figures 4.21, 4.22, and 4.23 plotted for the average of the three batches of NH_2 liposomes at each power density, using parameters estimated for each model fit. From the parity plot, it can be noticed that Hixson-Crowell and Hopfenberg (colored overlapping as grey) were the second closest models after Korsmeyer-Peppas (colored in black) to the actual model (colored in red). The fourth closest was the Weibull model, while the rest of the models failed to accurately represent the release data. Baker-Lonsdale model was not included in the parity plot because $CFR_{(BL)}$ can not be estimated mathematically and iterations would be needed. But the model had a low R^2 value (0.8687), and therefore was considered one of the poor models to fit the data.

Further analysis for both liposome types and their compatibility with the models are discussed in section 4.5.11.

4.5.11. Models accuracy for immunoliposomes. The same analysis implemented for NH_2 liposomes was done also for immunoliposomes, where all the models graphs can be seen in the appendices. The summary for the R^2 values are presented in Tables 4.10, and 4.11, in which Korsmeyer-Peppas also demonstrated to have the highest R^2 averaged value follow by the zero-order, and Weibull models. This can also be visualized in the parity plot in Figures 4.24, 4.25, and 4.26, where the black colored Korsmeyer-Peppas model was the closest to the red colored actual CFR values, followed by the green colored Weibull model, and then the blue colored zero-order model, and finally the Hixson-Crowell and Hopfenberg models overlapping as grey color.

This shows that both types of liposomes have similar behavior and consequently similar mechanisms. The Korsmeyer-Peppas model reveals the apparent diffusion release mechanism by calculating the n value in the model. The n values were found to be 0.7742 and 0.7896 for NH_2 liposomes and immunoliposomes, respectively. This could be averaged for both as 0.7819. This value falls in the non-Fickian transport upper limit, and close to the super transport region. The adherence of the data to Korsmeyer-Peppas, Hopfenberg, and Hixson-Crowell, assume diffusion-driven and dissolution-driven mechanism [116]. This could be understood considering that ultrasound induces the formation of pore-like deformations during sonication allowing the drug to diffuse easily and rapidly to the outer environment.
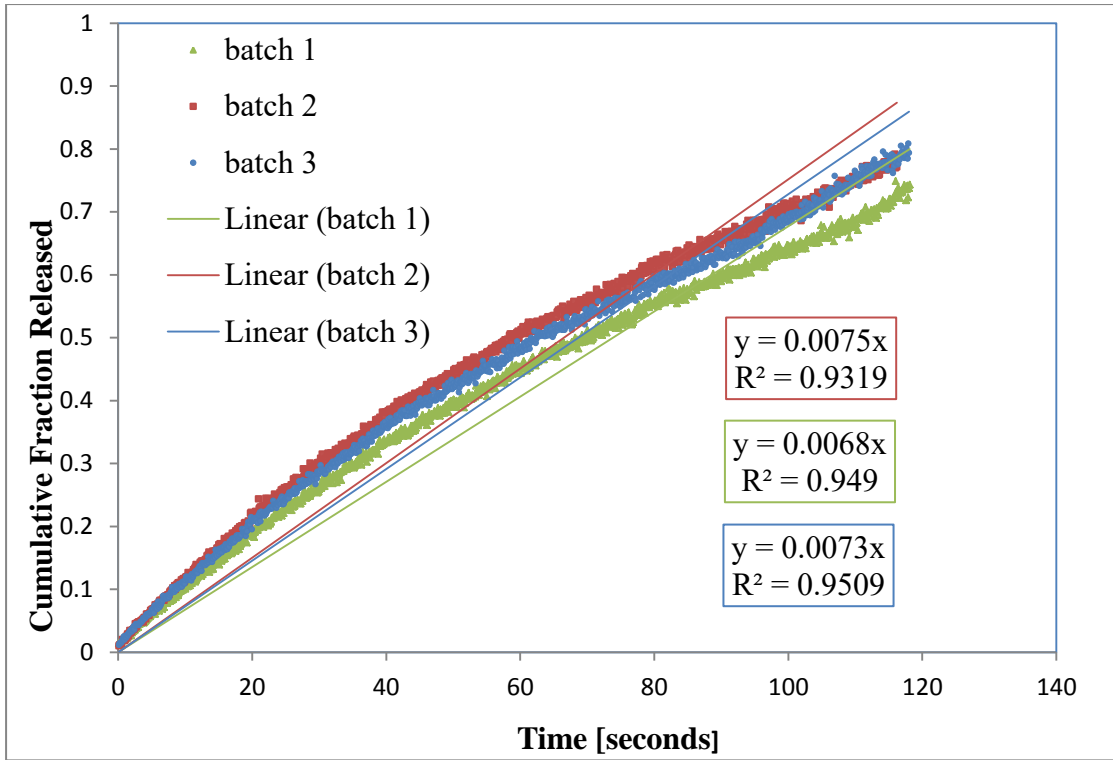
Figure 4.12: Zero-order plot for NH2 liposomes at 7.46 mW/cm^2.
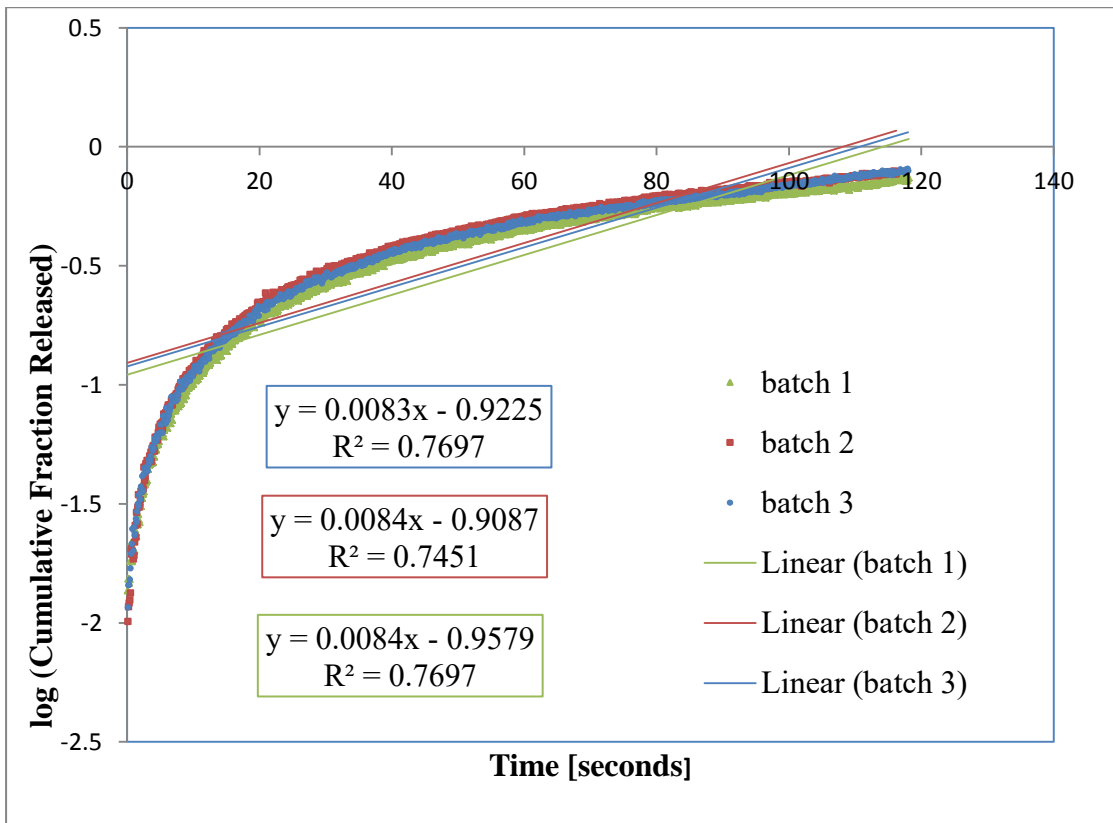
Figure 4.13: First-order plot for NH2 liposomes at 7.46 mW/cm^2.
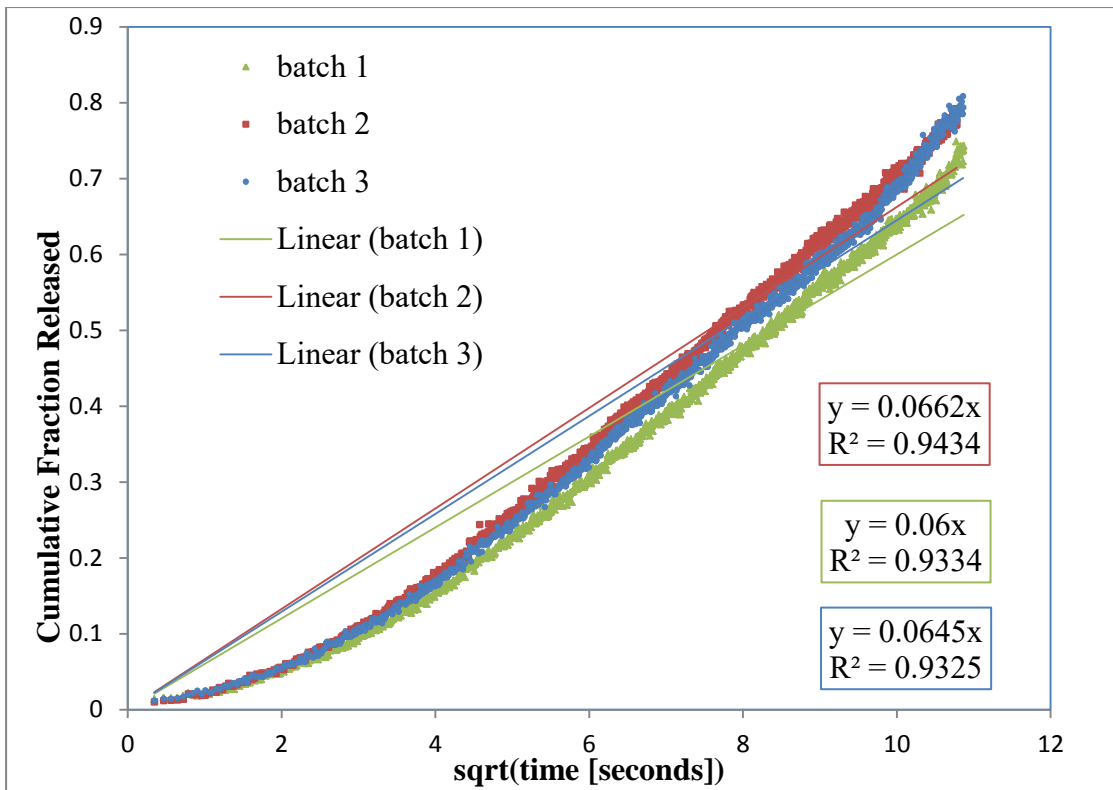
Figure 4.14: Higuchi model for NH2 liposomes at 7.46 mW/cm^2.
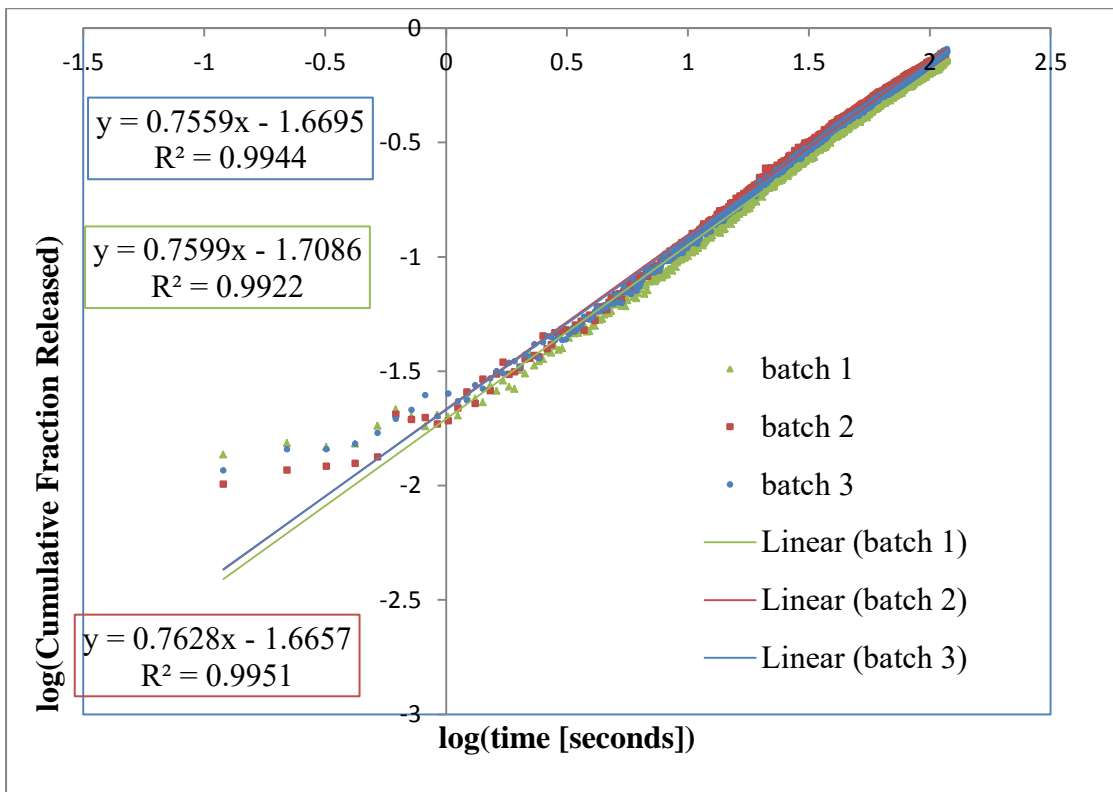
Figure 4.15: Korsmeyer-Peppas model for NH2 liposomes at 7.46 mW/cm^2.
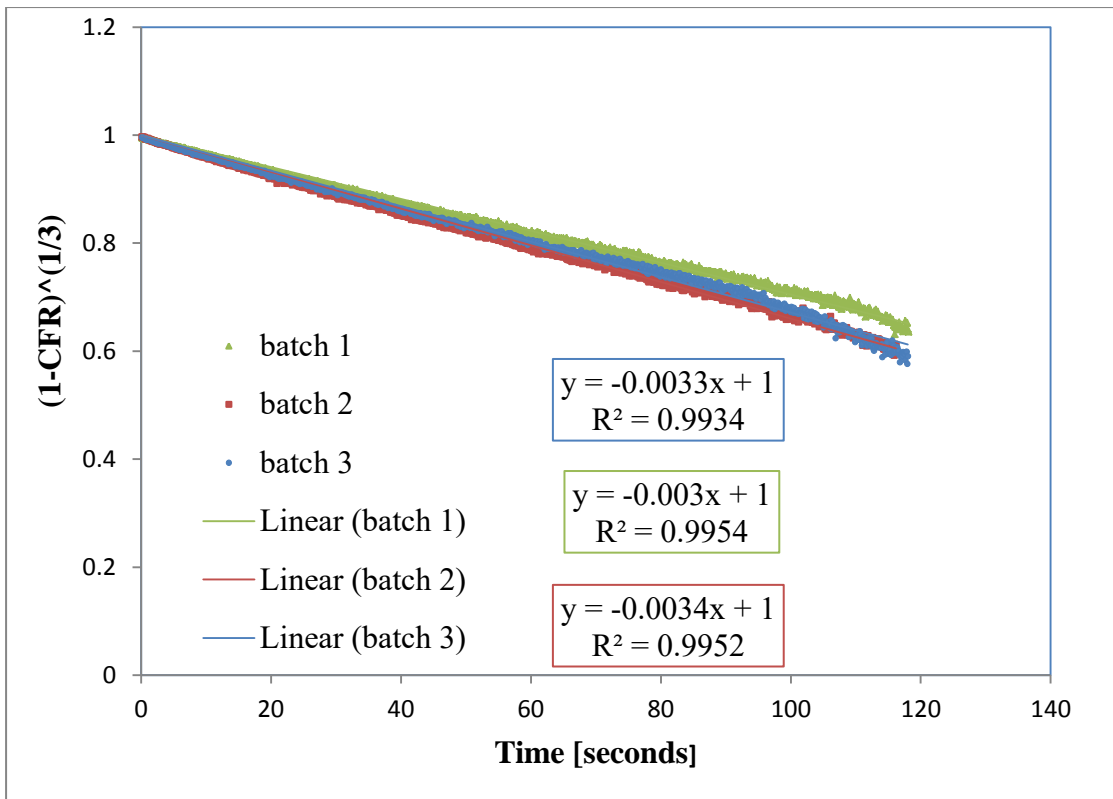
Figure 4.16: Hixson-Crowell model for NH2 liposomes at 7.46 mW/cm^2.
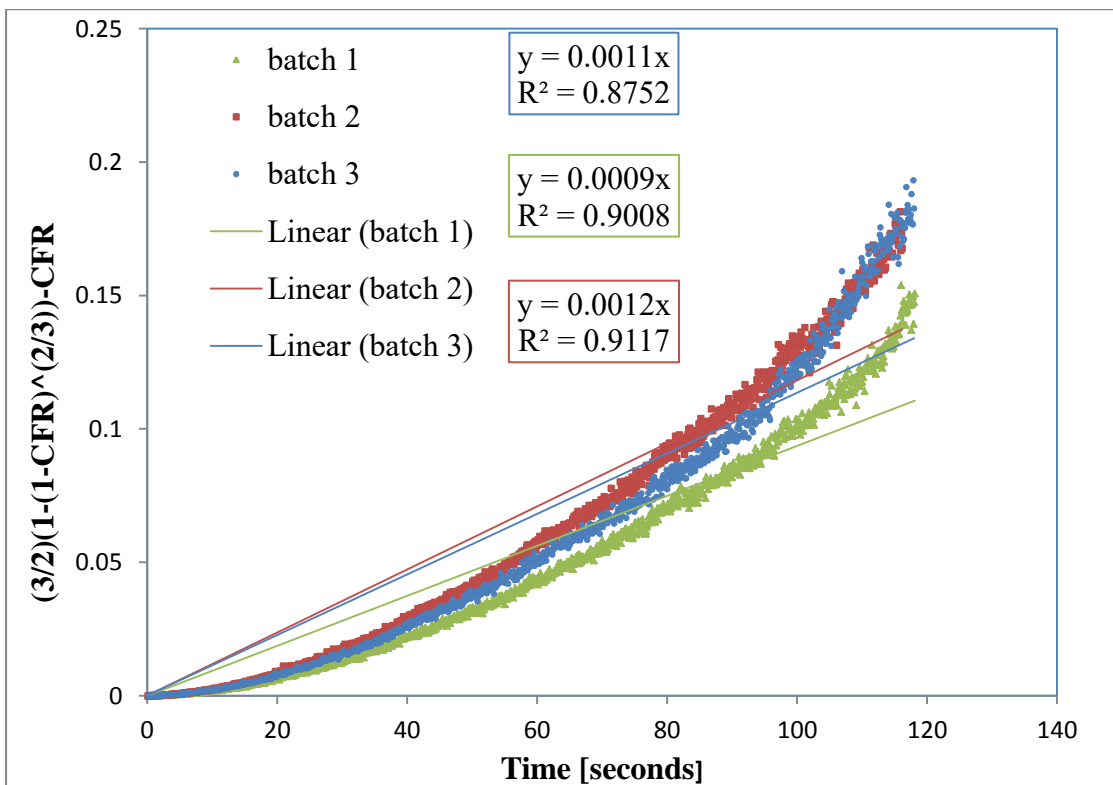
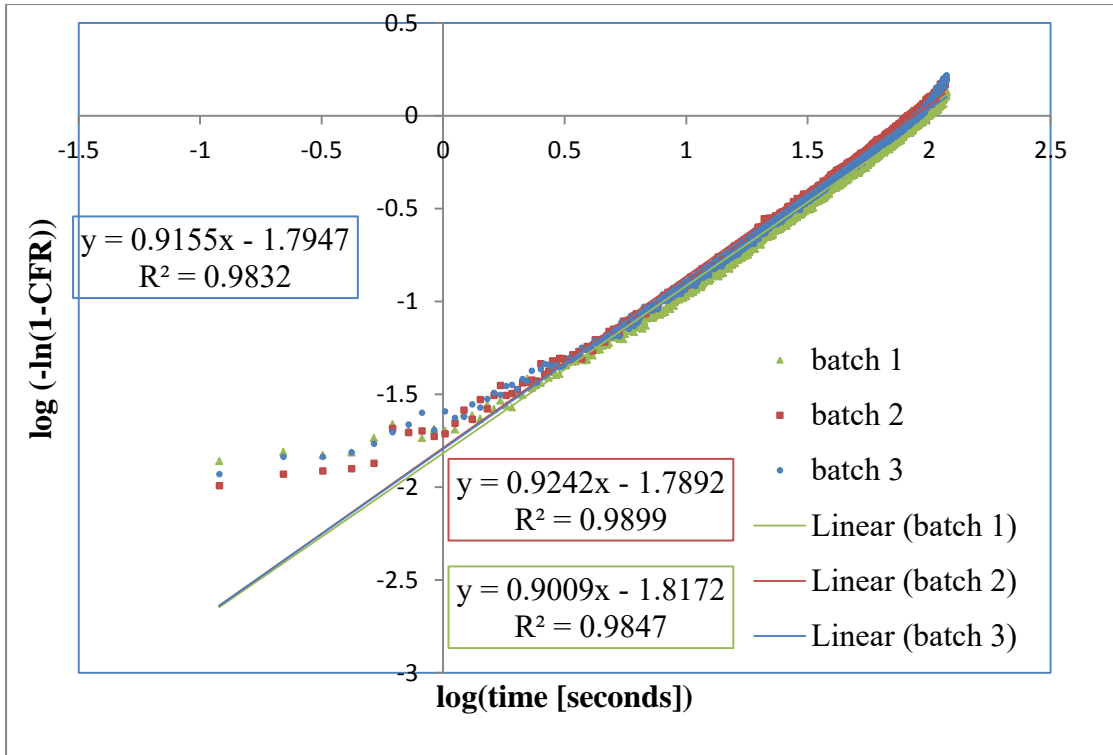Figure 4.17: Baker-Lonsdale model for NH2 liposomes at 7.46 mW/cm^2.

81

Figure 4.18: Weibull model for NH2 liposomes at 7.46 mW/cm^2.
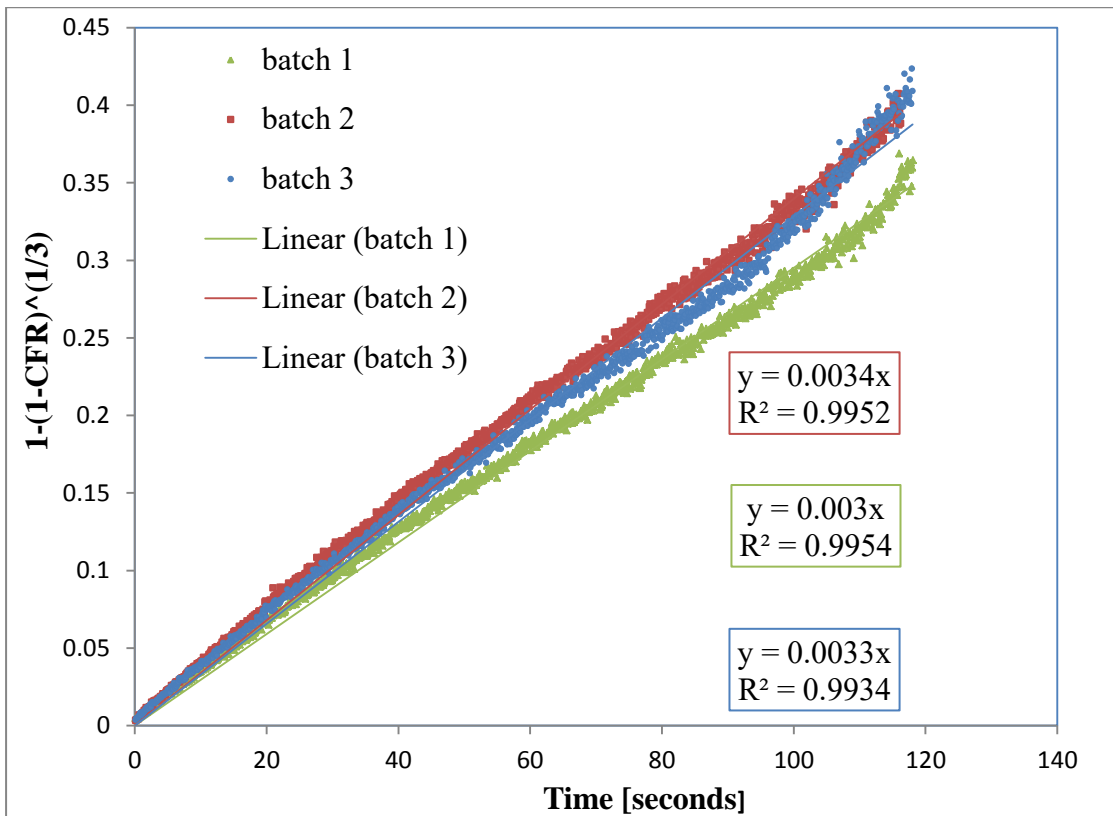
Figure 4.19: Hopfenberg model for NH2 liposomes at 7.46 mW/cm^2.

82
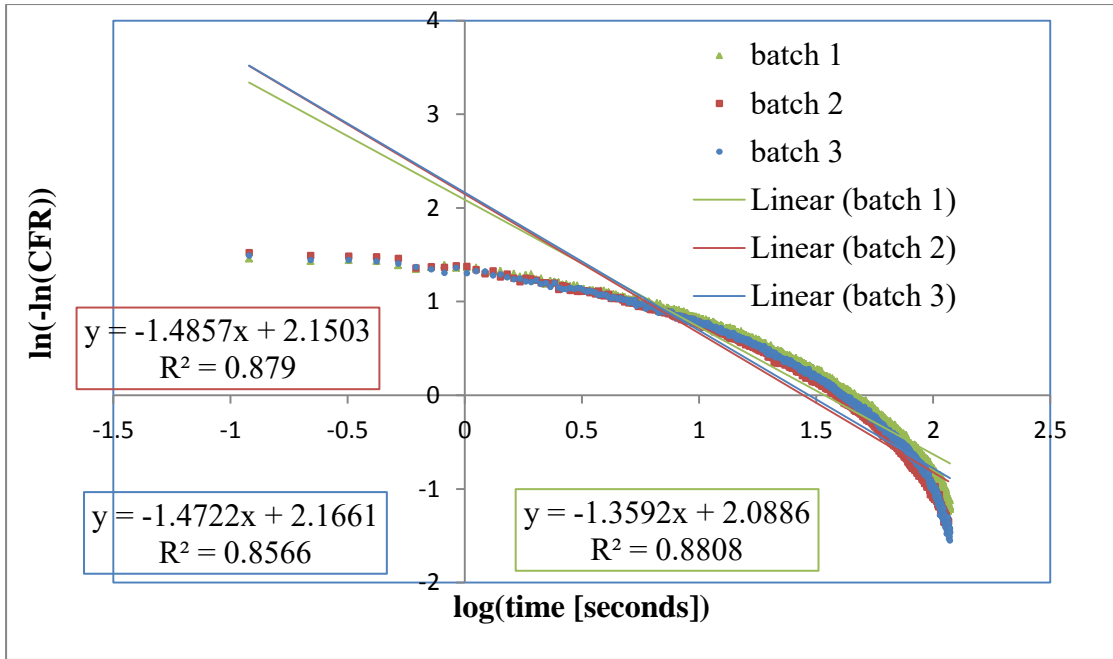
Figure 4.20: Gompertz model for NH2 liposomes at 7.46 mW/cm^2.

Table 4.8: R^2 values of different models for NH2 liposomes at each power density.

R^2 values	NH2 liposomes batch	Zero order	First order	Higuchi	Korsmeyer-Peppas
7.46 (mW/cm^2)	1	0.9490	0.7697	0.9334	0.9922
	2	0.9319	0.7451	0.9434	0.9951
	3	0.9509	0.7697	0.9325	0.9944
9.85 (mW/cm^2)	1	0.9688	0.7811	0.9163	0.9961
	2	0.9558	0.7658	0.9280	0.9953
	3	0.9618	0.7821	0.9224	0.9952
17.31 (mW/cm^2)	1	0.9718	0.7928	0.9094	0.9950
	2	0.9567	0.7642	0.9282	0.9973
	3	0.9724	0.7823	0.9089	0.9965
Average		0.9577	0.7725	0.9247	0.9952

Table 4.9: R^2 values of different models for NH2 liposomes at each power density.

R^2 values	NH2 liposomes batch	Hixson-Crowell	Baker-Lonsdale	Weibull	Hopfenberg	Gompertz
7.46 (mW/cm^2)	1	0.9954	0.9008	0.9847	0.9954	0.8808
	2	0.9952	0.9117	0.9899	0.9952	0.879
	3	0.9934	0.8752	0.9832	0.9934	0.8566
9.85 (mW/cm^2)	1	0.9957	0.8718	0.9868	0.9958	0.8744
	2	0.9967	0.8853	0.987	0.9967	0.8689
	3	0.992	0.8606	0.9831	0.9920	0.8571
17.31 (mW/cm^2)	1	0.9839	0.8251	0.9801	0.9839	0.8422
	2	0.9932	0.8662	0.9878	0.9932	0.8576
	3	0.9822	0.8212	0.9815	0.9822	0.8333
Average		0.9920	0.8687	0.9849	0.9920	0.8611
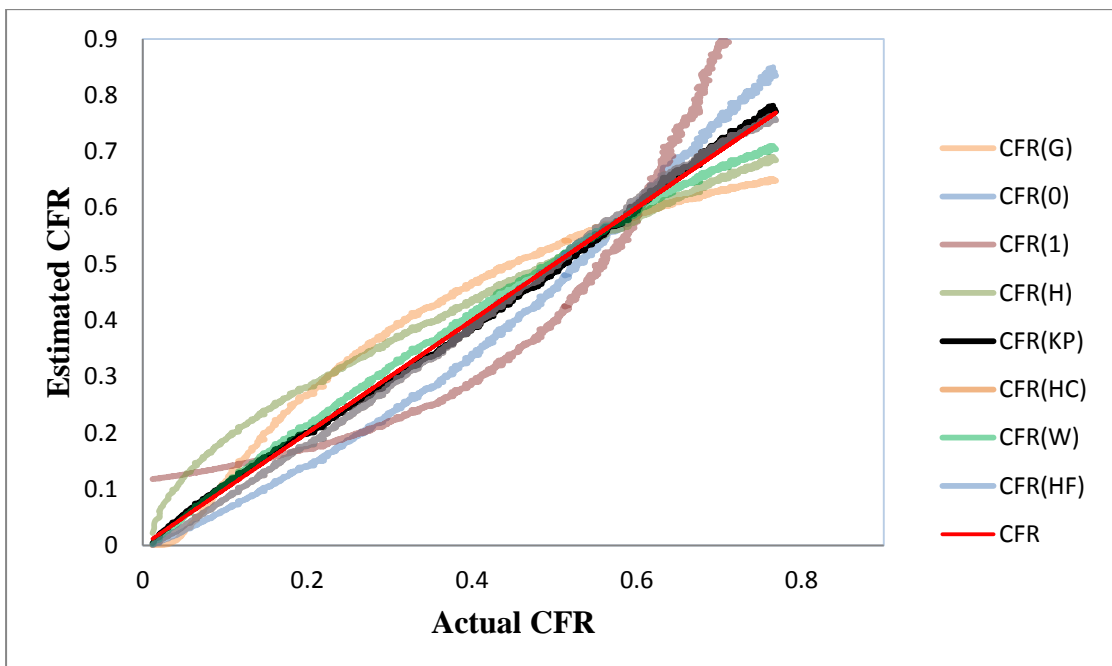
Figure 4.21: Parity plot for 3-batch averaged NH2 liposomes at 7.46 (mW/cm^2).
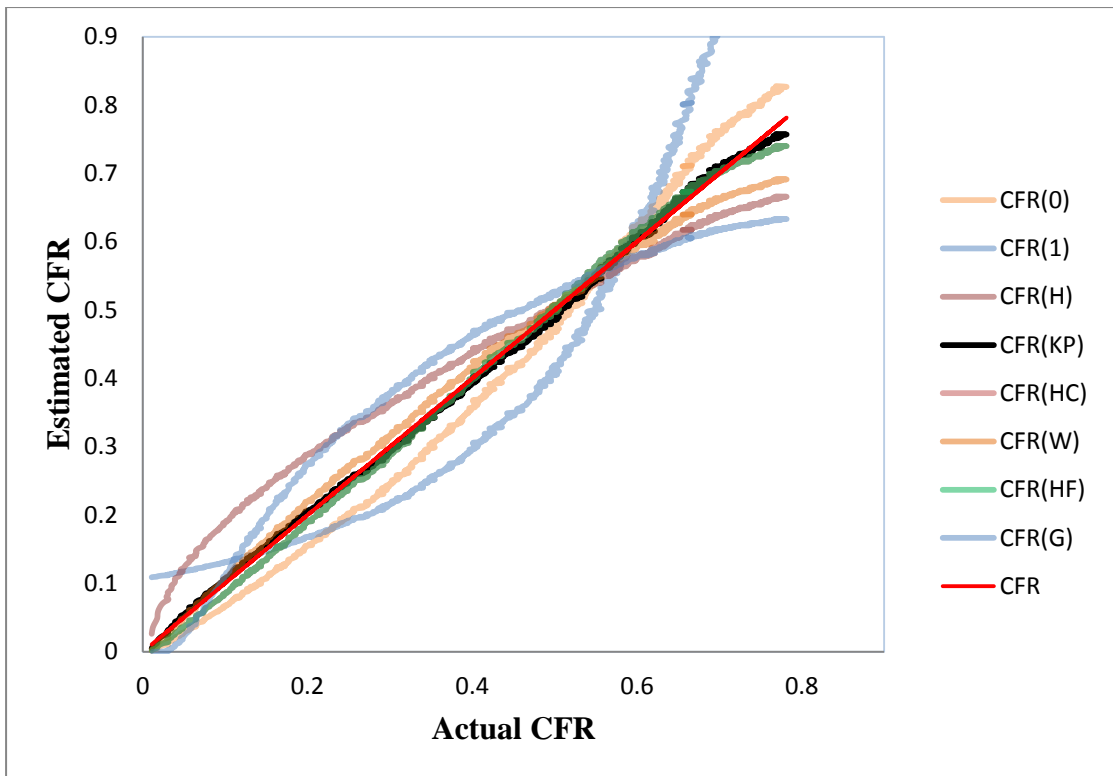
Figure 4.22: Parity plot for 3-batch averaged NH2 liposomes at 9.85 (mW/cm^2).
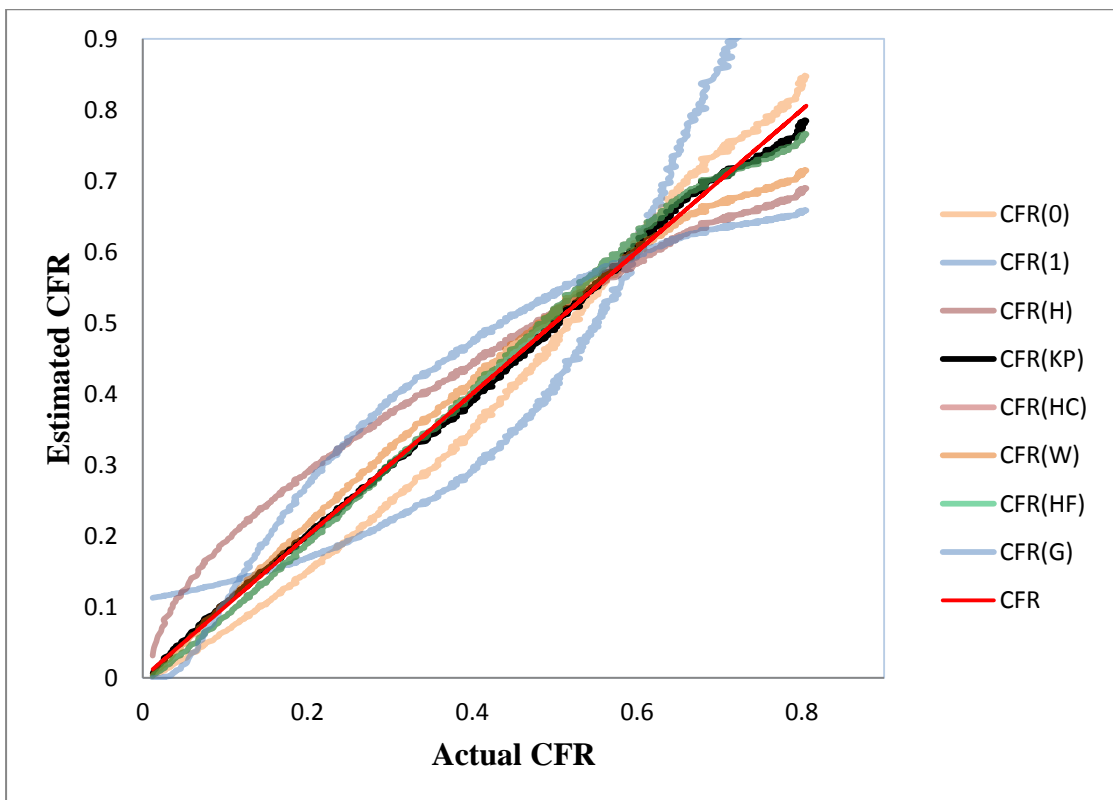
Figure 4.23: Parity plot for 3-batch averaged NH2 liposomes at 17.31 (mW/cm^2).
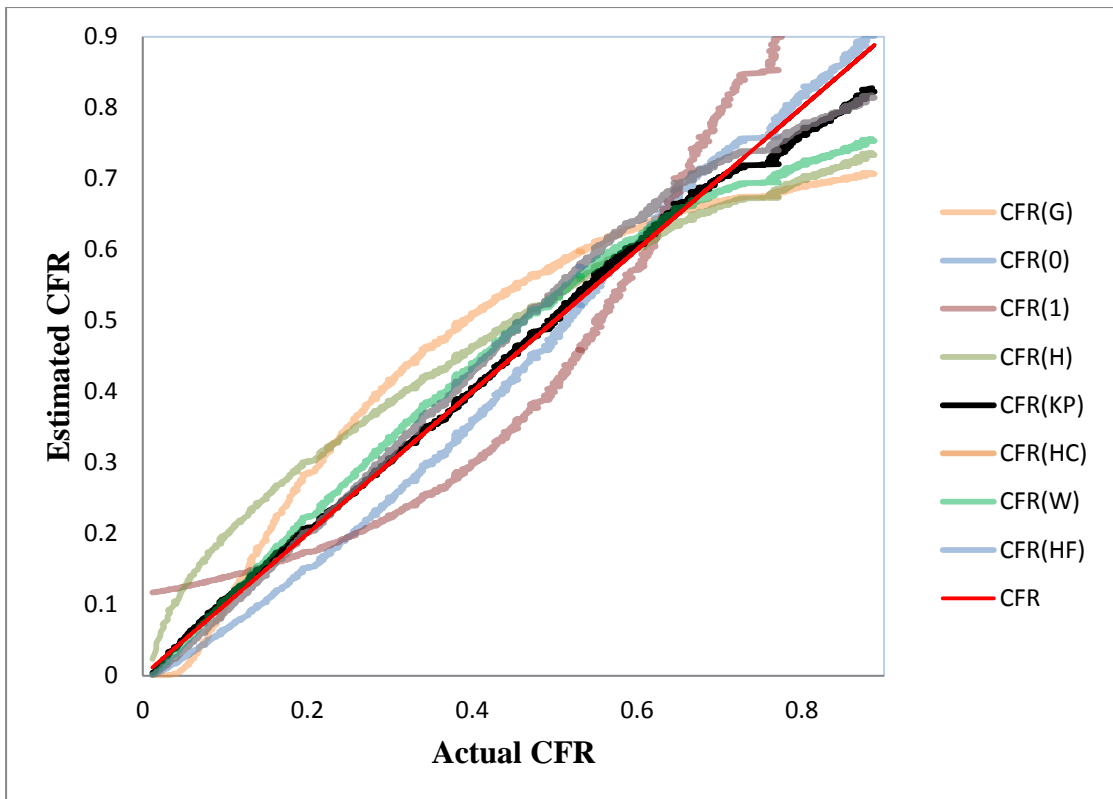
Figure 4.24: Parity plot for 3-batch averaged immunoliposomes at 7.46 (mW/cm^2).
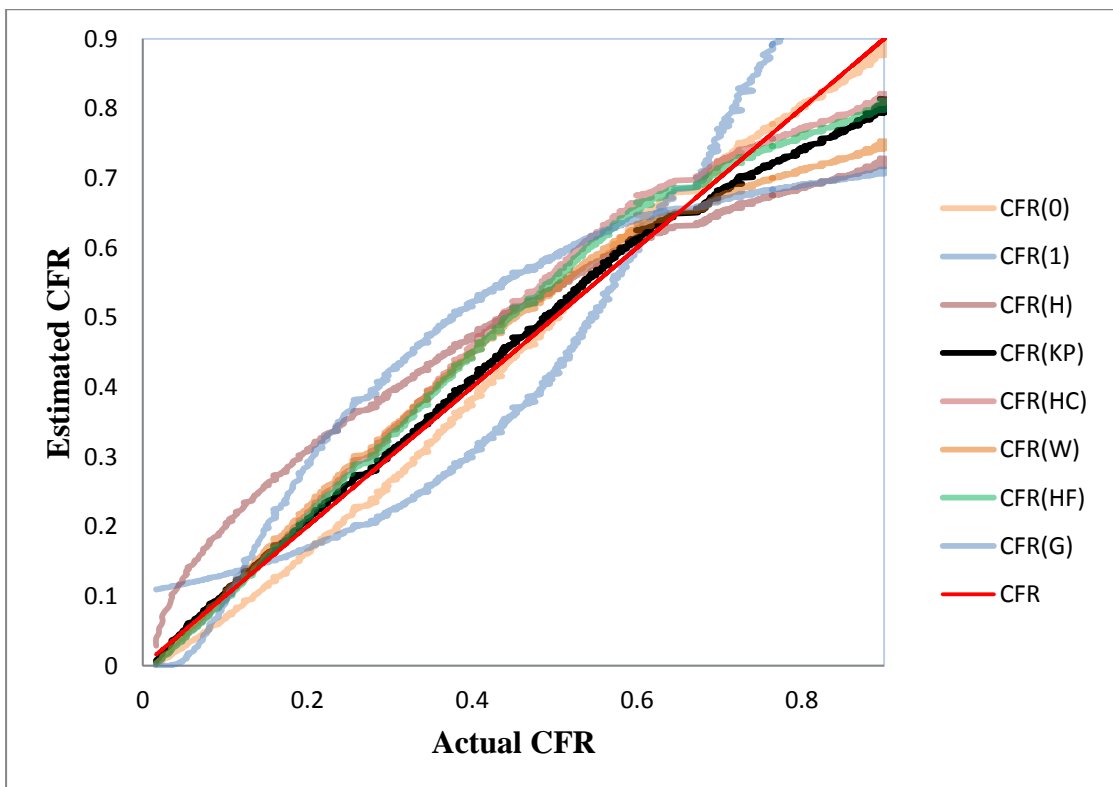
Figure 4.25: Parity plot for 3-batch averaged immunoliposomes at 9.85 (mW/cm^2).
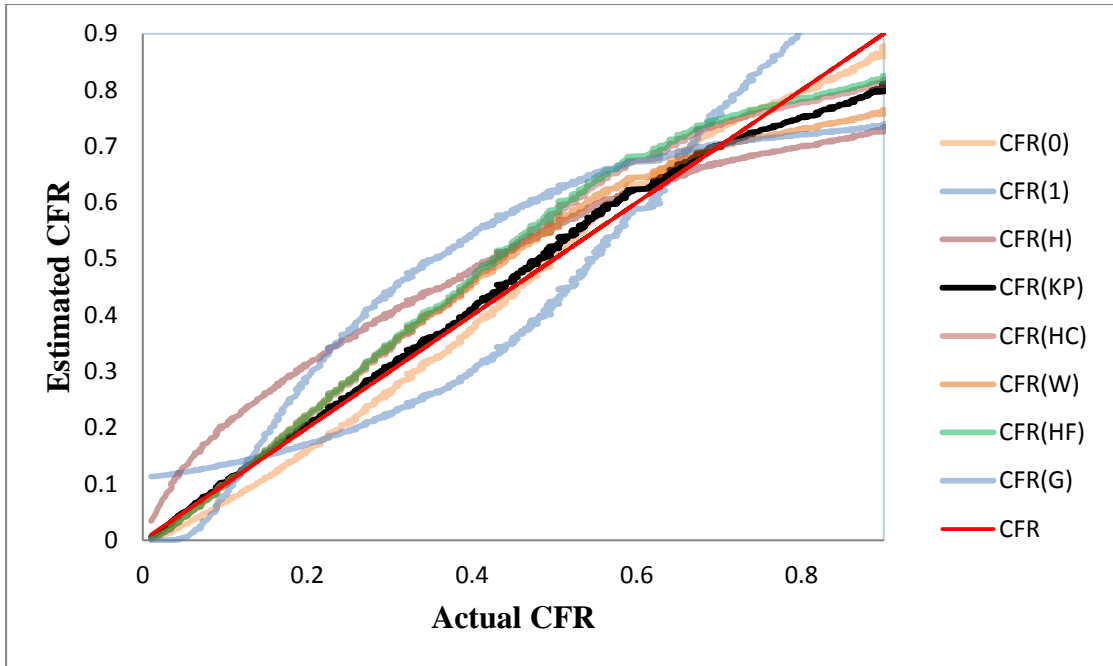
Figure 4.26: Parity plot for 3-batch averaged immunoliposomes at 17.31 (mW/cm^2).

Table 4.10: R^2 values of different models for immunoliposomes at each power density.

R^2 values	Immunoliposomes batch	Zero order	First order	Higuchi	Korsmeyer-Peppas
7.46 (mW/cm^2)	1	0.9729	0.7991	0.9027	0.9937
	2	0.9784	0.7924	0.9050	0.9936
	3	0.9838	0.8135	0.8856	0.9915
9.85 (mW/cm^2)	1	0.9812	0.8136	0.8782	0.9919
	2	0.9892	0.8221	0.8745	0.9906
	3	0.9892	0.8431	0.8528	0.9847
17.31 (mW/cm^2)	1	0.9820	0.8160	0.8560	0.9936
	2	0.9905	0.8066	0.8642	0.9957
	3	0.9886	0.8399	0.8640	0.9887
Average		0.9840	0.8163	0.8759	0.9916

Table 4.11: R^2 values of different models for immunoliposomes at each power density.

R^2 values	immunoliposomes batch	Hixson-Crowell	Baker-Lonsdale	Weibull	Hopfenberg	Gompertz
7.46 (mW/cm^2)	1	0.9509	0.7587	0.9616	0.9509	0.7554
	2	0.9784	0.8116	0.9712	0.9784	0.7991
	3	0.9560	0.7667	0.9582	0.9560	0.7599
9.85 (mW/cm^2)	1	0.9379	0.7209	0.9612	0.9379	0.7611
	2	0.9433	0.7386	0.9557	0.9433	0.7472
	3	0.9066	0.7044	0.9276	0.9066	0.6735
17.31 (mW/cm^2)	1	0.8851	0.6641	0.9409	0.8851	0.6675
	2	0.9208	0.7231	0.9517	0.9208	0.7020
	3	0.9186	0.7121	0.9379	0.9186	0.6963
Average		0.9331	0.7334	0.9518	0.9331	0.7291

4.5.12. Calculations of k_{KP} values. According to Korsmeyer-Peppas model, a log-inverse of the intersect value yields the k_{kp} rate constant. The constant values are shown in Table 4.12.

Looking at Table 4.13, a two-factor ANOVA analysis shows that the F-value is lower than the F-critical value, and hence no significant difference exists between k_{kp} values for both types. This indicates that the release rate constant is not affected by the type of carrier. This means that immunoliposomes follow the exact same release pattern as the control ones. The second F-value is shown to be higher than the F-critical, which indicates that k_{kp} are significantly affected by the power density. This is expected since a higher release rate was obtained with increased power density.

Table 4.12: Rate constant of Korsmeyer-Peppas model for both types of liposomes at each power density.

K_{kp} values (n=0.7742)			
NH2 liposomes	7.46 (mW/cm^2)	9.85 (mW/cm^2)	17.31 (mW/cm^2)
Batch # 1	1.96E-02	2.32E-02	3.17E-02
Batch # 2	2.16E-02	2.63E-02	3.41E-02
Batch # 3	2.14E-02	2.69E-02	3.13E-02
average	2.09E-02	2.55E-02	3.24E-02
Std. dev.	1.12E-03	1.97E-03	1.55E-03
Immunoliposomes (n=0.7896)			
Batch # 1	2.26E-02	2.56E-02	3.24E-02
Batch # 2	1.98E-02	2.53E-02	3.04E-02
Batch # 3	2.05E-02	2.73E-02	3.51E-02
average	2.09E-02	2.61E-02	3.26E-02
Std. dev.	1.47E-03	1.05E-03	2.34E-03

Table 4.13: Two-factor ANOVA analysis of K_{KP} values.

Source of Variation	SS	df	MS	F	P-value	F crit
Sample	4.14E-07	1	4.14E-07	0.15	0.70	4.75
Columns	4.06E-04	2	2.03E-04	74.82	1.67E-07	3.89
Interaction	1.93E-07	2	9.63E-08	0.04	0.97	3.89
Within	3.26E-05	12	2.72E-06			
Total	4.40E-04	17				

Chapter 5. Conclusion and Recommendations

Conventional cancer therapy results in critical side effects limiting its use. Drug delivery systems have changed the way chemotherapy work, by enhancing its pharmacokinetics and bio-distribution in the vicinity of tumors. Nanocarriers shield healthy cells and allow the drug to only interact with cancer cells, thus reducing unwanted side effects. Liposomes in modern drug delivery systems are used as nanocarriers. They are physically attracted to tumor cells via the enhanced permeability and retention effect (EPR). They can also be engineered to increase their selectivity toward cancer cells by conjugating targeting moieties to their surface. Once these targeted liposomes reach the tumor site, the drug can be released using low-frequency ultrasound, thus, resulting in a well-controlled, extremely specific, and highly cytotoxic cancer treatment. The system suggested in this thesis is immunoliposomes targeting HER2 breast cancer. The monoclonal antibody, Trastuzumab, is used as a targeting moiety due to its high affinity toward HER2 breast cancer.

In this thesis, the behavior of immunoliposomes encapsulating a model drug, namely calcein, was compared to conventional liposomes (NH_2 liposomes), to study the effect of incorporating the targeting ligand. Liposomes were made by the lipid hydration method. Then immunoliposomes were made by the conjugate of Trastuzumab to their surface. Moiety attachment was confirmed by the methods of Stewart and BCA assays. After that, both types of liposomes were tested for their release under low-frequency ultrasound at 20 kHz. Finally, release kinetics were investigated using 9 kinetic models.

This thesis is the first to report successful drug release from immunoliposomes upon exposure to LFUS. Immunoliposomes were found sensitive to ultrasound and do not agglomerate upon sonication. They were found to successfully release their contents at low frequency (of 20 kHz) and intensities ranging from 7.46 to 17.31 mW/cm^2. These parameters are considered a starting point for drug delivery studies *in vivo*. Ultrasound results in a well-controlled and highly effective cancer treatment.

Nine Trastuzumab molecules were attached to each liposome vesicle, which was considered enough to induce the affinity effect needed to target HER2 overexpressed on breast cancer cells.

Liposome sizes were found to fall within the optimal range for the EPR effect to take place, with a radius of about 101.1 and 89.5 (nm) for immunoliposomes and NH_2 liposomes, respectively.

Low-frequency ultrasound studies showed ideal release profiles that would be needed for successful controlled release, in which a large amount of the drug is initially released, to reach therapeutic levels, followed by a sustained release to maintain therapeutic effectiveness. Both liposomes types exhibited sensitivity and released their contents in a stable manner upon exposure to LFUS at relatively low intensities. Immunoliposomes were found more responsive to ultrasound than NH2 control liposomes, which was due to the attached moiety absorbing more acoustic energy. The release rate was shown to be proportional to the power density and exposure time of LFUS. The release is a result of mechanical effects only and not thermal effects. It is cumulative, allowing for different modes of operation to results in the same release amount after the same exposure time. This was considered important in controlling release rates over prolonged periods of time. The LFUS used was considerably below the safety limit for human exposure, which allows for the flexibility of increasing the intensity whenever needed for *in vivo* studies.

Modeling release kinetics was done to reduce the number of unnecessary bio-studies conducted to measure release. Korsmeyer-Peppas model was found to be the best fitting model for the release data of both types of liposomes. This suggests that both types have similar behavior, hence similar mechanisms. The rate constant was affected by the type of carrier, but by the parameters of ultrasound.

For future work, firstly, the integrity of the attached antibody should be confirmed by cytotoxicity studies on the SKBR3 cell line overexpressing HER2 receptors. Secondly, the release profile for an actual drug (Doxorubicin) should be tested. This thesis is considered a starting point for optimizing ultrasound parameters for the release of a chemotherapeutic drug from immunoliposomes. Testing the release at higher frequencies, and intensities can provide additional insights into the best way to implement drug delivery *in vivo* and in clinics. The complexity of the human body makes it more unpredictable for clinical trials, bearing in mind the safety limits. It all starts, however, with the knowledge of this study results, and the capability of the drug to respond to ultrasound effectively and in a controlled manner.

References

[1]   K. Hunt and S. M. Love. (2016, 2017/1/25). "Breast cancer and other breast disorders." *AccessScience.* Available: http://www.accessscience.com/content/breast-cancer-and-other-breast-disorders/094800

[2]   O. R. Oakley. (2015, 2017/1/25). "Cancer, immunotherapy, and mouse avatars." *AccessScience.* Available: http://www.accessscience.com/content/cancer-immunotherapy-and-mouse-avatars/YB150670

[3]   G. Sharma, S. Anabousi, C. Ehrhardt, and M. N. V. Ravi Kumar, "Liposomes as targeted drug delivery systems in the treatment of breast cancer," *Journal of Drug Targeting,* vol. 14, no. 5, pp. 301-310, 2006.

[4]   C. GM., *The Cell: A Molecular Approach.* Sunderland, MA: Sinauer Associates; 2000.

[5]   S. P. Hammar. (2016, 2017/1/25). "Cancer." *AccessScience*. Available: http://www.accessscience.com/content/cancer/105800

[6]   D. L. Longo. (2016, 2017/1/25). "Oncology." *AccessScience*. Available: http://www.accessscience.com/content/oncology/469000

[7]   P. Masuzzo and L. Martens, "An open data ecosystem for cell migration research," *Trends in Cell Biology*, vol. 25, no. 2, pp. 55-58, Dec., 2014.

[8]   Y. Kato *et al.*, "Acidic extracellular microenvironment and cancer," *Cancer Cell International,* vol. 13, no. 1, pp. 1-8, 2013.

[9]   M. W. Pickup, J. K. Mouw, and V. M. Weaver, "The extracellular matrix modulates the hallmarks of cancer," *EMBO reports,* vol. 15, no. 12, pp. 1243-1253, 2014.

[10]   S. Parbhoo, "Breast cancer overview," ed. London: Cancerkin, Royal Free Hospital, 2005.

[11]   A. Dittrich, H. Gautrey, D. Browell, and A. Tyson-Capper, "The HER2 Signaling Network in Breast Cancer—Like a Spider in its Web," *Journal of Mammary Gland Biology and Neoplasia,* vol. 19, no. 3-4, pp. 253-270, 2014.

[12]   S. M na rd, S. Fortis, F. astiglioni, . g resti, and .   alsari, HE 2 as a prognostic factor in breast cancer," *Oncology,* vol. 61, no. 2, pp. 67-72, 2001.

[13]   R. Kurzrock and M. Markman, *Targeted cancer therapy* (Current clinical oncology; Current clinical oncology), Totowa: Humana Press, 2008.

[14]   R. H. Alvarez, *Handbook of HER2-targeted agents in breast cancer*. Switzerland: Adis, 2016.

[15]   G. W. Sledge, "VEGF-Targeting Therapy for Breast Cancer," *Journal of Mammary Gland Biology and Neoplasia,* vol. 10, no. 4, pp. 319-23, 2005.

[16]   C. P. Burns and D. A. Vaena. (2016, 2017/2/5). "Chemotherapy and other antineoplastic drug treatments." *AccessScience*. Available: http://www.accessscience.com/content/chemotherapy-and-other-antineoplastic-drug-treatments/128900

[17]   J. Kan-Mitchell and M. S. Mitchell. (2014, 2017/1/25). "Immunotherapy." *AccessScience.* Available: http://www.accessscience.com/content/immunotherapy/338970

[18]   D. Escors, "Tumour Immunogenicity, Antigen Presentation, and Immunological Barriers in Cancer Immunotherapy," *New Journal of Science,* vol. 2014, no. 7, pp. 1-25, 2014.

[19]   D. G. Duda. (2016, 2017/2/5). "Immune checkpoint blockade." *AccessScience*. Available: http://www.accessscience.com/content/immune-checkpoint-blockade/337970

[20]   W. M. Saltzman and V. P. Torchilin. (2014, 2017/2/19). "Drug delivery systems." *AccessScience*. Available: http://www.accessscience.com/content/drug-delivery-systems/757275

[21]   R. Langer, "New Methods of Drug Delivery," *Science,* vol. 249, no. 4976, pp. 1527-1533, 1990.

[22]   M. S. El-Shall. (2014, 2017/3/10). "Nanoparticles." *AccessScience*. Available: http://www.accessscience.com/content/nanoparticles/802960

[23]   M. A. Elkhodiry *et al.*, "Synergistic Nanomedicine: Passive, Active, and Ultrasound-Triggered Drug Delivery in Cancer Treatment," *Journal of nanoscience and nanotechnology,* vol. 16, no. 1, pp. 1-18, 2016.

[24]   A. M. Martins, S. A. Elgaili, R. F. Vitor, and G. A. Husseini, "Ultrasonic Drug Delivery Using Micelles and Liposomes," in *Handbook of Ultrasonics and Sonochemistry*: Singapore : Springer Singapore : Springer, 2016, pp. 1127-1161.

[25]   N. Mohammad and G. A. Hussieni, "Acoustically activated release of estrone-targeted liposomes used for breast cancer treatment," M.S. thesis, American University of Sharjah, United Arab Emirates, 2016.

[26]   S. E. Ahmed, A. M. Martins, and G. A. Husseini, "The use of ultrasound to release chemotherapeutic drugs from micelles and liposomes," *Journal of Drug Targeting,* vol. 23, no. 1, 2015.

[27]   R. C. MacDonald, "Liposomes," *AccessScience*. 2014, Available: https://www-accessscience-com.aus.idm.oclc.org/content/liposomes/385650

[28]   M. Oula Penate, Z. Ying, and K. Kalevi, "Targeted Liposomal Drug Delivery in Cancer," *Current Pharmaceutical Design,* vol. 10, pp. 2981-2989, 2004.

[29]   V. P. Torchilin, "Recent advances with liposomes as pharmaceutical carriers," *Nature Reviews Drug Discovery,* vol. 4, no. 2, pp. 145-160, 2005.

[30]   M. U. Ahmad, *Lipids in Nanotechnology*. Academic Press and AOCS Press: Elsevier Inc., 2013.

[31]   T. M. Allen and F. J. Martin, "Advantages of liposomal delivery systems for anthracyclines," *Seminars in oncology,* vol. 31, no. 6 Suppl 13, pp. 5-15, 2004.

[32]   B. Bahrami *et al.*, "Folate-conjugated nanoparticles as a potent therapeutic approach in targeted cancer therapy," *Tumor Biology : Tumor Markers, Tumor Targeting and Translational Cancer Research,* vol. 36, no. 8, pp. 5727-5742, 2015.

[33]   Z. Cao, L. Zhang, and S. Jiang, "Superhydrophilic zwitterionic polymers stabilize liposomes," *Langmuir : the ACS journal of surfaces and colloids,* vol. 28, no. 31, pp. 11625-32, 2012.

[34]   G. Bendas, A. Krause, U. Bakowsky, J. Vogel, and U. Rothe, "Targetability of novel immunoliposomes prepared by a new antibody conjugation technique," *International Journal of Pharmaceutics,* vol. 181, no. 1, pp. 79-93, 1999.

[35]   H. Maeda, "Vascular permeability in cancer and infection as related to macromolecular drug delivery, with emphasis on the EPR effect for tumor-selective drug targeting," *Proceedings of the Japan Academy. Series B, Physical and biological sciences,* vol. 88, no. 3, pp. 53-71, 2012.

[36]   H. Maeda, J. Wu, T. Sawa, Y. Matsumura, and K. Hori, "Tumor vascular permeability and the EPR effect in macromolecular therapeutics: a review,"

Journal of controlled release : official journal of the Controlled Release Society, vol. 65, no. 1-2, pp. 271-84, 2000.

[37] A. M. Jhaveri and V. P. Torchilin, "Multifunctional polymeric micelles for delivery of drugs and siRNA," *Frontiers in pharmacology,* vol. 5, pp. 40-77, 2014.

[38] Y. Matsumura and H. Maeda, "A new concept for macromolecular therapeutics in cancer chemotherapy: mechanism of tumoritropic accumulation of proteins and the antitumor agent smancs," (in eng), *Cancer Res,* vol. 46, no. 12 Pt 1, pp. 6387-6392, Dec 1986.

[39] Y. Noguchi *et al.*, "Early Phase Tumor Accumulation of Macromolecules: A Great Difference in Clearance Rate between Tumor and Normal Tissues," *Japanese Journal of Cancer Research,* vol. 89, no. 3, pp. 307-314, 1998.

[40] H. Hashizume *et al.*, "Openings between Defective Endothelial Cells Explain Tumor Vessel Leakiness," *The American Journal of Pathology,* vol. 156, no. 4, pp. 1363-1380, 2000.

[41] D. H. Shin, M. J. Koo, and J. S. Kim, "Herceptin-conjugated temperature-sensitive immunoliposomes encapsulating gemcitabine for breast cancer," *Archives of pharmacal research : a publication of the Pharmaceutical Society of Korea.,* vol. 39, no. 3, pp. 350-358, 2016.

[42] M. Mishra, *Liposomes: Clinical aspects and challenges*. 2018.

[43] R. I. Nicholson, J. M. W. Gee, and M. E. Harper, "EGFR and cancer prognosis," *European Journal of Cancer: Supplement 4,* vol. 37, no. Supplement 4, pp. 9-15, 2001.

[44] A. Gabizon *et al.*, "Targeting folate receptor with folate linked to extremities of poly(ethylene glycol)-grafted liposomes: in vitro studies," *Bioconjugate chemistry,* vol. 10, no. 2, pp. 289-98, 1999.

[45] H. S. Yoo and T. G. Park, "Folate receptor targeted biodegradable polymeric doxorubicin micelles," *Journal of Controlled Release,* vol. 96, no. 2, pp. 273-283, 2004.

[46] W. Guo, T. Lee, J. Sudimack, and R. J. Lee, "Receptor-Specific Delivery of Liposomes Via Folate-Peg-Chol," *Journal of Liposome Research,* vol. 10, no. 2-3, pp. 179-195, 2008.

[47] D. A. Eavarone, X. Yu, and R. V. Bellamkonda, "Targeted drug delivery to C6 glioma by transferrin-coupled liposomes," (in eng), *J Biomed Mater Res,* vol. 51, no. 1, pp. 10-14, Jul 2000.

[48] J. Huwyler, D. Wu, and W. M. Pardridge, "Brain drug delivery of small molecules using immunoliposomes," *Proceedings of the National Academy of Sciences of the United States of America,* vol. 93, no. 24, pp. 14164-14169, 1996.

[49] A. M. Master and A. Sen Gupta, "EGF receptor-targeted nanocarriers for enhanced cancer treatment," *Nanomedicine (London, England),* vol. 7, no. 12, pp. 1895-906, 2012.

[50] R. Bazak, M. Houri, S. El Achy, S. Kamel, and T. Refaat, "Cancer active targeting by nanoparticles: a comprehensive review of literature," *Journal of Cancer Research and Clinical Oncology,* vol. 141, no. 5, pp. 769-784, 2015.

[51] P. Sapra and T. M. Allen, "Internalizing antibodies are necessary for improved therapeutic efficacy of antibody-targeted liposomal drugs," (in eng), *Cancer Res,* vol. 62, no. 24, pp. 7190-4, Dec 15 2002.

[52] M. J. Polley and Z. Cohen. (2014, 2017/4/18). "Antigen." *AccessScience*. Available: http://www.accessscience.com/content/antigen/040600

[53]   J. J. Cohen. (2016, 2017/4/18). "Antibody." *AccessScience*. Available: http://www.accessscience.com/content/antibody/040100

[54]   A. Baumgarten. (2014, 2017/4/6). "Antigen-antibody reaction." *AccessScience*. Available: http://www.accessscience.com/content/antigen-antibody-reaction/040700

[55]   J. K. H. Liu, "The history of monoclonal antibody development – Progress, remaining challenges and future innovations," *Annals of Medicine and Surgery,* vol. 3, no. 4, pp. 113-116, 2014.

[56]   F. M. Brodsky. (2014, 2017/1/28). "Monoclonal antibodies." *AccessScience*. Available: http://www.accessscience.com/content/monoclonal-antibodies/432975

[57]   R. Abramson. (2016). *Overview of Targeted Therapies for Cancer*. Available: https://www.mycancergenome.org/content/molecular-medicine/overview-of-targeted-therapies-for-cancer/

[58]   F. A. Harding, M. M. Stickler, J. Razo, and R. B. DuBridge, "The immunogenicity of humanized and fully human antibodies: Residual immunogenicity resides in the CDR regions," *MAbs,* vol. 2, no. 3, pp. 256-265, May-Jun 2010.

[59]   S. M. Ansell, T. O. Harasym, P. G. Tardi, S. S. Buchkowsky, M. B. Bally, and P. R. Cullis, "Antibody Conjugation Methods for Active Targeting of Liposomes," in *Drug Targeting : Strategies, Principles, and Applications* (Methods in Molecular Medicine™ 1940-6037) Totowa, NJ : Humana Press, 2000, pp. 51-68.

[60]   K. Garnock-Jones, G. Keating, and L. Scott, "Spotlight on Trastuzumab as Adjuvant Treatment in Human Epidermal Growth Factor Receptor 2 (HER2)-Positive Early Breast Cancer," *BioDrugs,* vol. 24, no. 3, pp. 207-209, 2010.

[61]   H. G. Moussa, A. M. Martins, and G. A. Husseini, "Review on triggered liposomal drug delivery with a focus on ultrasound," *Current Cancer Drug Targets,* vol. 15, no. 4, pp. 282-313, 2015.

[62]   Y. Barenholz *et al.*, "Stability of liposomal doxorubicin formulations: problems and prospects," *Medicinal research reviews,* vol. 13, no. 4, pp. 449-491, 1993.

[63]   E. L. Cussler, *Controlled drug delivery: Fundamentals and Application,* vol. 29, Joseph R. Robinson and Vincent H.L. Lee, Eds. New York: Marcel Dekker, 1987.

[64]   . S ve rkr p,   Modeling and data treatment in the pharmaceutical sciences, *European Journal of Pharmaceutics and Biopharmaceutics,* vol. 44, no. 1, pp. 105-106, 1997.

[65]   J. H. Lee and Y. Yeo, "Controlled drug release from pharmaceutical nanocarriers," *Chemical Engineering Science,* vol. 125, pp. 75-84, 2015.

[66]   A. K. Bajpai, S. K. Shukla, S. Bhanu, and S. Kankane, "Responsive polymers in controlled drug delivery," *Progress in Polymer Science,* vol. 33, no. 11, pp. 1088-1118, 2008.

[67]   S. Dash, P. N. Murthy, L. Nath, and P. Chowdhury, "Kinetic modeling on drug release from controlled drug delivery systems," *Acta poloniae pharmaceutica,* vol. 67, no. 3, pp. 217-23, 2010.

[68]   S. K. Ei-Arini and H. Leuenberger, "Modelling of drug release from polymer matrices: Effect of drug loading," *International Journal of Pharmaceutics,* vol. 121, no. 2, pp. 141-148, 1995.

[69] J. W. Park *et al.*, "Tumor targeting using anti-her2 immunoliposomes," *Journal of controlled release : official journal of the Controlled Release Society,* vol. 74, no. 1-3, pp. 95-113, 2001.

[70] J. O. Eloy, R. Petrilli, D. L. Chesca, F. P. Saggioro, R. J. Lee, and J. M. Marchetti, "Anti-HER2 immunoliposomes for co-delivery of paclitaxel and rapamycin for breast cancer therapy," *European Journal of Pharmaceutics and Biopharmaceutics,* vol. 115, no. 4, pp. 159-167, 2017.

[71] M. Kullberg, K. Mann, and T. J. Anchordoquy, "Targeting Her-2+ breast cancer cells with bleomycin immunoliposomes linked to LLO," *Molecular pharmaceutics,* vol. 9, no. 7, pp. 2000-2008, 2012.

[72] L. Nobs, F. uchegger, . Gurny, and E. ll mann, urrent methods for attaching targeting ligands to liposomes and nanoparticles," *Journal of Pharmaceutical Sciences,* vol. 93, no. 8, pp. 1980-1992, 2004.

[73] M. Mercadal, J. C. Domingo, J. Petriz, J. Garcia, and M. A. de Madariaga, "A novel strategy affords high-yield coupling of antibody to extremities of liposomal surface-grafted PEG chains," *BBA - Biomembranes,* vol. 1418, no. 1, pp. 232-238, 1999.

[74] C. B. Hansen, G. Y. Kao, E. H. Moase, S. Zalipsky, and T. M. Allen, "Attachment of antibodies to sterically stabilized liposomes: evaluation, comparison and optimization of coupling procedures," *Biochimica et Biophysica Acta (BBA) - Biomembranes,* vol. 1239, no. 2, pp. 133-144, 1995.

[75] V. P. Torchilin *et al.*, "p-Nitrophenylcarbonyl-PEG-PE-liposomes: fast and simple attachment of specific ligands, including monoclonal antibodies, to distal ends of PEG chains via p-nitrophenylcarbonyl groups," *BBA - Biomembranes,* vol. 1511, no. 2, pp. 397-411, 2001.

[76] K. Maruyama, T. Takizawa, T. Yuda, S. J. Kennel, L. Huang, and M. Iwatsuru, "Targetability of novel immunoliposomes modified with amphipathic poly(ethylene glycol) s conjugated at their distal terminals to monoclonal antibodies," *Biochimica et Biophysica Acta (BBA) - Biomembranes,* vol. 1234, no. 1, pp. 74-80, 1995.

[77] H. Chen *et al.*, "Preparation and characterization of PE38KDEL-loaded anti-HER2 nanoparticles for targeted cancer therapy," *Journal of controlled release : official journal of the Controlled Release Society,* vol. 128, no. 3, pp. 209-216, 2008.

[78] F. J. Martin and D. Papahadjopoulos, "Irreversible coupling of immunoglobulin fragments to preformed vesicles. An improved method for liposome targeting," *The Journal of biological chemistry,* vol. 257, no. 1, pp. 286-288, 1982.

[79] K. Laginha, D. Mumbengegwi, and T. Allen, "Liposomes targeted via two different antibodies: Assay, B-cell binding and cytotoxicity," *BBA - Biomembranes,* vol. 1711, no. 1, pp. 25-32, 2005.

[80] D. Kirpotin *et al.*, "Sterically stabilized anti-HER2 immunoliposomes: design and targeting to human breast cancer cells in vitro," *Biochemistry,* vol. 36, no. 1, pp. 66-75, 1997.

[81] T. Kitagawa, T. Shimozono, T. Aikawa, T. Yoshida, and H. Nishimura, "Preparation and characterization of hetero-bifunctional cross-linking reagents for protein modifications," *Chemical & Pharmaceutical Bulletin,* vol. 29, no. 4, pp. 1130-1135, 1981.

[82] A. M. Yacynych and T. Kuwana, "Cyanuric chloride as a general linking agent for modified electrodes: attachment of redox groups to pyrolytic graphite," *Analytical Chemistry,* vol. 50, no. 4, pp. 640-645, 1978.

[83] R. R. Hood, "Microfluidic-enabled synthesis of immunoliposomes," D. L. DeVoe, Ed., ed. USA: University of Maryland College Park, 2015.

[84] G. Steinberg, K. Stromsborg, L. Thomas, D. Barker, and C. Zhao, "Strategies for covalent attachment of DNA to beads," *Biopolymers,* vol. 73, no. 5, pp. 597-605, 2004.

[85] M. Afadzi *et al.*, "Effect of Ultrasound Parameters on the Release of Liposomal Calcein," *Ultrasound in Medicine & Biology,* vol. 38, no. 3, pp. 476-486, 2012.

[86] T. J. Evjen, E. A. Nilssen, S. Barnert, R. Schubert, M. Brandl, and S. L. Fossheim, "Ultrasound-mediated destabilization and drug release from liposomes comprising dioleoylphosphatidylethanolamine," *European Journal of Pharmaceutical Sciences,* vol. 42, no. 4, pp. 380-386, 2011.

[87] H.-Y. Lin and J. L. Thomas, PEG−Lipids and Oligo(ethylene glycol) Surfactants Enhance the Ultrasonic Permeabilizability of Liposomes," *Langmuir,* vol. 19, no. 4, pp. 1098-1105, 2003.

[88] D. D. Lasic, *Liposomes in gene delivery*. Boca Raton, FL: CRC Press, 1997.

[89] Z. Mirafzali. (2011). *Is it necessary to add cholesterol to a liposome formulation?* Available: https://www.quora.com/Is-it-necessary-to-add-cholesterol-to-a-liposome-formulation

[90] H. Shmeeda, D. Tzemach, L. Mak, and A. Gabizon, "Her2-targeted pegylated liposomal doxorubicin: Retention of target-specific binding and cytotoxicity after in vivo passage," *Journal of Controlled Release,* vol. 136, no. 2, pp. 155-160, 2009.

[91] J. Li *et al.*, "A review on phospholipids and their main applications in drug delivery systems," *Asian Journal of Pharmaceutical Sciences,* vol. 10, no. 2, pp. 81-98, 2015.

[92] D. Needham, J.-Y. Park, A. M. Wright, and J. Tong, "Materials characterization of the low temperature sensitive liposome (LTSL): effects of the lipid composition (lysolipid and DSPE–PEG2000) on the thermal transition and release of doxorubicin," *Faraday Discuss.,* vol. 161, no. 1, pp. 515-534, 2013.

[93] R. Turki and G. A. Hussieni. "Preparation of albumin-targeted liposomes and the study of their release characteristics using ultrasound," M.S. thesis, American University of Sharjah, United Arab Emirates, 2016.

[94] S. E. Ahmed and G. A. Hussieni. "Dynamics of chemotherapeutic drug release from liposomes using low-frequency ultrasound," M.S. thesis, American University of Sharjah, Sharjah, United Arab Emirates, 2015.

[95] A. L. Polar. (26 April). *Products 16:0 PC (DPPC) | 850355*. Available: https://avantilipids.com/product/850355/

[96] N. C. f. B. Information. *Compound Summary for CID 102547*. Available: https://pubchem.ncbi.nlm.nih.gov/compound/102547

[97] A. L. Polar. (26 April). *Phase Transition Temperatures for Glycerophospholipids*. Available: https://avantilipids.com/tech-support/physical-properties/phase-transition-temps/

[98] A. L. Polar. (26 April). *Products DSPE-PEG(2000) Amine | 880128*. Available: https://avantilipids.com/product/880128/

[99] J. C. M. Stewart, "Colorimetric determination of phospholipids with ammonium ferrothiocyanate," *Analytical Biochemistry,* vol. 104, no. 1, pp. 10-14, 1980.

[100] B. J. Olson and J. Markwell, "Assays for determination of protein concentration," (in eng), *Curr Protoc Protein Sci,* vol. Chapter 3, p. Unit 3.4, May 2007.

[101] P. K. Smith *et al.*, "Measurement of protein using bicinchoninic acid," *Analytical Biochemistry,* vol. 150, no. 1, pp. 76-85, 1985.

[102] Sigma-aldrich, "Product information: QuantiPro BCA Assay Kit," ed: sigma-aldrich.

[103] B. Maherani, E. Arab-Tehrany, A. Kheirolomoom, D. Geny, and M. Linder, "Calcein release behavior from liposomal bilayer; influence of physicochemical/mechanical/structural properties of lipids," *Biochimie,* vol. 95, no. 11, pp. 2018-2033, 2013.

[104] Cohen-Levi, "Ultrasound for targeted delivery of cytotoxic drugs from liposomes," M.S. thesis, Ben Gurion University, Beer Sheva, 2000.

[105] G. Husseini and M. Mahmoud, "The Effect of Ultrasound on the Drug Delivery of RGD-Targeted Liposomes," M.S. thesis, American University of Sharjah, United Arab Emirates, 2018.

[106] B. J. Staples, B. L. Roeder, G. A. Husseini, O. Badamjav, G. B. Schaalje, and W. G. Pitt, "Role of frequency and mechanical index in ultrasonic-enhanced chemotherapy in rats," *Cancer Chemotherapy and Pharmacology,* vol. 64, no. 3, pp. 593-600, 2009.

[107] J. Wolfe. *What is acoustic impedance and why is it important*. Available: https://newt.phys.unsw.edu.au/jw/z.html

[108] A. Schroeder *et al.*, "Controlling liposomal drug release with low frequency ultrasound: mechanism and feasibility," *Langmuir : the ACS journal of surfaces and colloids,* vol. 23, no. 7, pp. 4019-4025, 2007.

[109] P. Costa and J. M. Sousa Lobo, "Modeling and comparison of dissolution profiles," *European Journal of Pharmaceutical Sciences,* vol. 13, no. 2, pp. 123-133, 2001.

[110] R. K.H, "Mathematical Models of Drug Dissolution: A Review," vol. 3, D. P.A, Ed., ed: Scholars Academic Journal of Pharmacy, 2014, pp. 388-396.

[111] T. Higuchi, "Rate of release of medicaments from ointment bases containing drugs in suspension," *Journal of Pharmaceutical Sciences,* vol. 50, no. 10, pp. 874-875, 1961.

[112] R. W. Korsmeyer, R. Gurny, E. Doelker, P. Buri, and N. A. Peppas, "Mechanisms of solute release from porous hydrophilic polymers," *International Journal of Pharmaceutics,* vol. 15, no. 1, pp. 25-35, 1983.

[113] K. H. Ramteke, "Mathematical Models of Drug Dissolution: A Review," vol. 3, P. A. Dighe, Ed., ed: Scholars Academic Journal of Pharmacy, pp. 388-396, 2014.

[114] R. W. Baker and H. K. Lonsdale, "Controlled Release: Mechanisms and Rates," in *Controlled Release of Biologically Active Agents*: Springer US : Boston, MA, 1974, pp. 15-71.

[115] H. B. Hopfenberg, "Controlled Release from Erodible Slabs, Cylinders, and Spheres," in *Controlled Release Polymeric Formulations*: American Chemical Society : Washington, D. C., 1976, pp. 26-32.

[116] T. Hayashi *et al.*, "Formulation study and drug release mechanism of a new theophylline sustained-release preparation," *International Journal of Pharmaceutics,* vol. 304, no. 1, pp. 91-101, 2005.

Appendix A: Plots of Model Fitting for NH$_2$ Liposomes.
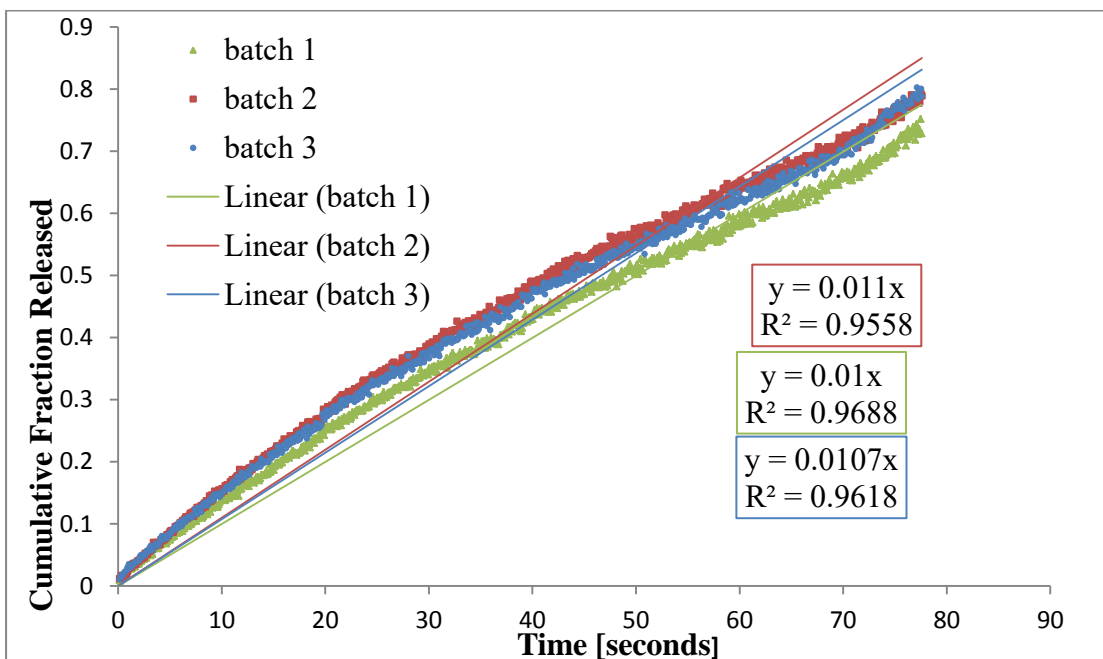
Figure A.1: Zero-order plot for NH2 liposomes at 9.85 (mW/cm^2).
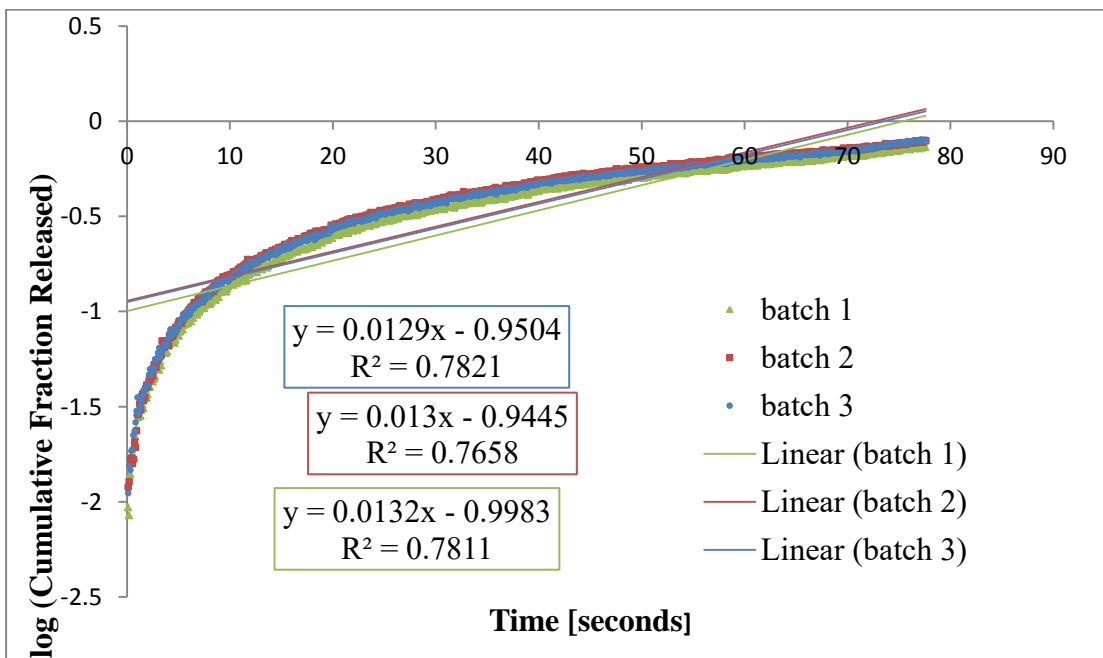
Figure A.2: First-order plot for NH2 liposomes at 9.85 (mW/cm^2).
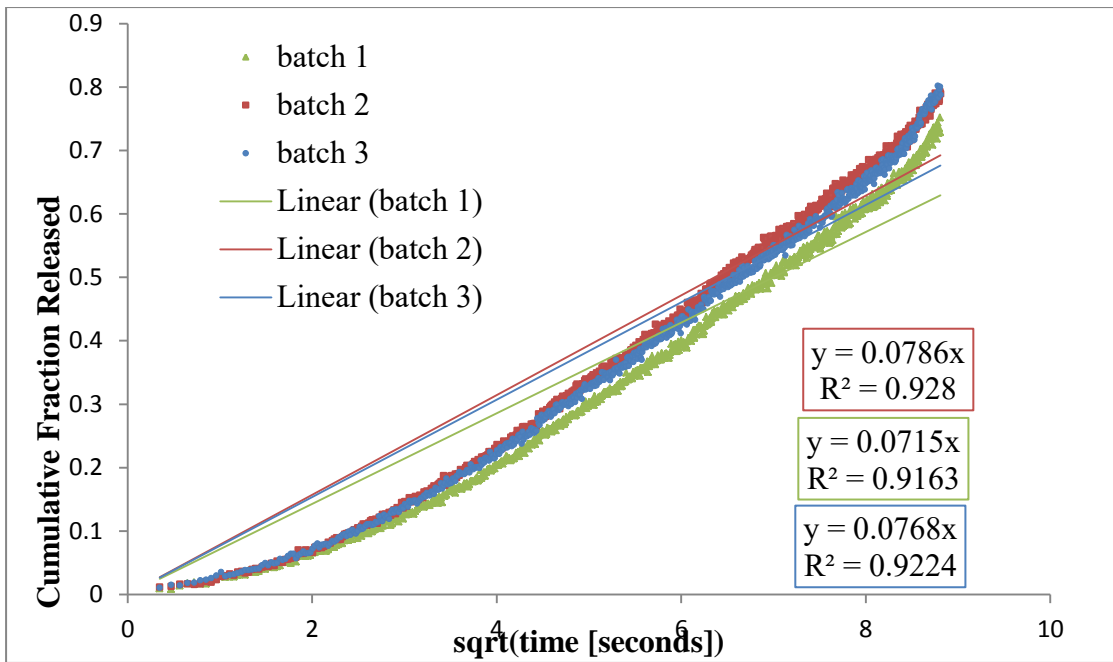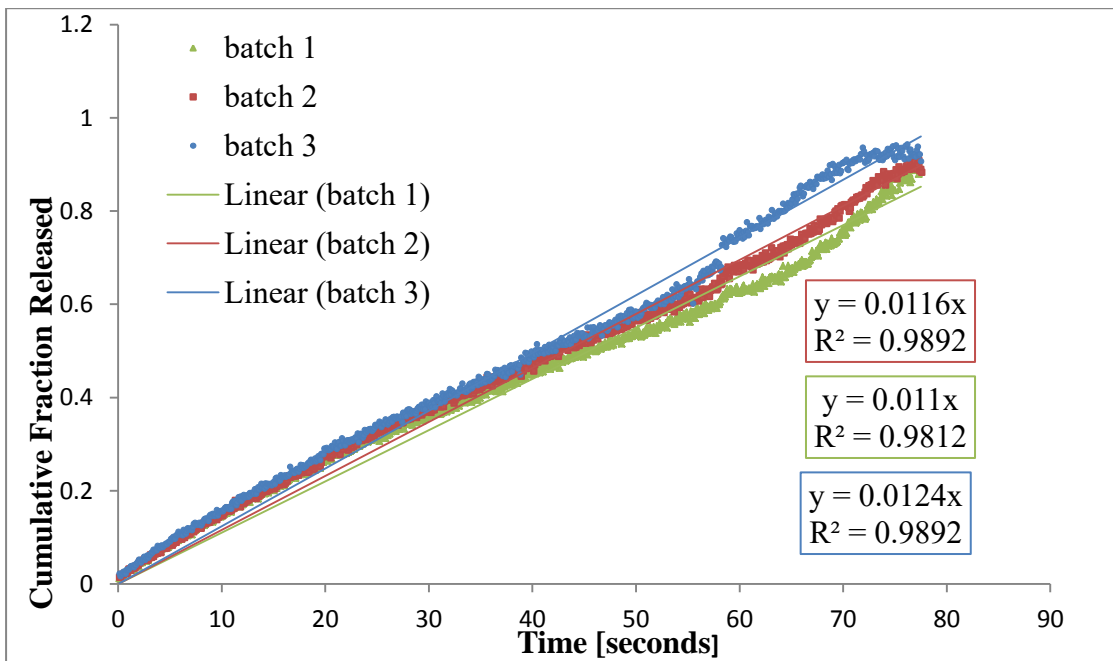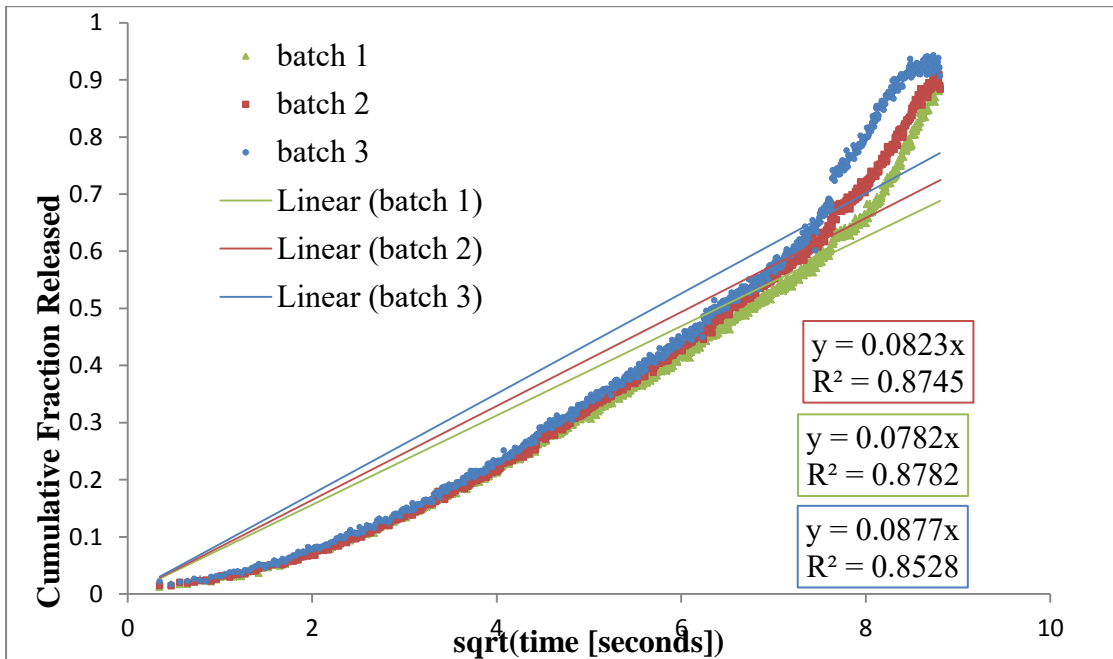
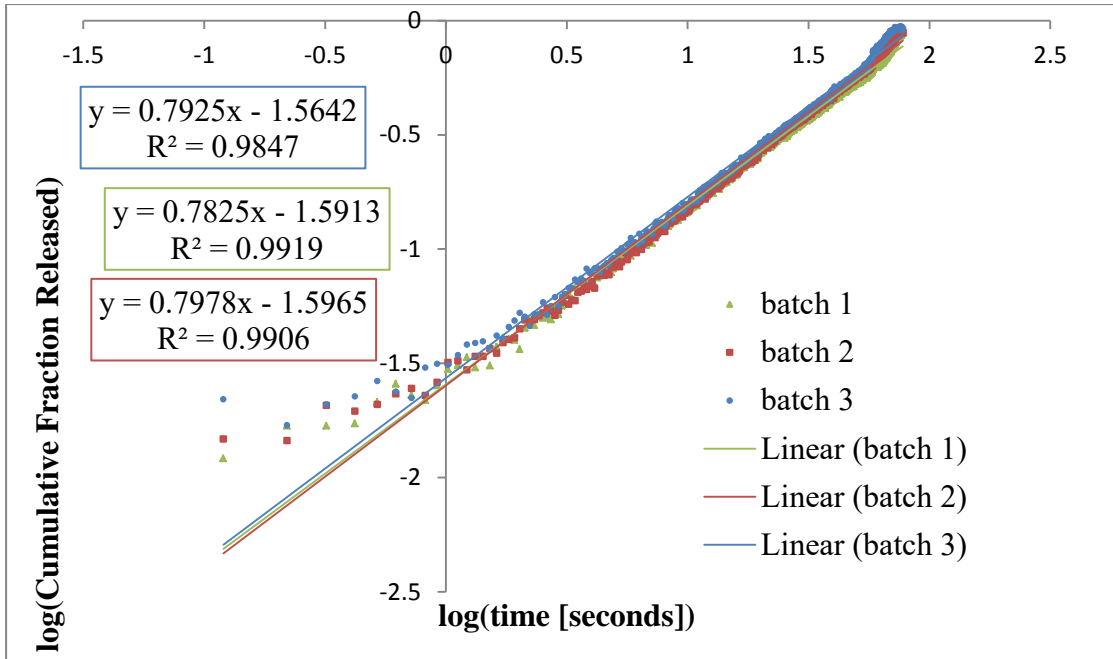Figure A.3: Higuchi model for NH2 liposomes at 9.85 (mW/cm^2).
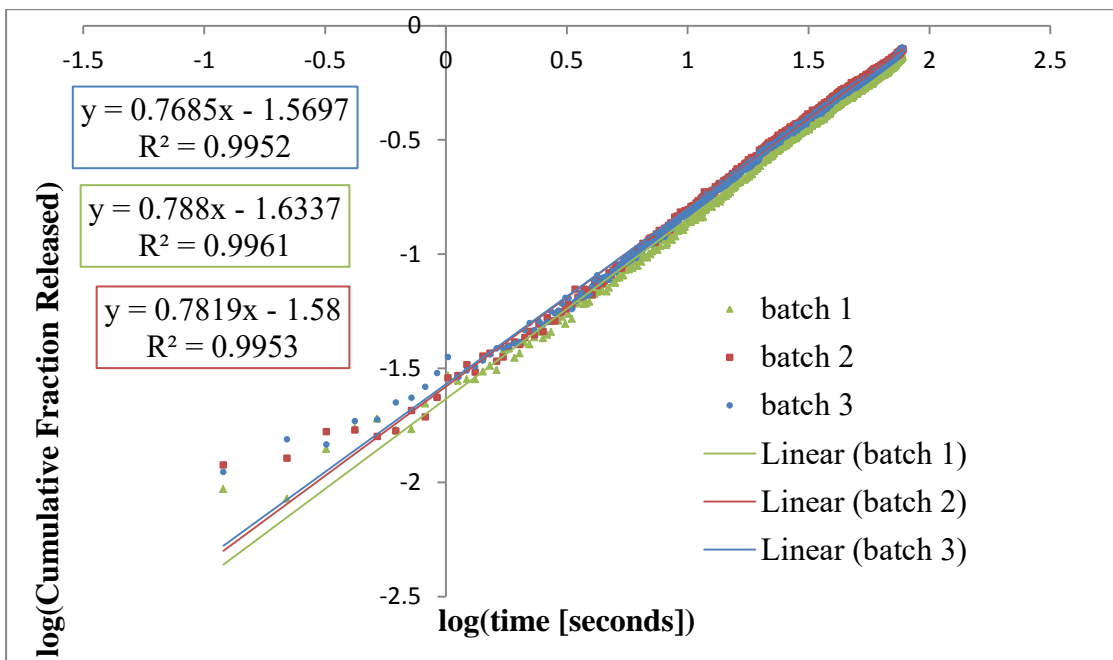
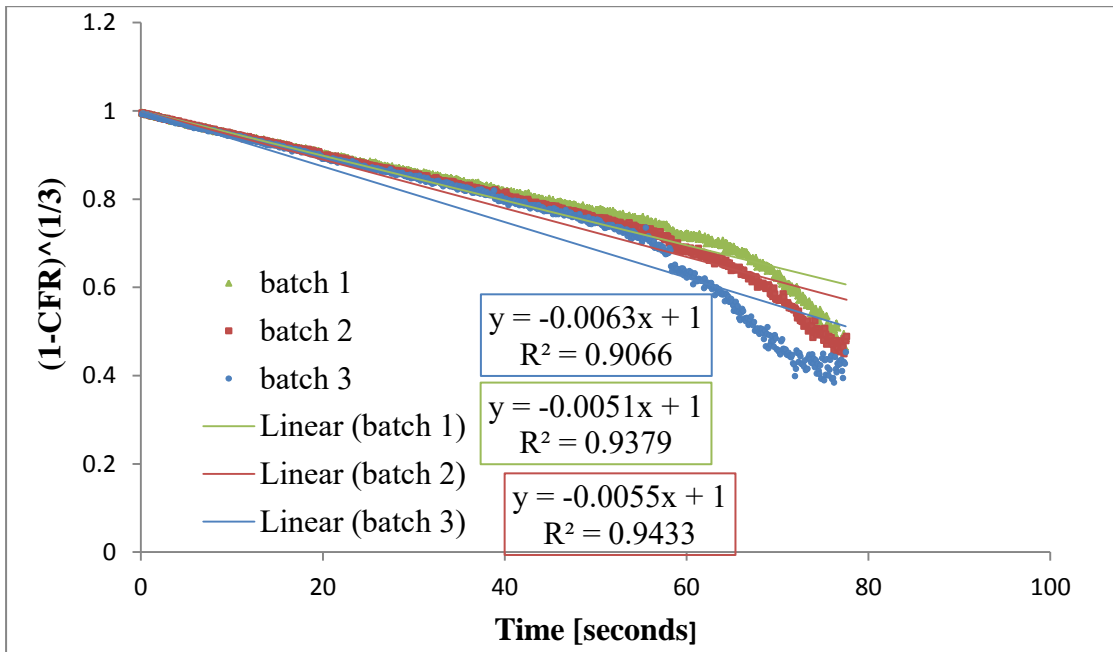Figure A.4: Korsmeyer-Peppas model for NH2 liposomes at 9.85 (mW/cm^2).
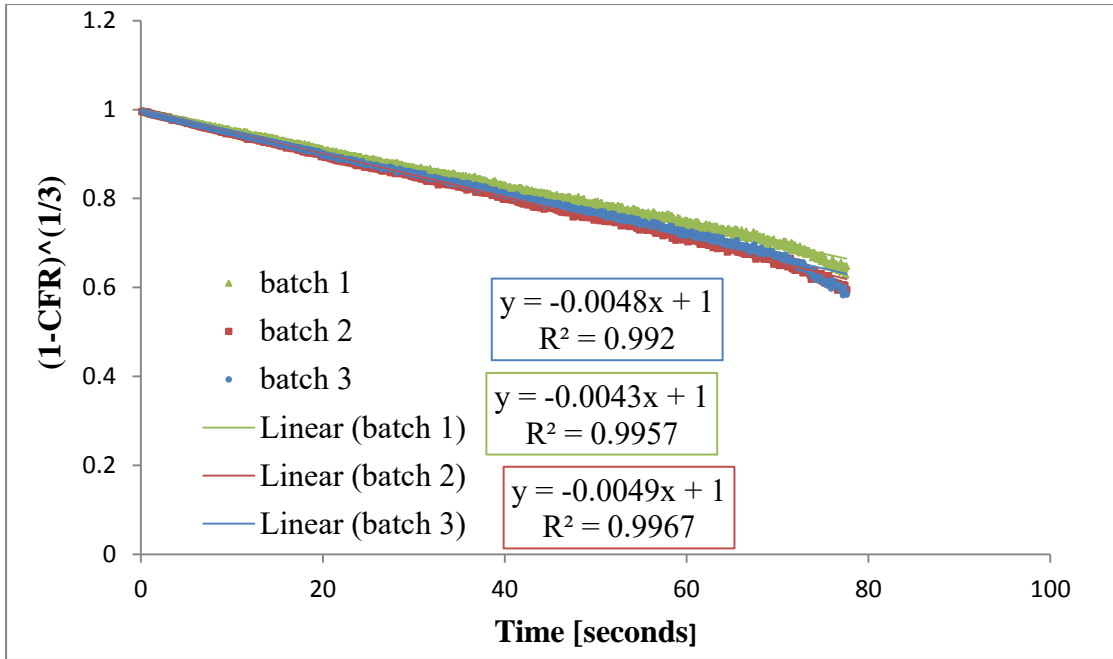
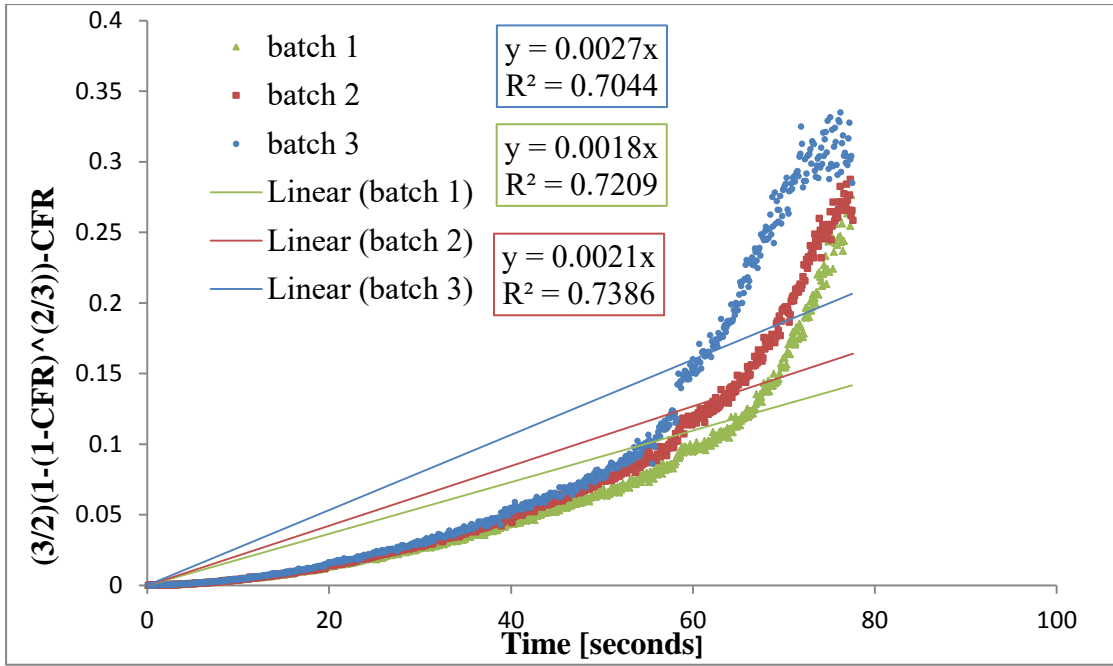Figure A.5: Hixson-Crowell model for NH2 liposomes at 9.85 (mW/cm^2).
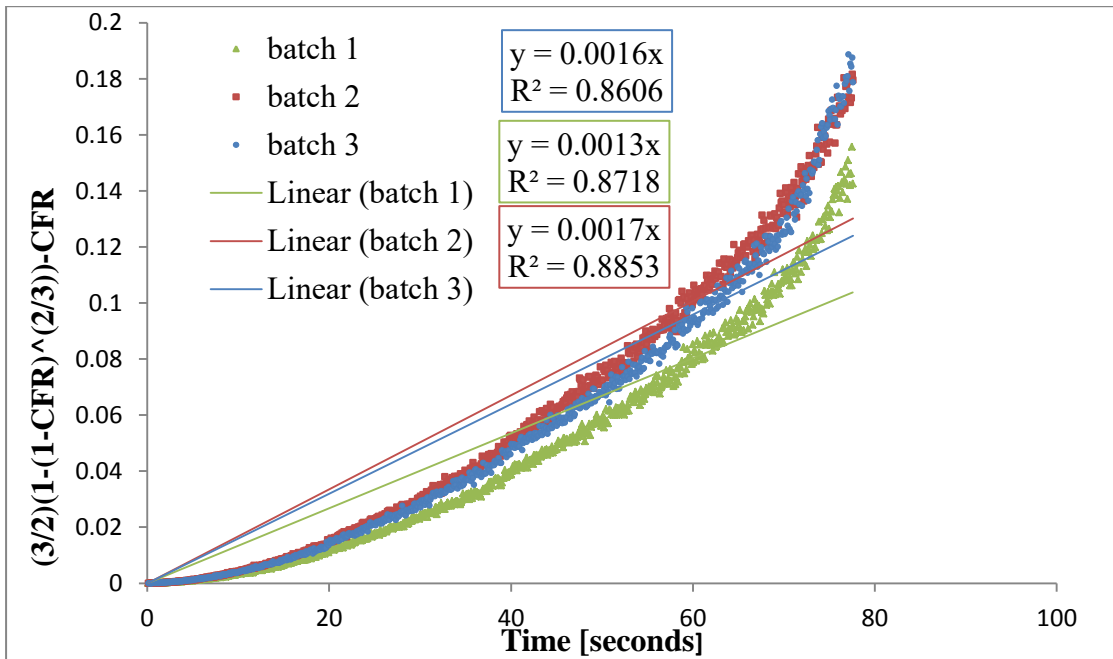
Figure A.6: Baker-Lonsdale model for NH2 liposomes at 9.85 (mW/cm^2).
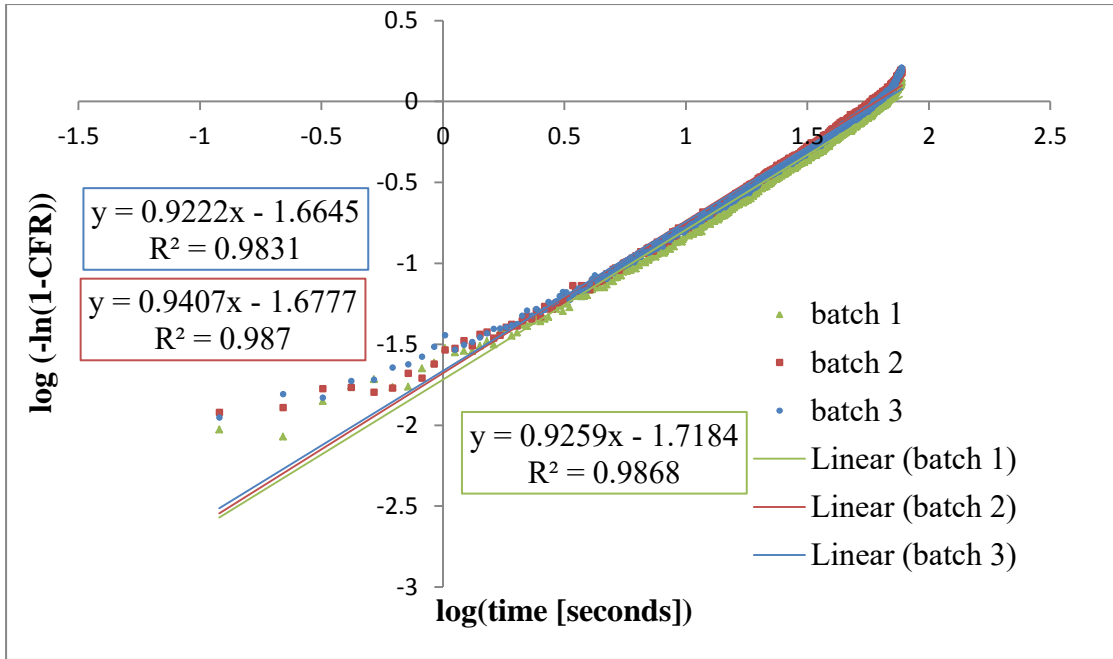
Figure A.7: Weibull model for NH2 liposomes at 9.85 (mW/cm^2).
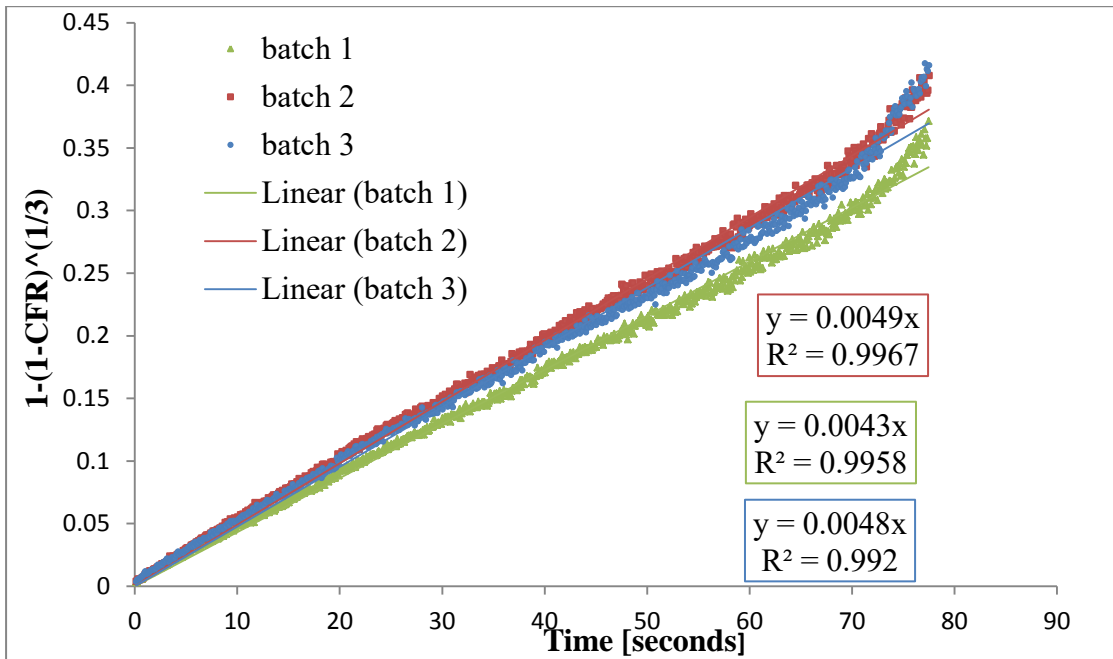
Figure A.8: Hopfenberg model for NH2 liposomes at 9.85 (mW/cm^2).
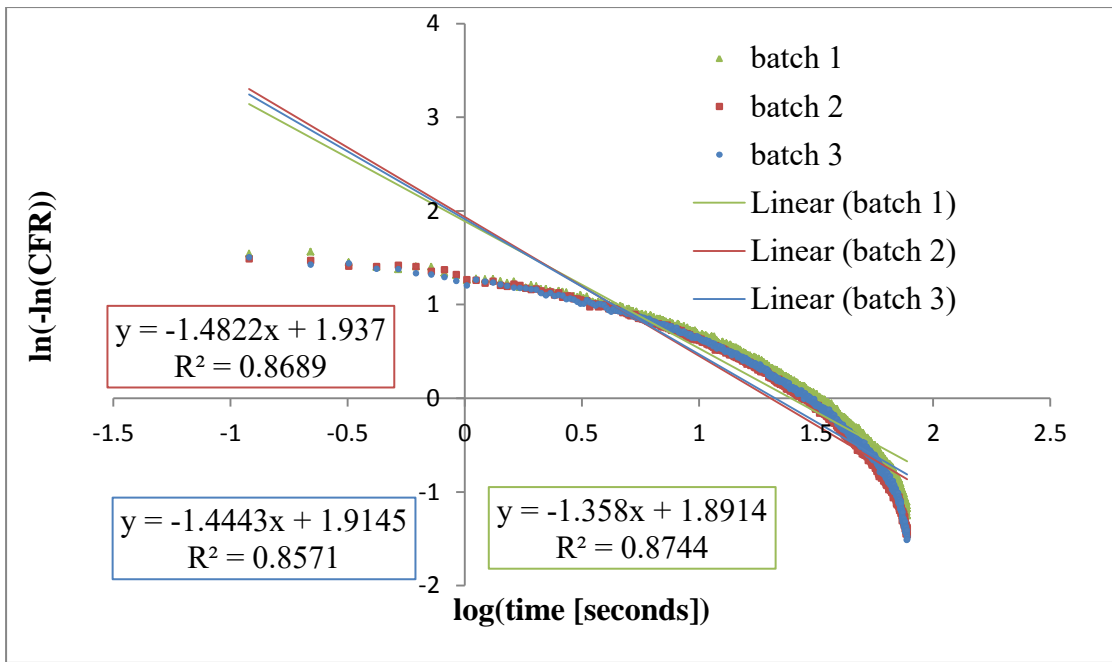
Figure A.9: Gompertz model for NH2 liposomes at 9.85 (mW/cm^2).
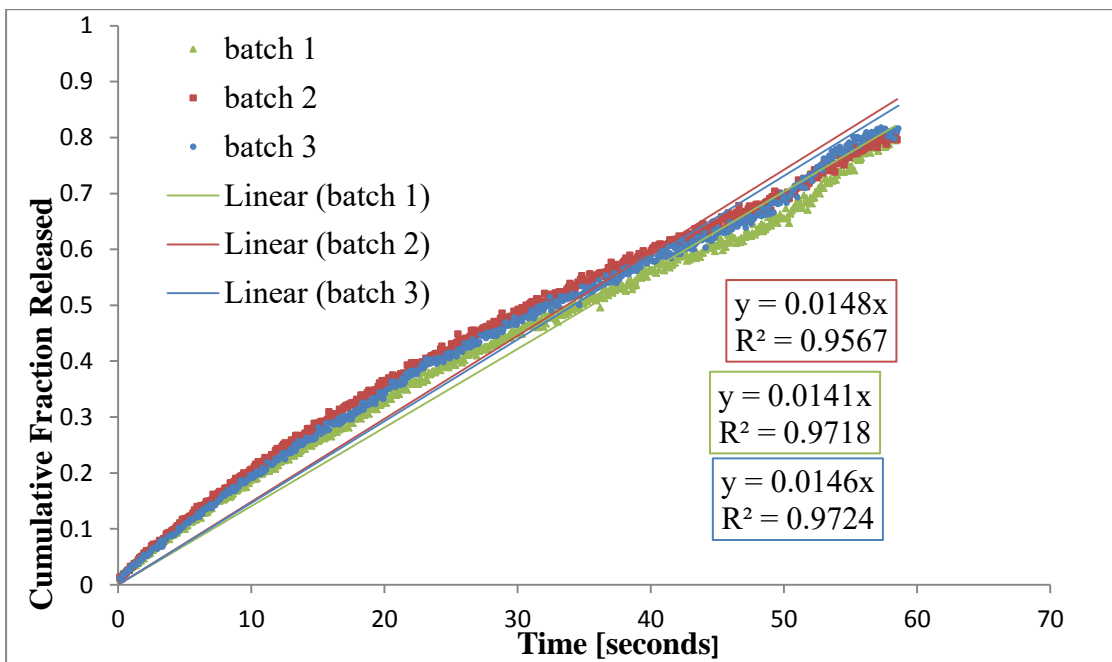
Figure A.10: Zero-order plot for NH2 liposomes at 17.31 (mW/cm^2).
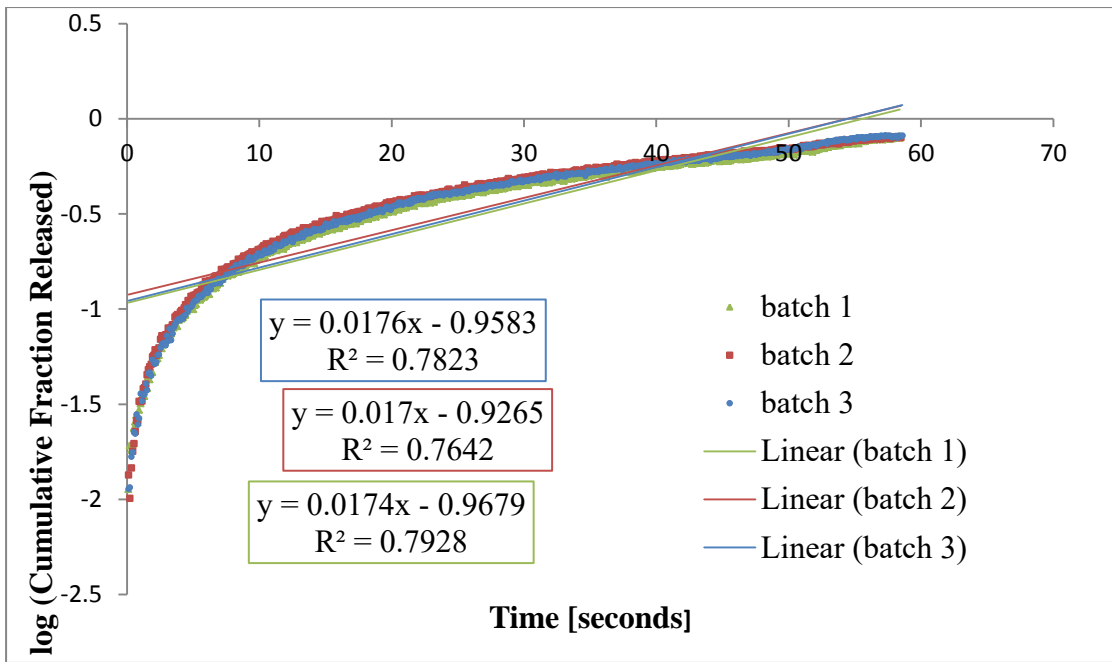
Figure A.11: First-order plot for NH2 liposomes at 17.31 (mW/cm^2).
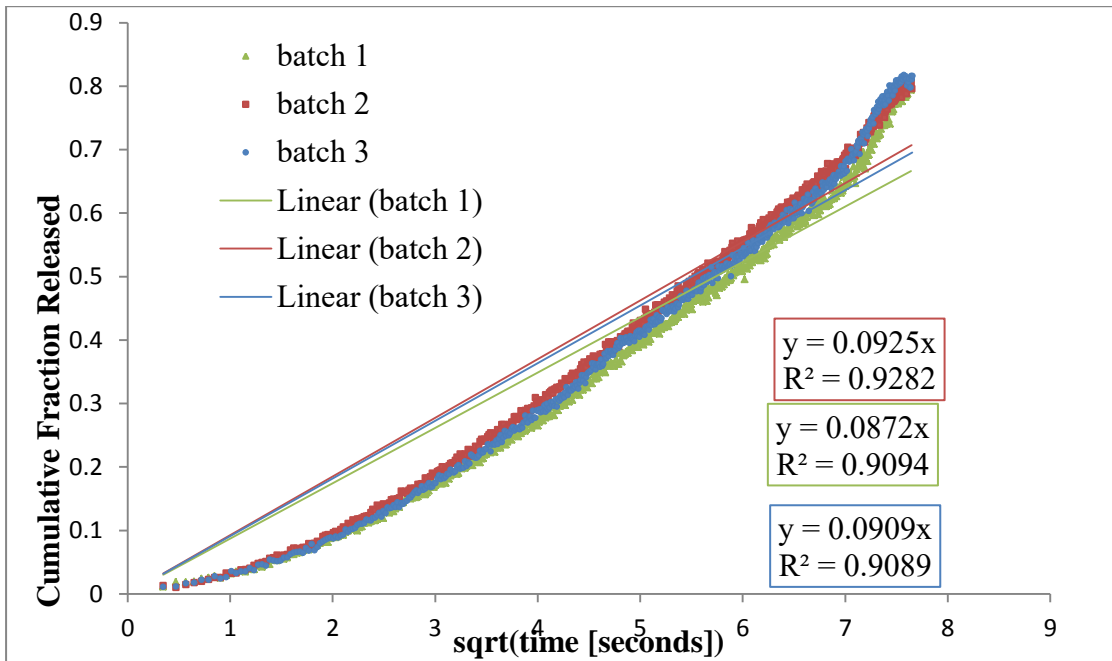
Figure A.12: Higuchi model for NH2 liposomes at 17.31 (mW/cm^2).
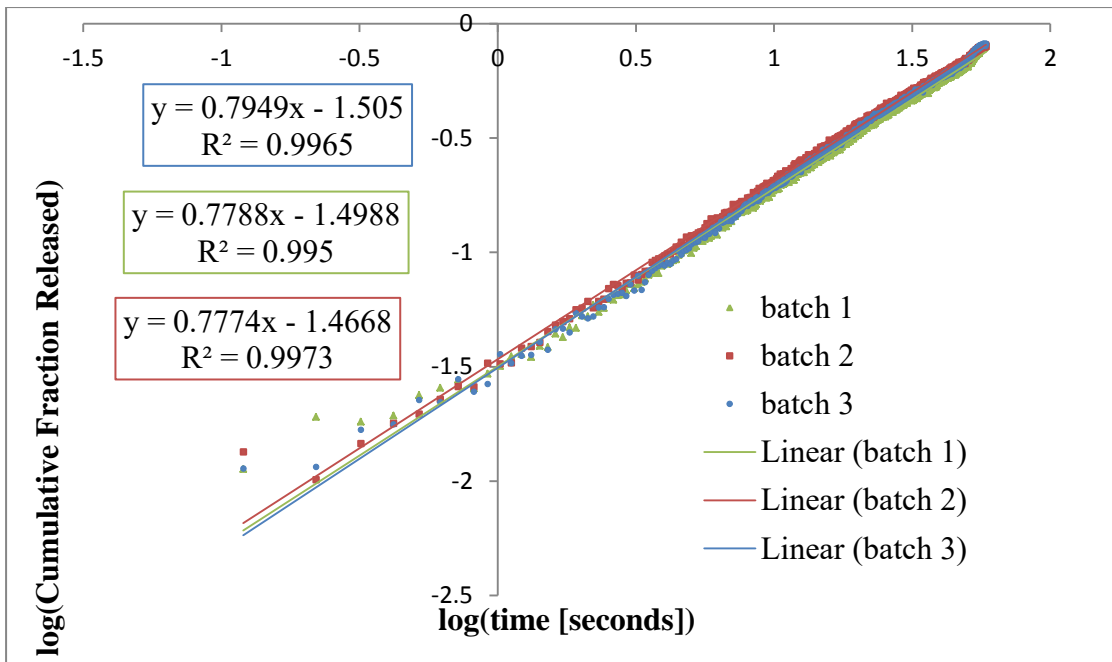
Figure A.13: Korsmeyer-Peppas model for NH2 liposomes at 17.31 (mW/cm^2).
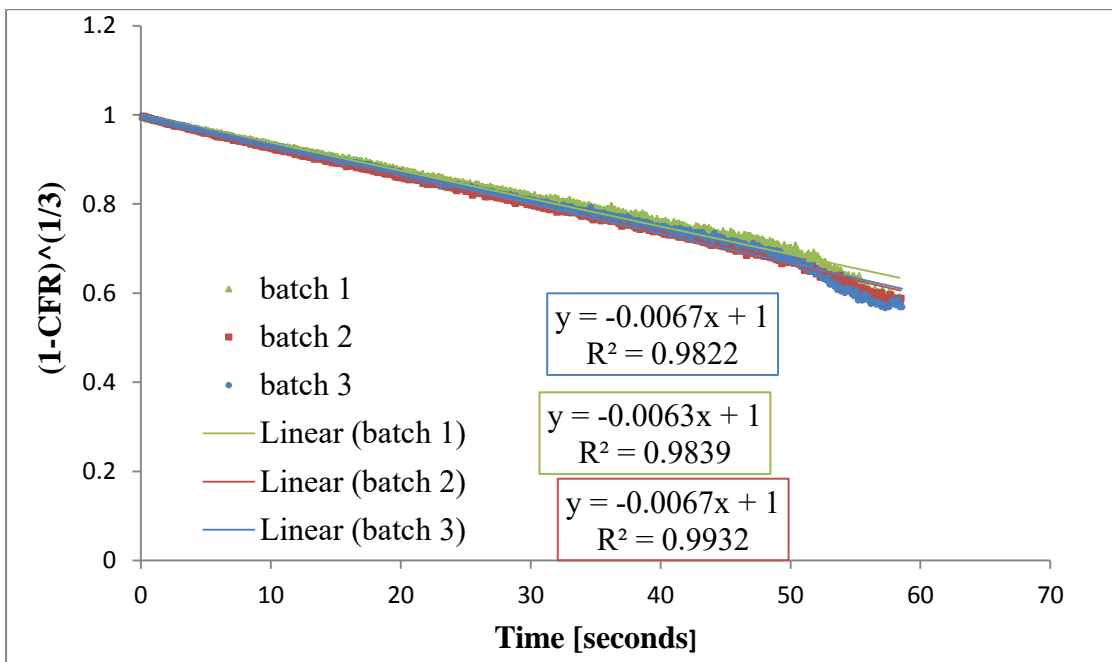
Figure A.14: Hixson-Crowell model for NH2 liposomes at 17.31 (mW/cm^2).
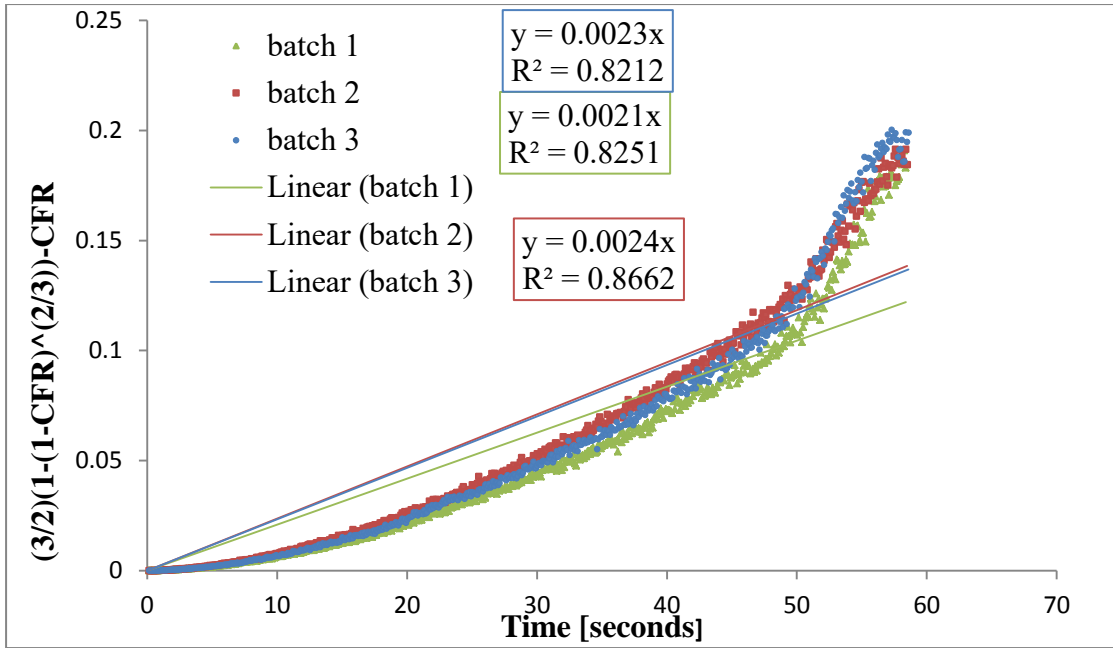
Figure A.15: Baker-Lonsdale model for NH2 liposomes at 17.31 (mW/cm^2).
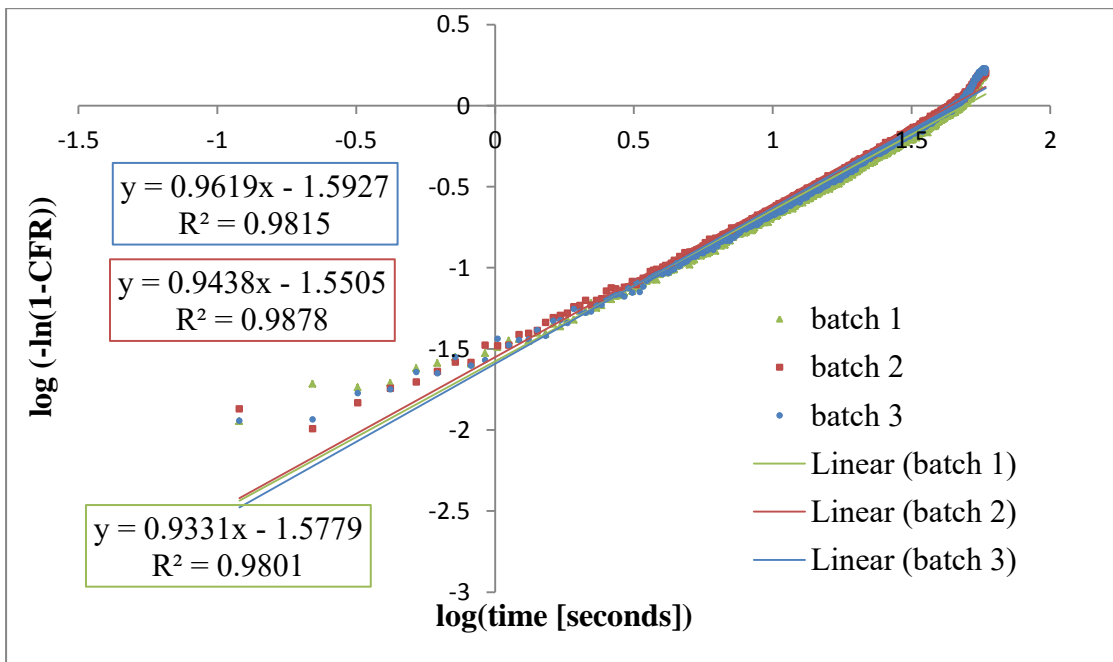
Figure A.16: Weibull model for NH2 liposomes at 17.31 (mW/cm^2).
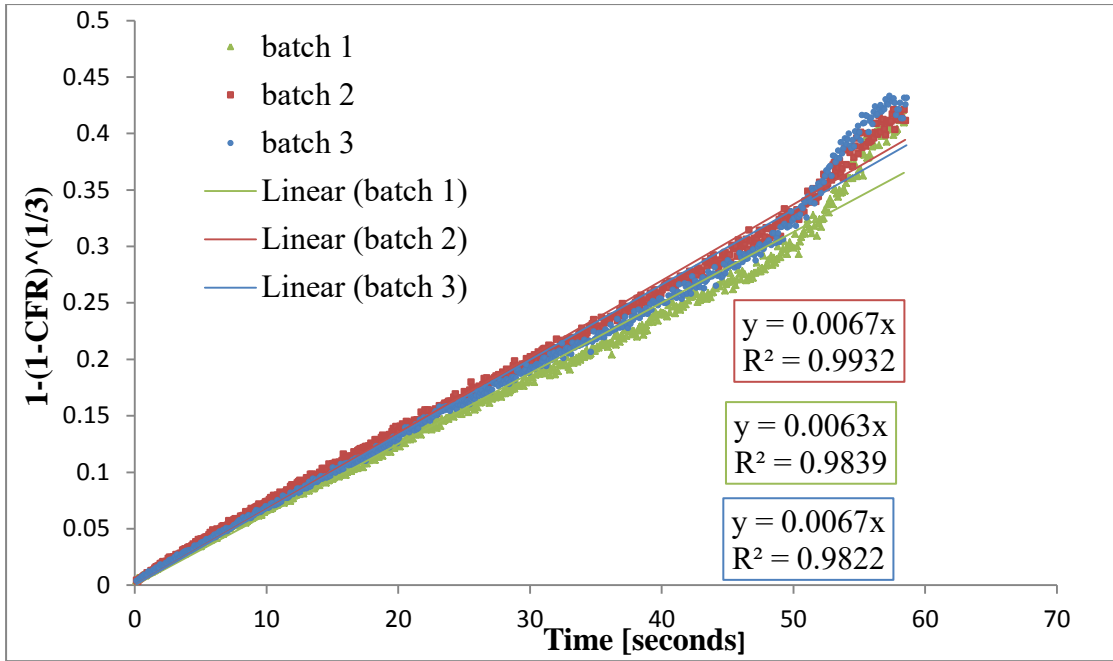
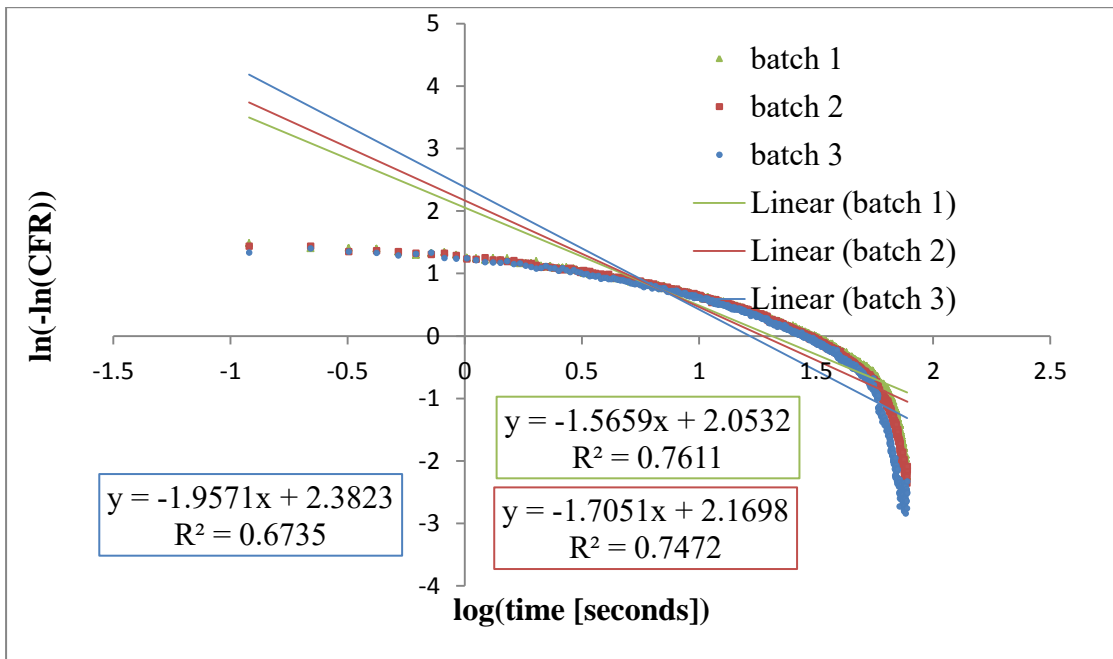Figure A.17: Hopfenberg model for NH2 liposomes at 17.31 (mW/cm^2).
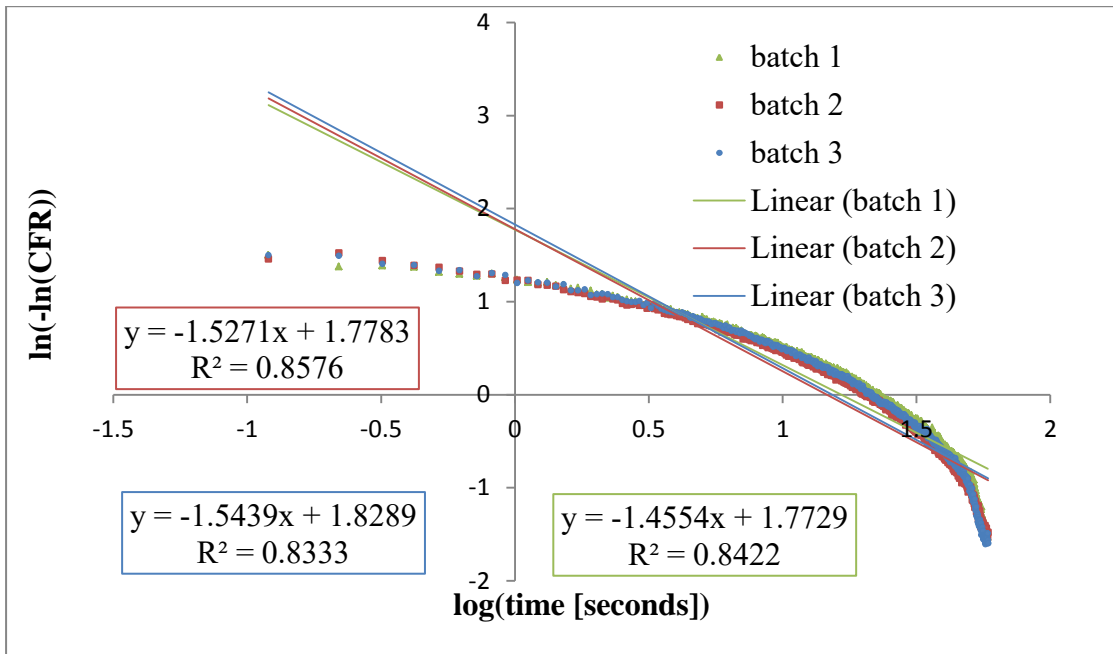
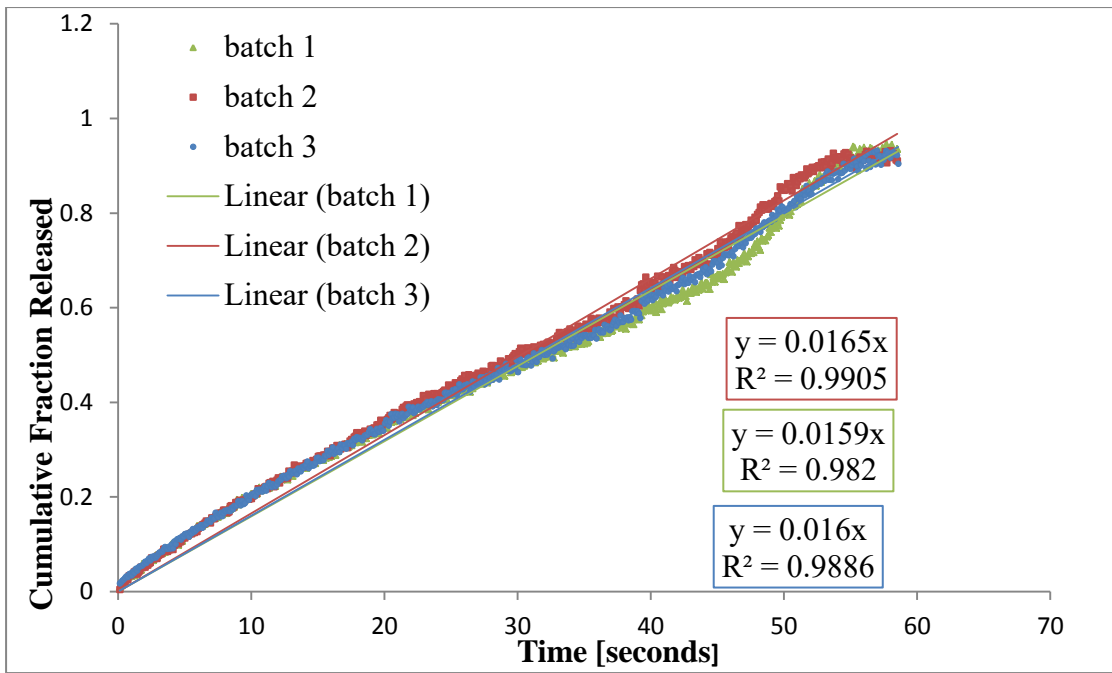Figure A.18: Gompertz model for NH2 liposomes at 17.31 (mW/cm^2).

Figure B.1: Zero-order plot for immunoliposomes at 7.46 (mW/cm^2).
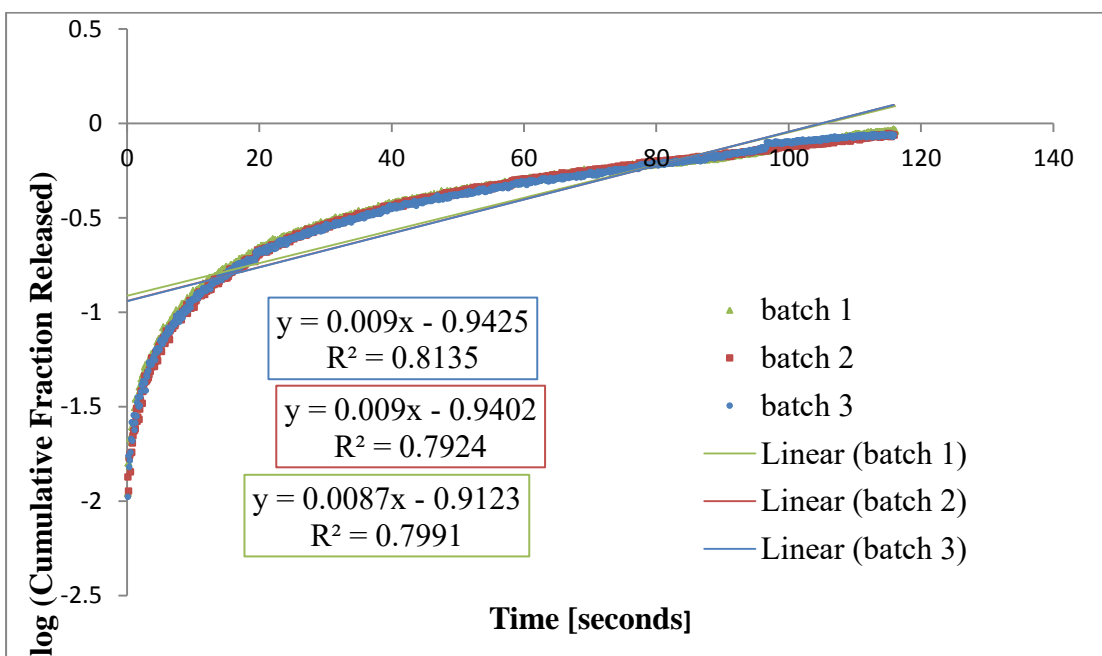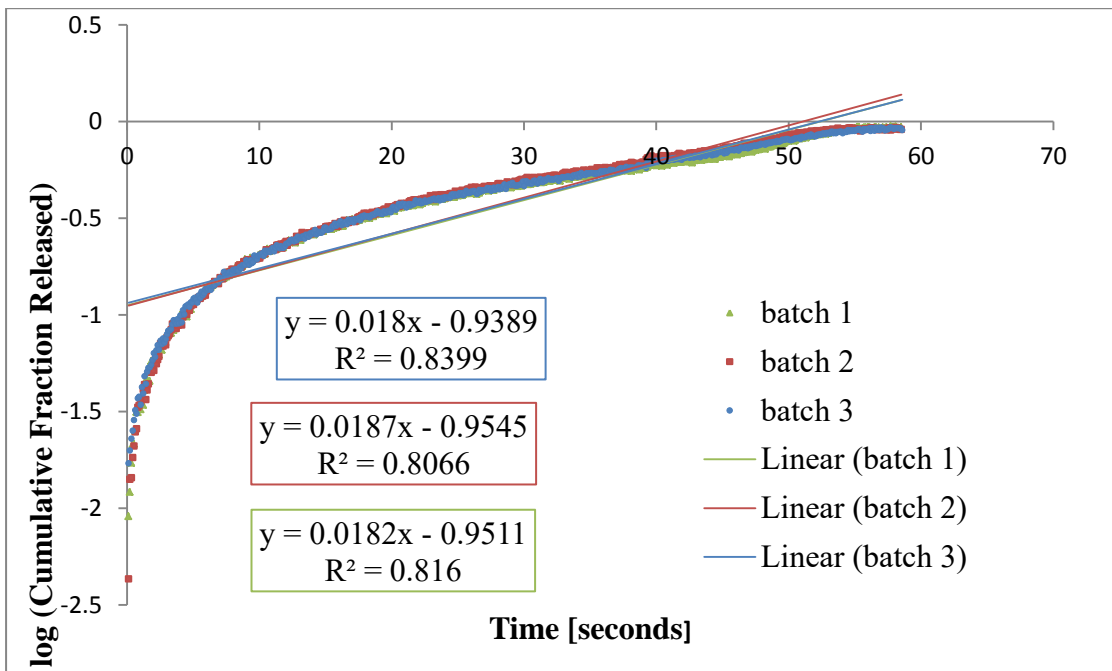

Figure B.2: First-order plot for immunoliposomes at 7.46 (mW/cm^2).
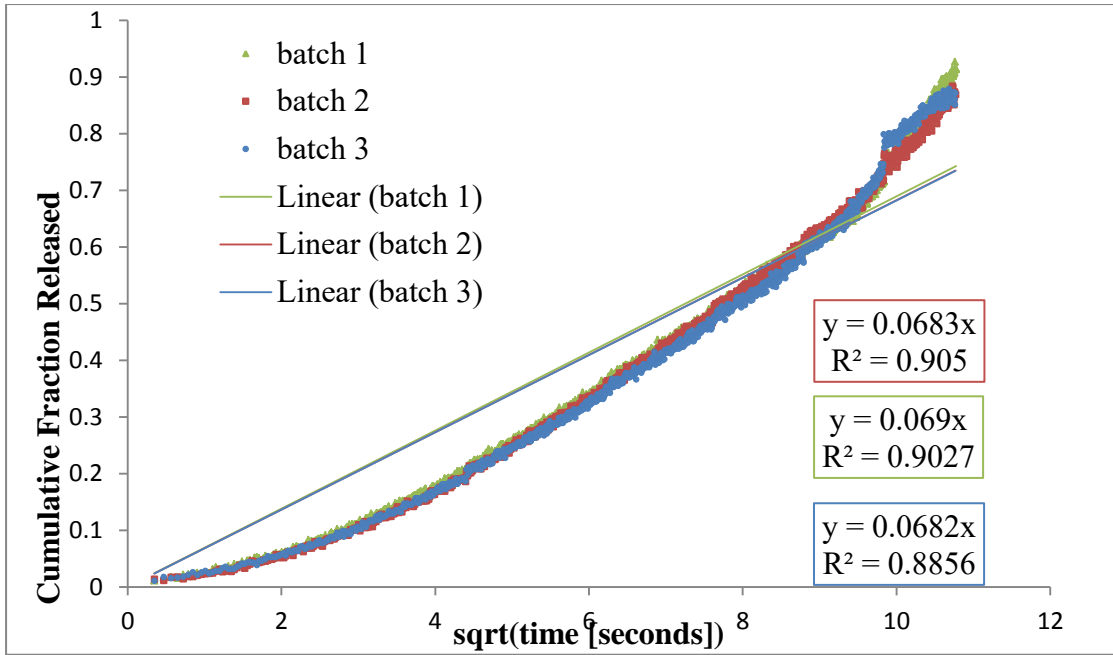
Figure B.3: Higuchi model for immunoliposomes at 7.46 (mW/cm^2).
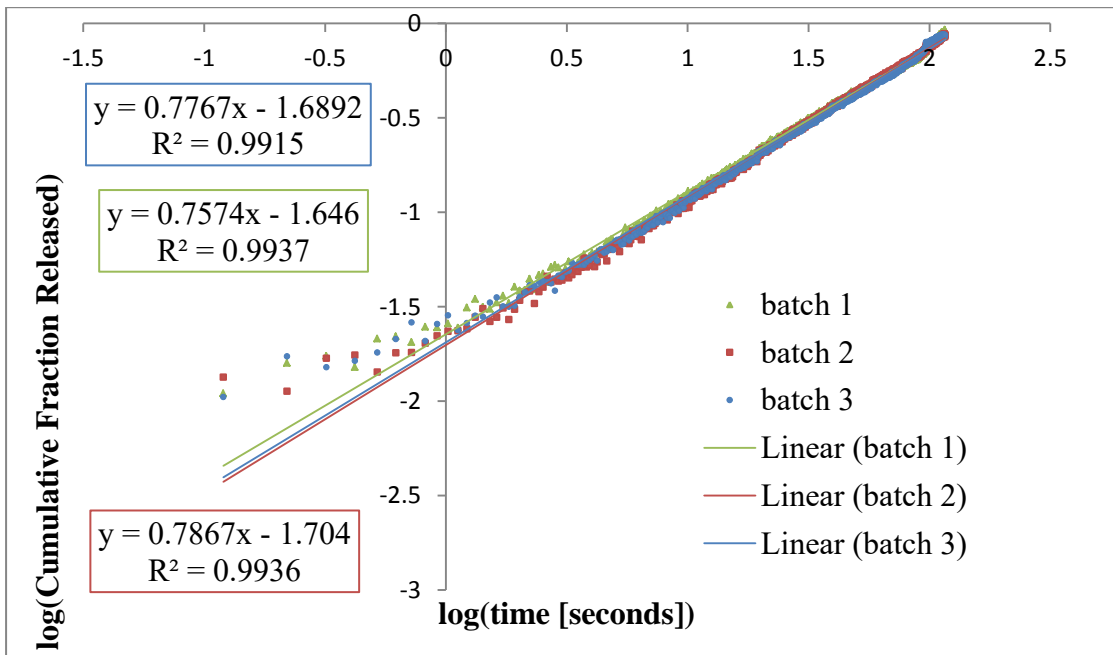
Figure B.4: Korsmeyer-Peppas model for immunoliposomes at 7.46 (mW/cm^2).
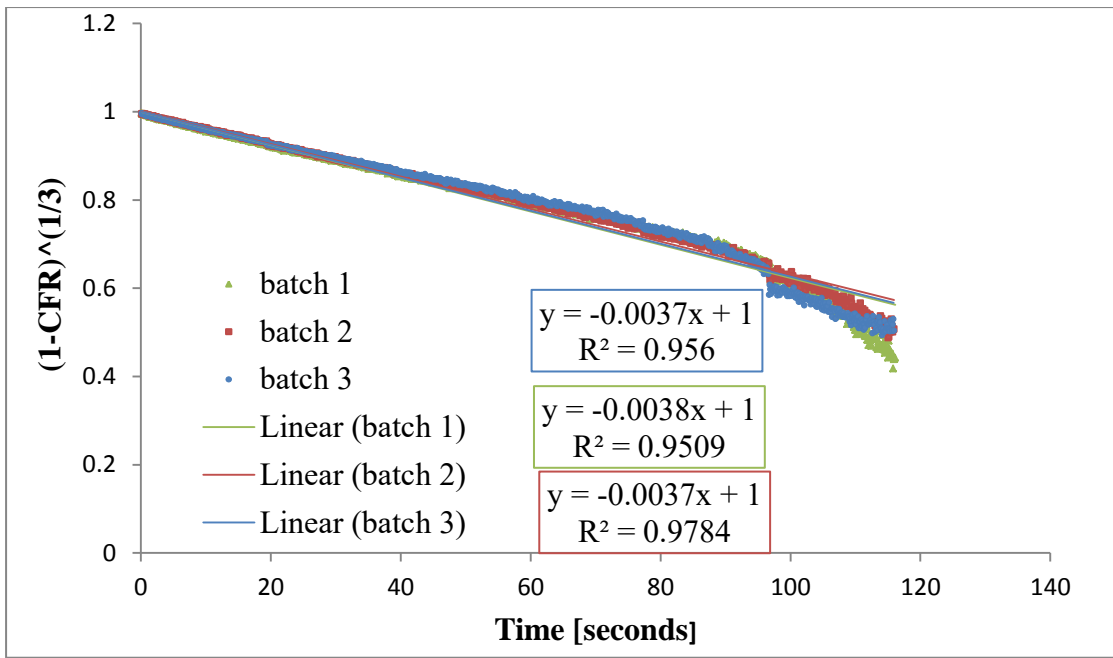
Figure B.5: Hixson-Crowell model for immunoliposomes at 7.46 (mW/cm^2).
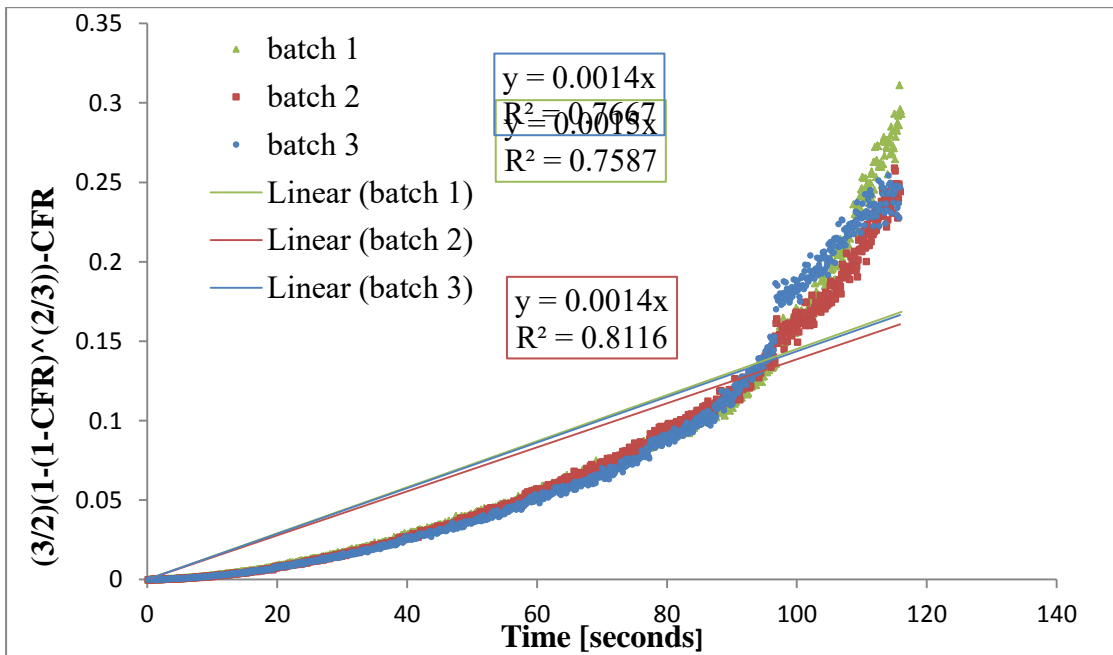
Figure B.6: Baker-Lonsdale model for immunoliposomes at 7.46 (mW/cm^2).
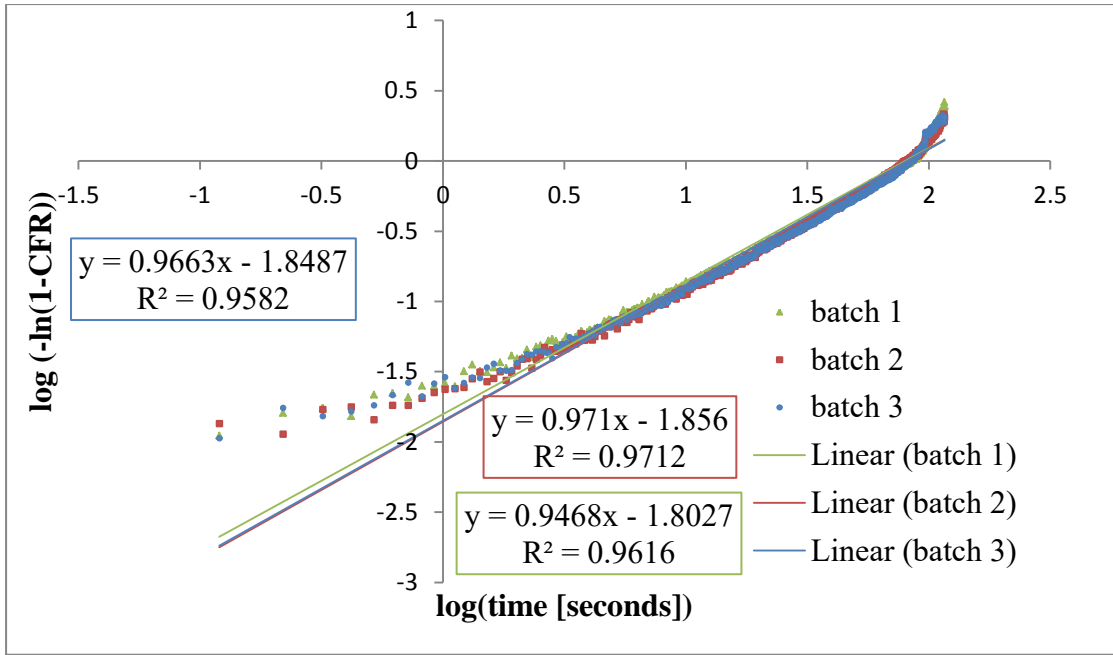
Figure B.7: Weibull model for immunoliposomes at 7.46 (mW/cm^2).
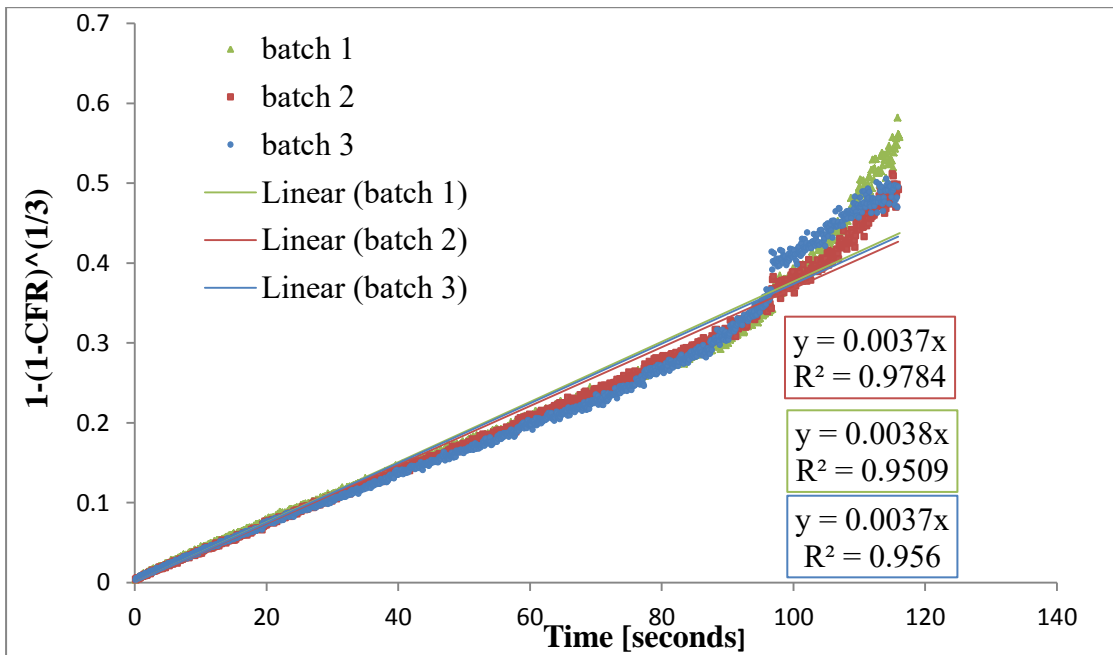
Figure B.8: Hopfenberg model for immunoliposomes at 7.46 (mW/cm^2).
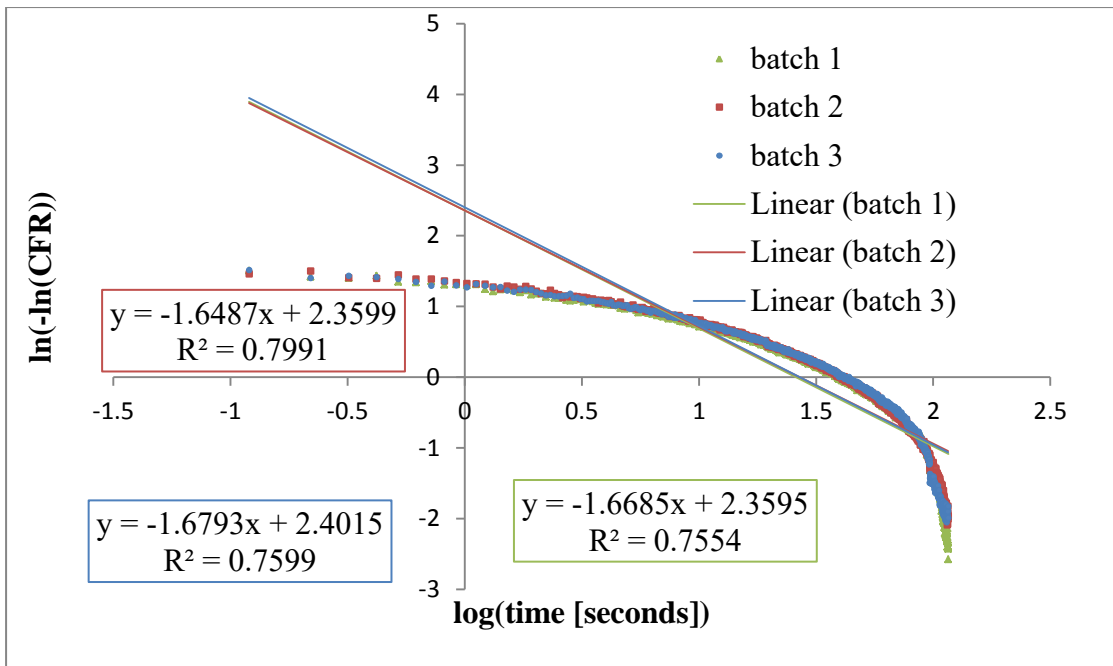
Figure B.9: Gompertz model for immunoliposomes at 7.46 (mW/cm^2).

Figure B.10: Zero-order plot for immunoliposomes at 9.85 (mW/cm^2).
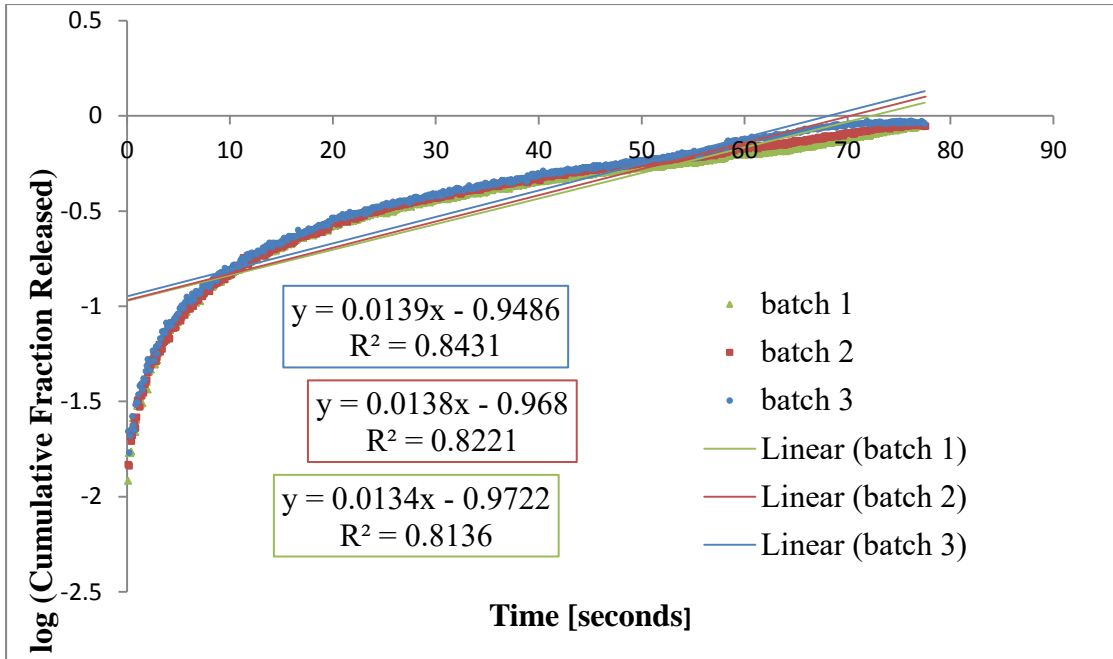
Figure B.11: First-order plot for immunoliposomes at 9.85 (mW/cm^2).
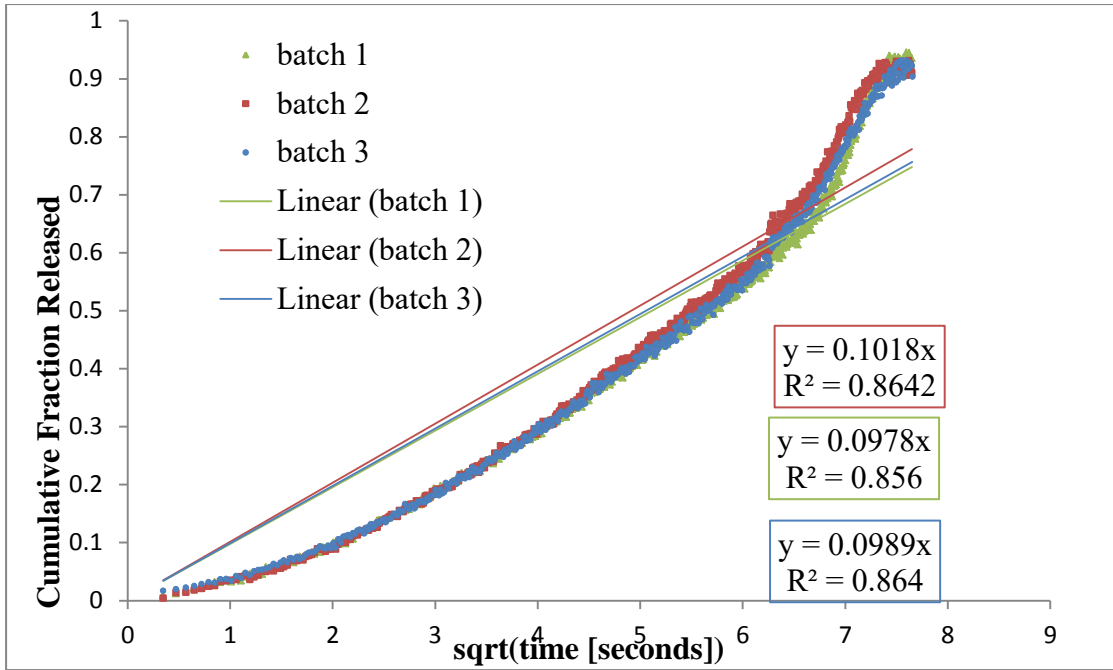

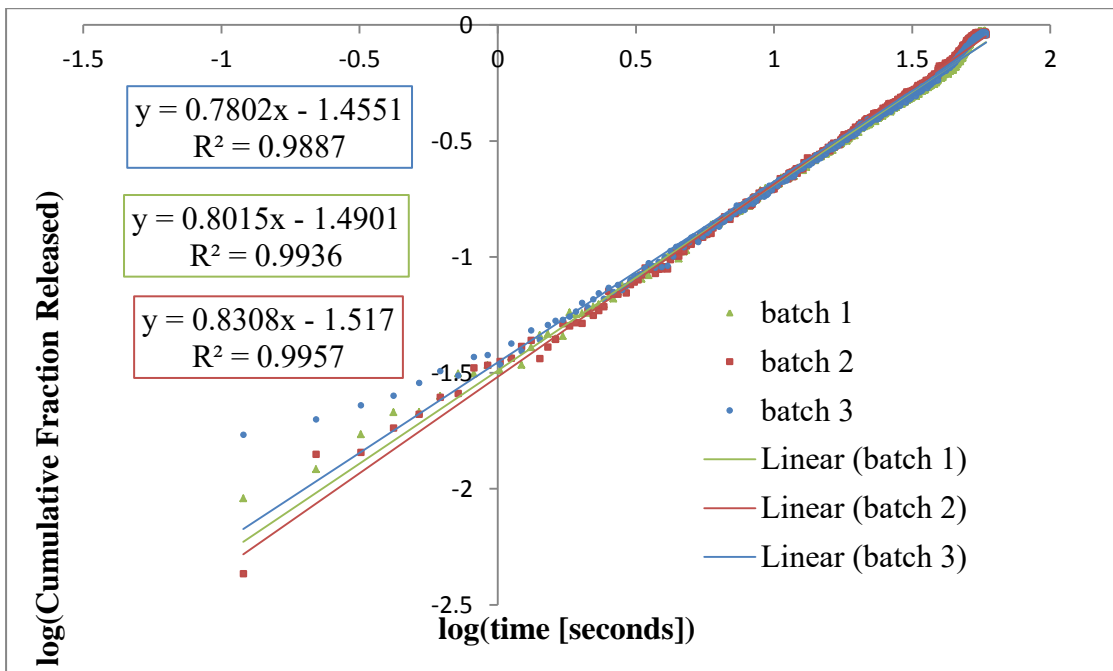Figure B.12: Higuchi model for immunoliposomes at 9.85 (mW/cm^2).

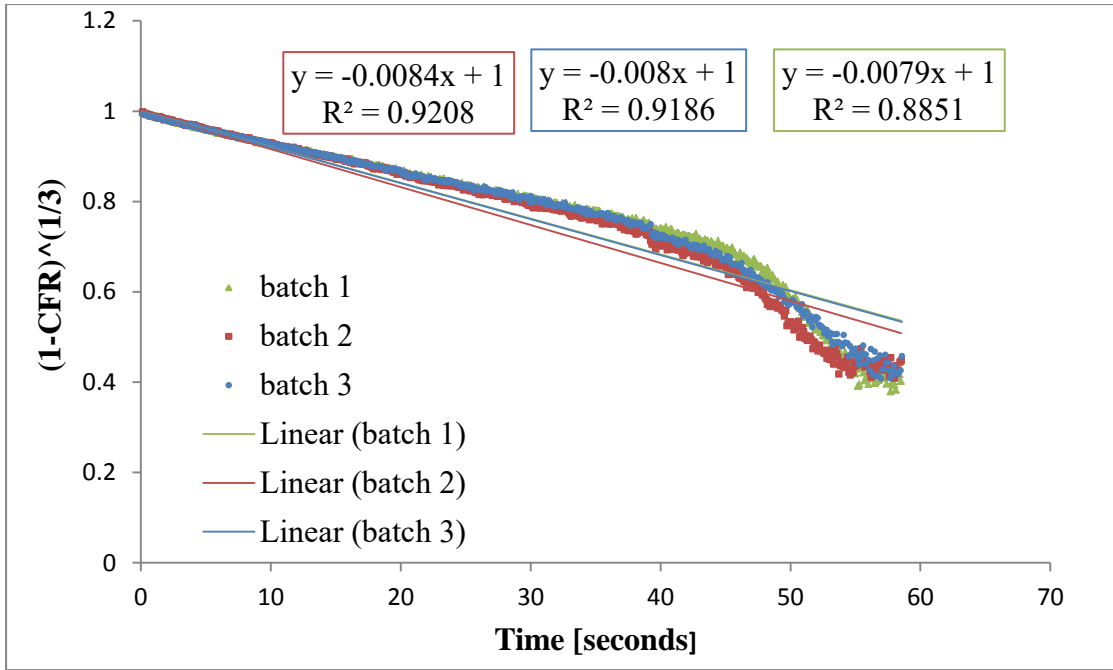Figure B.13 Korsmeyer-Peppas model for immunoliposomes at 9.85 (mW/cm^2).

Figure B.14: Hixson-Crowell model for immunoliposomes at 9.85 (mW/cm^2).

Figure B.15: Baker-Lonsdale model for immunoliposomes at 9.85 (mW/cm^2).
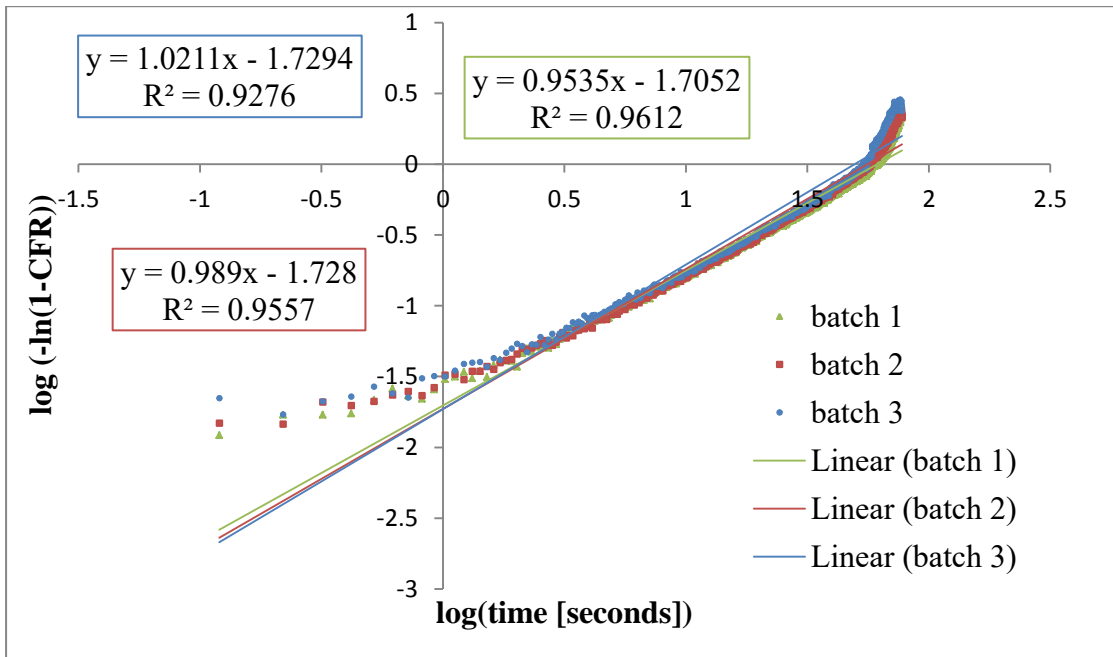
Figure B.16: Weibull model for immunoliposomes at 9.85 (mW/cm^2).

116
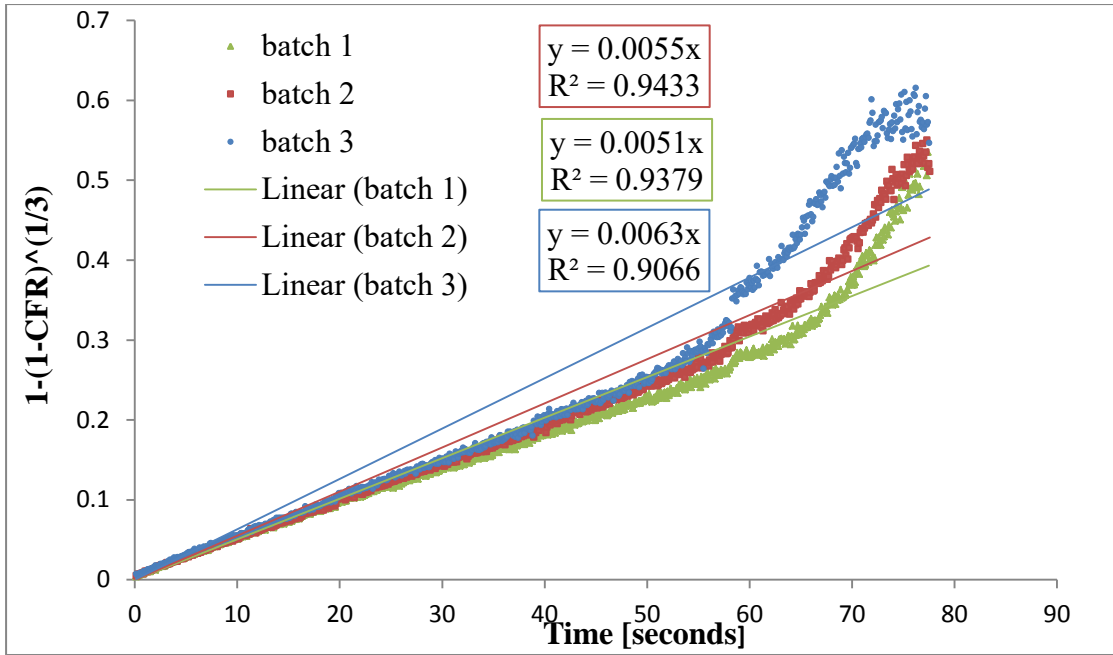
Figure B.17: Hopfenberg model for immunoliposomes at 9.85 (mW/cm^2).

Figure B.18: Gompertz model for immunoliposomes at 9.85 (mW/cm^2).

Figure B.19: Zero-order plot for immunoliposomes at 17.31 (mW/cm^2).

Figure B.20: First-order plot for immunoliposomes at 17.31 (mW/cm^2).

Figure B.21: Higuchi model for immunoliposomes at 17.31 (mW/cm^2).

Figure B.22: Korsmeyer-Peppas model for immunoliposomes at 17.31 (mW/cm^2).

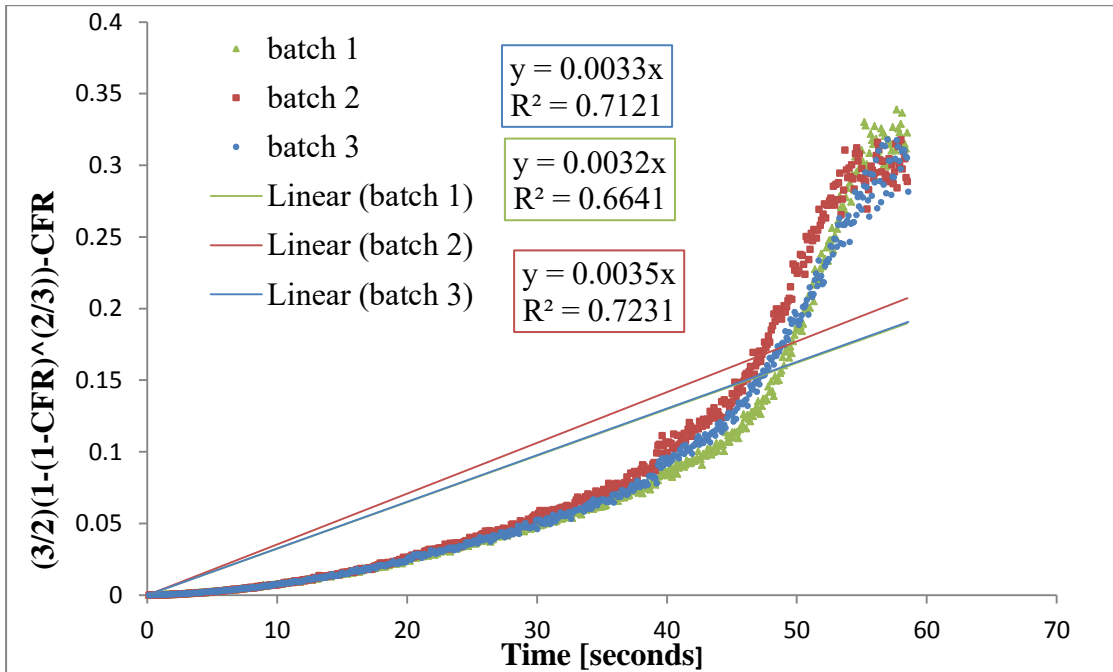Figure B.23: Hixson-Crowell model for immunoliposomes at 17.31 (mW/cm^2).

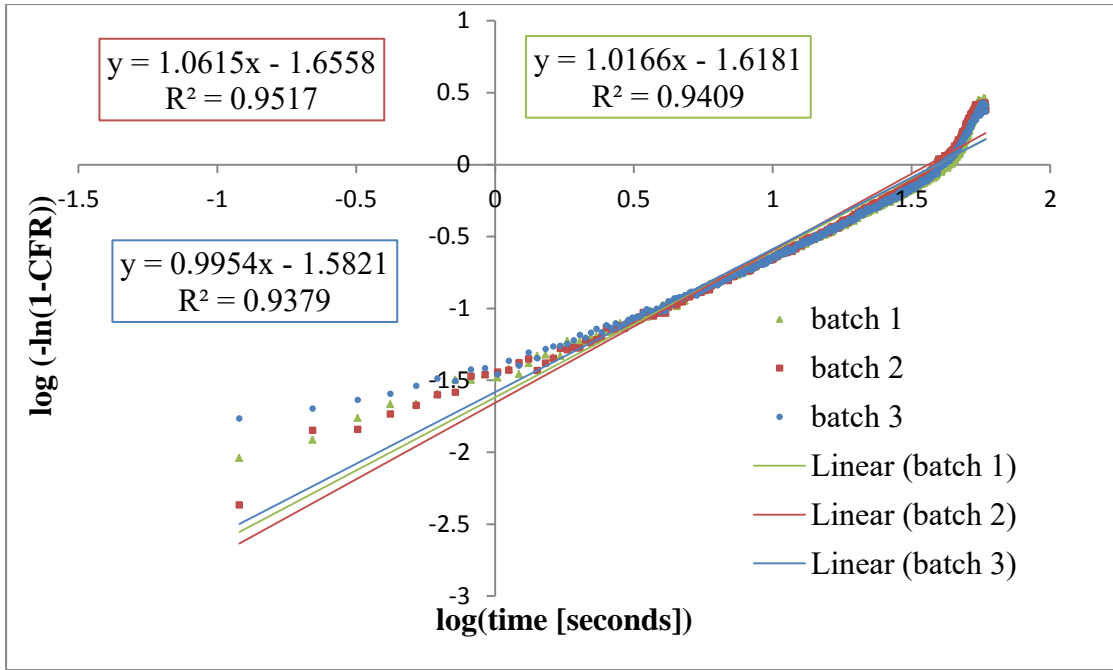Figure B.24: Baker-Lonsdale model for immunoliposomes at 17.31 (mW/cm^2).

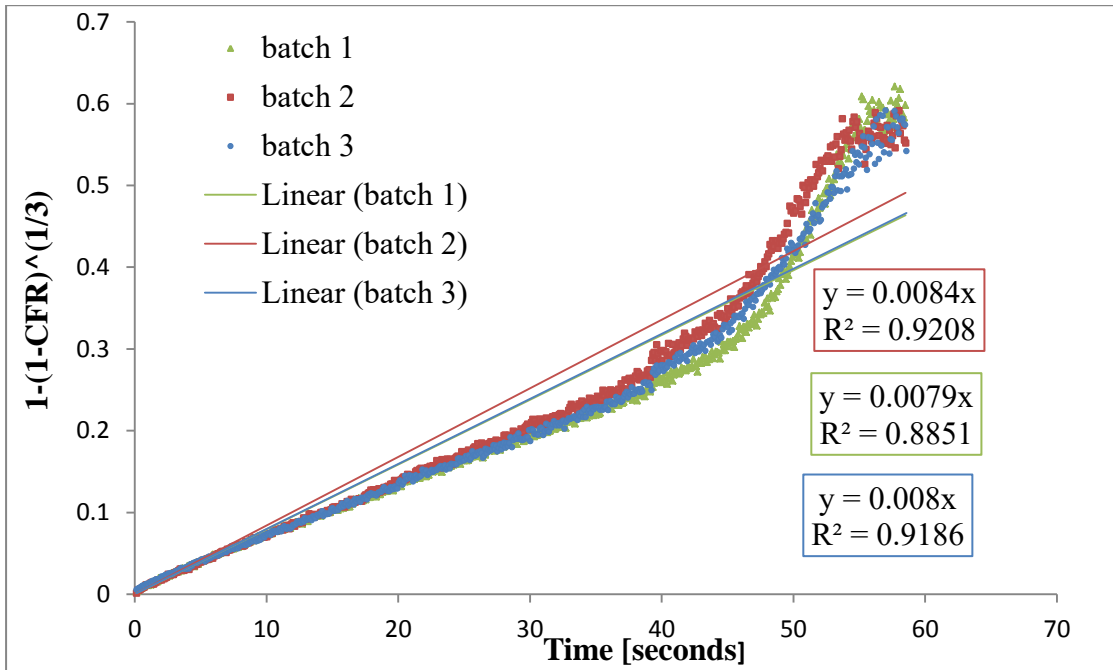Figure B.25: Weibull model for immunoliposomes at 17.31 (mW/cm^2).

Figure B.26: Hopfenberg model for immunoliposomes at 17.31 (mW/cm^2).
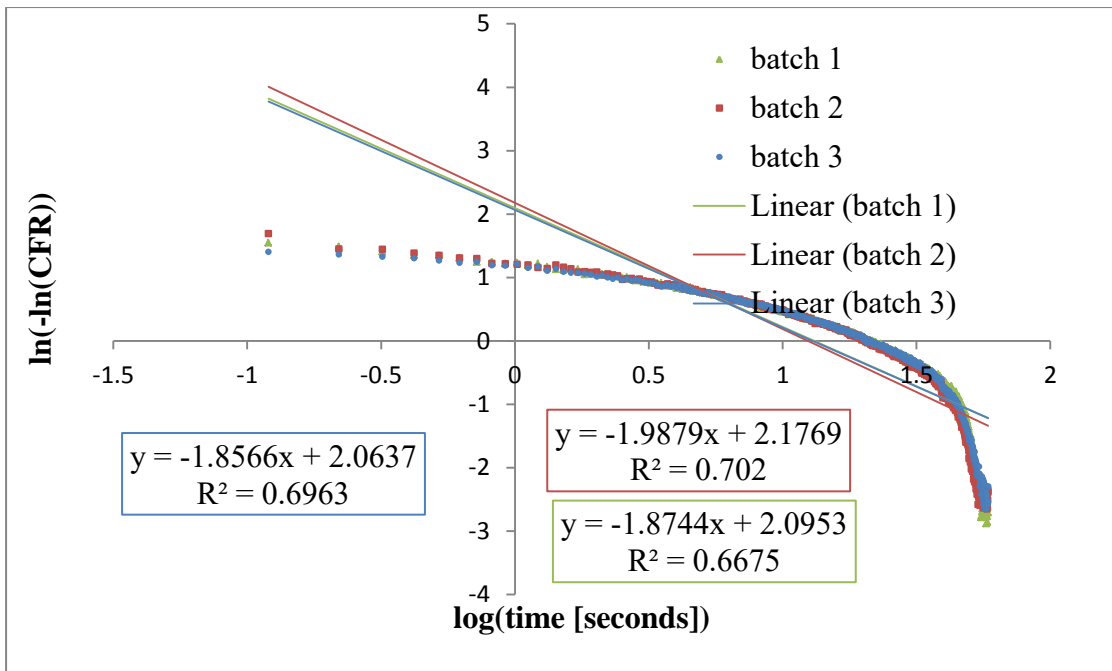
Figure B.27: Gompertz model for immunoliposomes at 17.31 (mW/cm^2).

Appendix C: Experimental Setup Photographs

Some of the steps in the methodology have been documented with pictures. These are shown in below figures. Figure C.1 shows the purification step of immunoliposomes after the conjugation reaction, where Sephacryl S-200 HR gel is used in the column to separate immunoliposomes (the lower color) from the free Trastuzumab and the calcein (the upper color). Separation is based on particle size using chromatography.
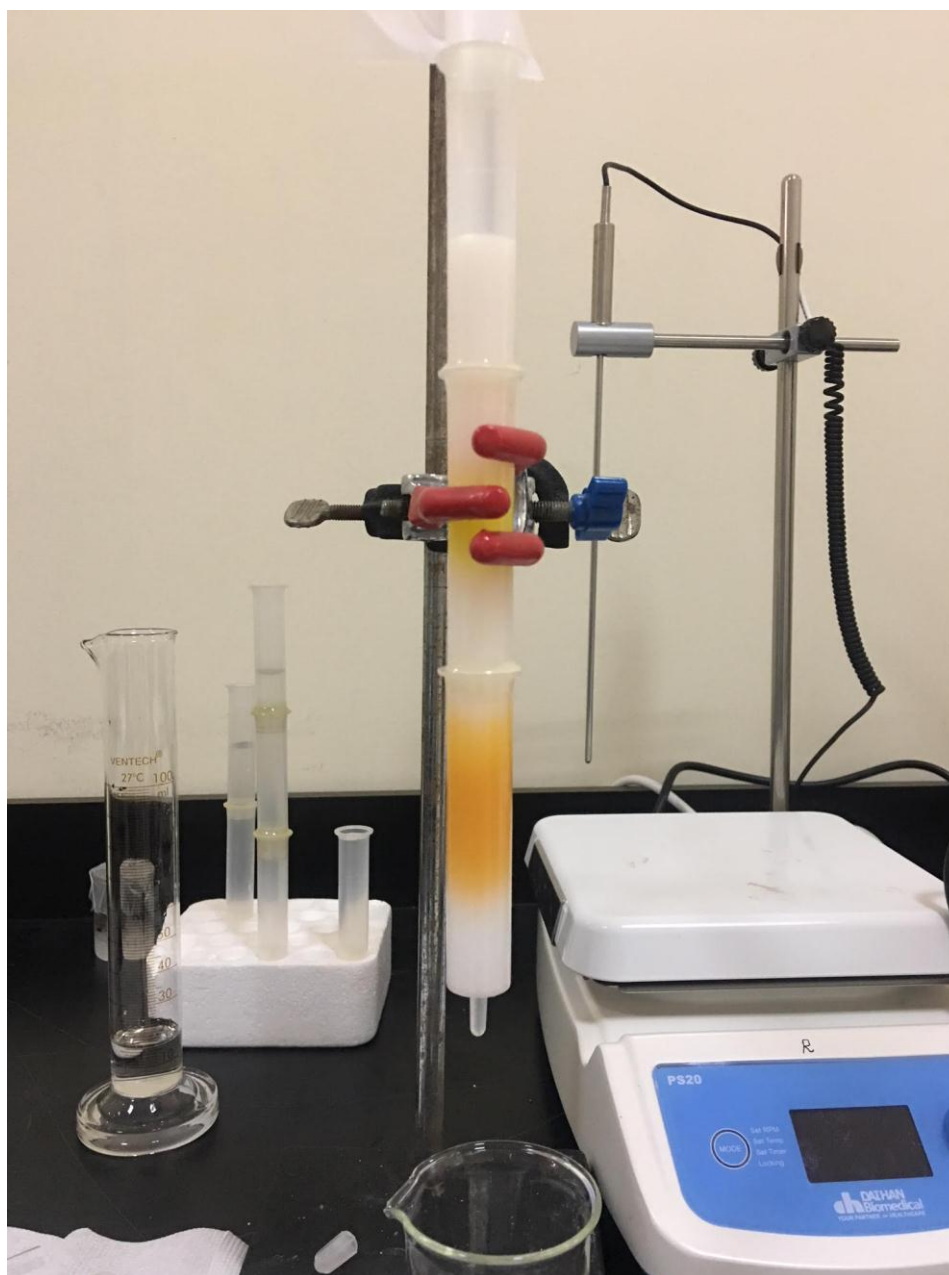

Figure C.1: Purifying immunoliposomes in Sephacryl S-200 HR from free Trastuzumab and calcein.

In Figure C.2, liposomes solutions after collection from the column are shown. Immunoliposomes, on the right, have slightly more yellowish color due to the presence of Trastuzumab that is distinguished by a light yellow color. The other sample on the left belongs to NH2 liposomes solution. In Figure C.3, the attachment confirmation is shown by the darker purple color that immunoliposomes sample exhibits after performing BCA assay. Darker purple color indicates more protein content which is caused by the attached Trastuzumab to immunoliposomes surface. The lighter purple color refers to the NH2 liposomes sample. Normally, samples with no protein attached shouldn't show purple color, but because of the presence of lipids in liposomes, some color is present. Lipids contain peptide bonds that are detected by the BCA assay.
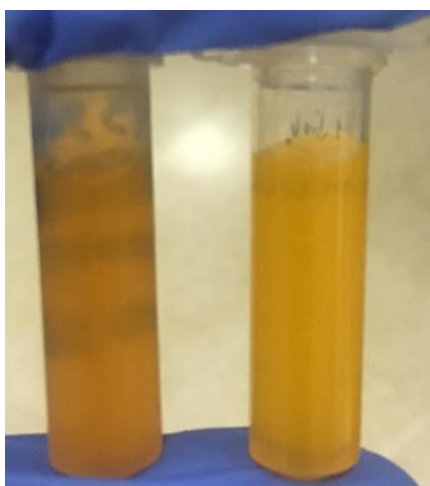

Figure C.2: NH2 liposomes and immunoliposomes solution after purification.

Figure C.3: Attachment confirmation with darker purple color for Immunoliposomes indicating more protein content, after performing BCA assay.

Vita

Amal Ahmed was born in 1991, in Abu Dhabi, United Arab Emirates. She received her primary and secondary education in Al Sila, Abu Dhabi, UAE. She received her B.Sc. degree in Chemical Engineering from the University of Khartoum, Sudan, in 2014. From 2014 to 2015, she enrolled in many courses, as well as worked as an executive secretary for three months in Abu Dhabi, Judicial department.

In January 2016, she joined the Chemical Engineering master's program in the American University of Sharjah as a graduate teaching assistant. During her master's study, she co-authored a paper in thermodynamics which was accepted in chemical engineering communications journal. She pursued her thesis in biomedical engineering and used the results to co-apply for a patent. During her time in AUS, she presented her thesis results in UAE Graduate Students Research Conference 2018 (UAEGSRC-2018). She also participated in U EU 's piano competition for higher education institutes, 2017. Additionally, she won second place in ―challenge yourself to be fit" competition organized by the sports complex in AUS.

Her current research focuses on nano-scale drug delivery of chemotherapy combined with ultrasound, for breast cancer treatment. Her research interests include drug delivery, thermodynamics, and clean energy production.